Co-funded by the



MIND

Microbiology In Nuclear waste Disposal

**(GRANT AGREEMENT: 661880)**

**DELIVERABLE 2.13**

# Anaerobic microbial corrosion of canister material

Editors: Tomáš Černoušek (CV Řež), Jakub Kokinda (CV Řež), Kateřina Vizelková (CV Řež), Rojina Shrestha (TUL), Alena Ševců (TUL)

Date of issue of this report: 15.1.2019

Report number of pages: 62

Start date of project: 01/06/2015
Duration: 48 Months

| This project has received funding from the Euratom research and training programme 2014-2018 under Grant Agreement no. 661880 | | |
|---|---|---|
| **Dissemination Level** | | |
| **PU** | Public | **PU** |
| **PP** | Restricted to other programme participants (including the Commission) | |
| **RE** | Restricted to a group specified by the partners of the MIND project | |
| **CO** | Confidential, only for partners of the MIND project | |

# Publishable Summary

The deep geological repository (DGR) was selected for disposal of spent fuel and high level radioactive waste due to its high radioactivity and significant content of long-lived radionuclides. In the DGR, a series of engineered and natural barriers will work together to isolate radioactive waste from the environment. First barrier will be a metal canister that will prevent direct release of radionuclides into the repository environment for as long as possible (up to ten thousand years). Microbially influenced corrosion (MIC) is one type of corrosion that may limit the lifetime of nuclear waste canisters. Although the risk of MIC is rather low, convincing proof is still missing.

Microorganisms are able to change the electrochemical conditions at the interface between a metal and an electrolyte solution by biofilm formation. These changes can range from acceleration of corrosion to complete corrosion inhibition. Sulphate-reducing bacteria (SRB) are the most important bacteria considered responsible for the MIC of carbon steel. On the other hand, archaeological analogues found under natural conditions with the presence of SRB confirm that these bacteria are not very aggressive for iron when the environment was strictly anaerobic.

The main goal of this study was to assess the impact of microbial activity on corrosion behavior of carbon steel and stainless steel in an anaerobic environment containing natural microbial community dominated by SRB. Therefore, granite groundwater from Josef Underground Research Center (Josef URC) containing SRB and synthetic bentonite pore water (bentonite BaM) inoculated with granite groundwater were used in our experiments. Electrochemical measurement, surface analysis, weight loss measurement and molecular biological tools were employed to evaluate the impact of MIC. This comprehensive analysis has given us a detailed overview about the impact of microorganisms and the processes of corrosion. Moreover, we were able to distinguish when biofilm formation began by comparison of sterile and non-sterile impedance spectrum.

To summarize, biofilm dualism was observed at the higher temperature (35°C) leading to an increase in the inhibitory action by barrier effect of the biofilm, while biofilm at $T_{LAB}$ accelerated corrosion. The seeding dispersal related to formation of biofilm at $T_{LAB}$ revealed in the form of second layer of biofilm, which was observed independently using EIS and SEM measurements. The unstable passivity and MIC inhibition of stainless steel was observed in the granite groundwater under anaerobic conditions. Severe local attack was observed only in the case of weight loss experiments with carbon steel using synthetic bentonite pore water inoculated with VITA water for samples taken after 3, 6 and 12 months. The samples collected after 18 months of exposure were without local attack under non-sterile conditions.

# Contents

# 1 Introduction

## 1.1 Microbially Influenced Corrosion (MIC)

Corrosion is the result of electrochemical reaction on the surface of the metal. It is influenced by the physiochemical condition such as pH, salt, oxygen, redox potential and conductivity at and around the surface of given metal. Moreover, corrosion induced by microorganisms is known as microbially influenced corrosion (MIC)[1]. Hence, MIC is the deterioration of the essential properties of metallic material due to reactions caused or promoted by the activity of microorganisms. Occurrence of MIC depends on the type of metal, the medium and the kinds of active microorganisms (Figure 1)[2].

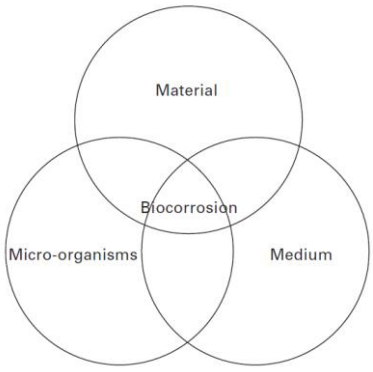


*Figure 1 Interaction material-medium-micro-organisms in the MIC*

MIC is a result of interactions, which are often synergistic, between the metal surface, abiotic corrosion products, and bacterial cells and their metabolites [3]. The appearance of the MIC does not differ from other types of abiotic corrosion (e.g. pitting, stress corrosion cracking or galvanic corrosion), and results from the metabolic activity of microorganisms within biofilms at the metal surfaces. Microorganisms tend to attach themselves to solid surfaces, colonize, proliferate, and form biofilms, which may in turn produce an environment at the biofilm/metal interface radically different from the bulk environment in terms of pH, dissolved organic and inorganic species [4]. Consequently, microorganisms within biofilms are involved in reactions that are not predicted by thermodynamic arguments based on the chemistry of the bulk medium.

MIC mechanisms can be classified into three types. Type I MIC involves respiration using sulfate or nitrate as electron acceptors. Cross-cell wall extracellular electron transfer (EET) is required for Type I MIC. Thus, Type I MIC is called EET-MIC. Microbes capable of EET are involved in microbial fuel cell (MFC) because they are electrogenic when EET direction is reversed to transport electrons from organic carbon oxidation in cytoplasm to an external anode. These electrogenic microbes can cause MIC, if there is a local shortage of organic carbon (electron donor). SRB-MIC and NRB-MIC mechanisms as discussed above belong to EET-MIC. Type II MIC is caused by secreted metabolites of microbes. Thus, Type II MIC is called metabolite MIC (M-MIC). Corrosive metabolites are oxidants such as protons, organic acids, and sulphides. Examples are MIC of steel by acids secreted by acid producing bacteria (APB) in biofilms, and copper MIC by $H_2S$ excreted by SRB. In the absence of an externally supplied oxidant, microbes such as APB can perform anaerobic fermentation, which often produces organic acids. With a sufficiently acidic pH under an APB biofilm, proton reduction can be coupled with iron oxidation to yield a thermodynamically favorable corrosion process. Like EET-MIC, M-MIC is also an electrochemical corrosion process, because iron oxidation and proton reduction are two separable electrode reactions. The word “metabolite” is used in M-MIC instead of the word “chemical,” because “chemical corrosion” refers to the direct reaction of a metal with an oxidant, usually at high



The MIND-project has received funding from the European Union’s Euratom research and training program (Horizon2020) under grant agreement 661880.

temperatures, without separable oxidation and reduction reactions, unlike in an electrochemical corrosion process. Unlike EET-MIC, M-MIC does not need biocatalysis. For example, proton is secreted by APB and it attacks metal extracellularly without enzymes. Because of this, M-MIC has abiotic counterparts. For example, acetic acid corrosion can be either due to APB excreting acetic acid or due to abiotic acetic acid. Apart from APB, fungi such as Aspergillus niger secret acidic metabolites (e.g., oxalic acid) that cause M-MIC.

A low $H_2S$ concentration in the culture medium caused less toxicity to sessile cells and also led to a thinner partially protective sulphide film than that with a high $H_2S$ concentration, which resulted in increased EET-MIC. They concluded that biogenic $H_2S$ corrosion is not a major contributor to carbon steel MIC by SRB. This means that M-MIC was not the main factor in carbon steel MIC by SRB, but rather EET-MIC. In other hand copper was not energetic enough as an electron donor for direct sulfate reduction by SRB. However, copper is corroded by SRB. Their thermodynamic analysis showed that the corrosion was caused by sulphide and proton with $Cu_2S$ as the corrosion product. Thus, copper corrosion by sulfate-respiring SRB belongs to M-MIC. This means that for SRB, both EET-MIC and M-MIC can occur depending on the metal type.

The characteristics of EET-MIC and M-MIC mechanisms provide useful insights into MIC by SRB, NRB, and APB, which dominate anaerobic MIC processes. In addition to Type I MIC and Type II MIC, Type III MIC can be classified as the biodegradation of organic materials such as organic polymers by microorganisms. Microbes, especially fungi in a warm and humid environment, excrete enzymes to degrade large molecules to produce utilizable small organic molecules. Type III MIC can damage polymer insulation of electrical systems, etc. [5].

## 1.2 Formation of Biofilms

The initial stage of MIC is the formation of a biofilm on the metallic surface. IUPAC has defined biofilm as an aggregate of microorganisms in which cells that are frequently embedded within a selfproduced matrix of extracellular polymeric substance (EPS) adhere to each other and/or to a surface [6]. Biofilm accumulation is the net result of cells attachment, growth, and detachment (Figure 2)[7]. The biofilm formation changes can range from acceleration of corrosion to complete corrosion inhibition.

Microorganisms accelerate corrosion by changing the nature or kinetics of the rate-controlling reaction or process. They can be directly involved in the electron transfer processes in the electrochemical cell or be less directly involved through a number of mechanisms. The major role in biofilm formation, maturation and maintenance is played by EPS and is composed of polysaccharide, nucleic acid and proteins. In biofilm, synergistic interaction of various microorganisms occurs which results in sharing of nutrient and energy among themselves causing a severe MIC [4]. The process of biofilm formation follows a sequence of steps that initiate by the adsorption of macromolecules (e.g. polysaccharides, nuclide acid) and micromolecules (fatty acids, lipids) at solid surfaces. A film is formed from the adsorbed molecules that can change the physiochemical condition of the environment including hydrophobicity and electrical charge. Diffusive transport owning to Brownian motion, convective transport due to liquid flow, and active movement of motile bacteria near the interface are the reasons behind transport and attachment of microorganism to an interface. After attachment, EPS is produced by microorganisms which provide the matrix to holds bacteria together and allows formation of microcolonies and eventually, formation of a mature biofilm. Dispersion is the final step of biofilm formation where the microorganisms are detach and dispersed by the process of sloughing and erosion. Hence, motile microorganisms are dispersed while some remains as sessile.


The MIND-project has received funding from the European Union's Euratom research and training program (Horizon2020) under grant agreement 661880.

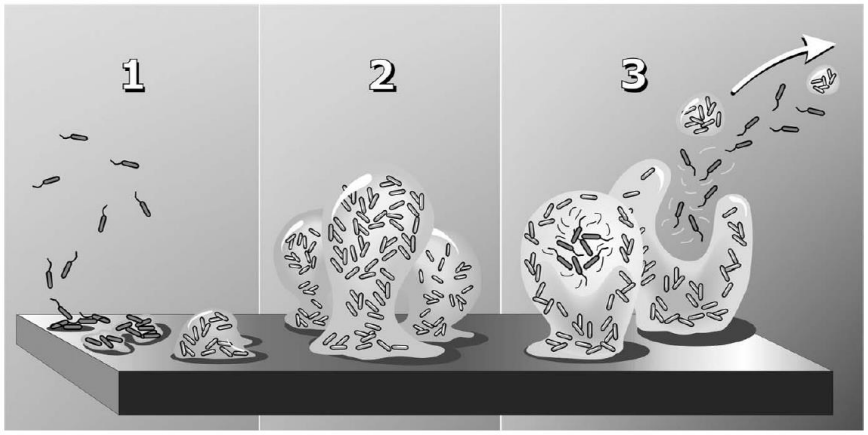


*Figure 2 The biofilm life cycle in three steps: 1) attachment, 2) growth of colonies, and 3) detachment in clumps or "seeding dispersal"[8]*

Biofilm at each phase may affect the process of corrosion differently and presence of biofilm does not necessarily brings out corrosion. Acceleration in corrosion was observed in a biofilm isolated from a drinking water system during the first 7 days of incubation but a protecting effect was found after 30 days of incubation [9]. It may have passivation effect on the metal surface protecting from corrosion as a coating. However, by the time the film may become week, porous and fragile having no more protecting effect [10]. Nevertheless, the biofilm is not just an accumulation of cells on a surface but that, compared to planktonic community, it represents a fundamentally different condition of microbial growth as evidenced by the current proteomic and transcriptomic analyses of SRB *Desulfovibrio vulgaris* [11].

The corrosion reaction can be modified by the metabolic reactions in biofilms in many ways, and we pointed four possible modifications here:

1. Biofilms consuming oxygen, the cathodic reactant.
2. Biofilm matrix increasing mass transport resistance near a metal surface.
3. Metabolic reactions in biofilms generating corrosive chemicals, such as acids.
4. Metabolic reactions in biofilms generating products that serves as cathodic reactants.

Bacteria are able to grow adhered to almost every surface, forming architecturally complex communities termed biofilms. In biofilms, cells grow in multicellular aggregates that are encased in an extracellular matrix produced by the bacteria themselves[12]. Microbial adhesion has been described in the literature in terms of DLVO theory [13]. According to this theory, the total potential energy of interaction ($V_T$) is obtained summing up the energy due to van der Waals interactions ($V_W$) and the energy arising from double-layer interactions ($V_{DL}$)[14]:

$$V_T = V_w + V_{DL}$$

The development of a biofilm at the surface will form a relatively stabilized matrix which may have numerous effects on the electrochemical processes but particularly in retaining a point source or chemical activity in a fixed position on near the metal surface. The opposite question of whether corroding metals encourage biofilm formation by providing localized regions with more favorable physiochemical properties onto which microorganisms could adhere, is a point considered[15].

The result of corrosion is that the surface of the metal will become coated with one or usually more of an enormous range of corrosion products. Most metals layers of corrosion product may begin to corrode again rapidly if the localized chemical conditions change. It is by mediating this change of conditions that microorganisms can interact with metallic surfaces. The composition of the biofilm itself is again highly dependent upon the environmental conditions. Initial attachment of individual bacteria will give rise to a very disjunctive community, and the development of this will be a feature of



The MIND-project has received funding from the European Union's Euratom research and training program (Horizon2020) under grant agreement 661880.

the mass transfer conditions, largely controlled by the number or cells in suspension, the now velocity and turbulence of the medium [16].

Metal corrosion can be influenced by:

- Physical effects – diffusion barrier, reduction of turbulence and surface flow, reduction of heat transfer
- Chemicals effects – anodic reaction (prevention of anodic polarization through metal ion complex and/or binding), cathodic reaction (modulation of reducible species; supply of reducible species)
- Dissolution of protective oxide/hydroxide layers
- Selectivity of ion permeability
- Effect upon pH

However, the most important aspect of all the diffusion and chemical effects is the creation of differential concentration cells producing galvanic corrosion cells.

The biofilm can acts as a barrier of mass transfer for the diffusion of organic carbon source. Generally, higher amount of carbon source is utilized by the top layer of biofilm resulting in less availability of carbon to sessile cells at the bottom layer. This leads to phase of starvation for sessile cells living close or directly on metal surface. Due to deprivation of electron donor (carbon source), starved cells switch to consume elemental iron as the source of electron donor for the generation of energy. An experiment on carbon starvation has demonstrated that corrosion of C1018 carbon steel was accelerated in spite of having lowered sessile cells because of carbon-limited environment. Due to lack of carbon source in media, sessile SRB obtained electrons directly from iron leading to severe corrosion of carbon steel than SRB biofilm in full supplement of nutrient media [17]. Such corrosion is known as electrical MIC.

## 1.3 Role of microorganisms in MIC

In the natural environment, microorganisms often exist as a biofilm, which is central to the occurrences of biofouling, biodegradation, and biocorrosion [18, 19]. Microorganisms require the following principal components to provide energy for their metabolism: an electron donor (energy source) and an electron acceptor [20]. Hydrocarbons and fatty acids (e.g., formate, pyruvate, acetate, methanol and lactate) usually serve as organic carbons for growth. They provide energy and carbon for growth. The biofilm in MIC is formed by bacteria, archaea and eukaryotes, whereas bacteria are the most responsible for MIC.

Prokaryotes involved in MIC are usually categorized into a few main groups, which comprise taxonomically diverse organisms varying considerably in their metabolic capabilities. MIC culprits are typically sulphate-reducing bacteria and archaea (SRP), methanogens, acid-producing bacteria (APB), hydrocarbon-degrading prokaryotes (HDP), acetogenic organisms, nitrate-reducing bacteria (NRB), nitriteoxidizing bacteria (NOB), metal-oxidizing bacteria (MOB) and metal-reducing bacteria (MRB), as well as fermentative hydrogen sulfide producing bacteria. These organisms typically coexist in naturally occurring biofilms, forming complex consortia on corroding metal surfaces [1]. All of the types of microorganisms described above, as well as many others that are less well characterized, usually thrive in biofilms as synergistic and/or syntrophic communities. Moreover, most severe deterioration of metal takes place when the biofilm is composed of different species due to interaction between multispecies [21] as shown in Figure 3.



The MIND-project has received funding from the European Union's Euratom research and training program (Horizon2020) under grant agreement 661880.

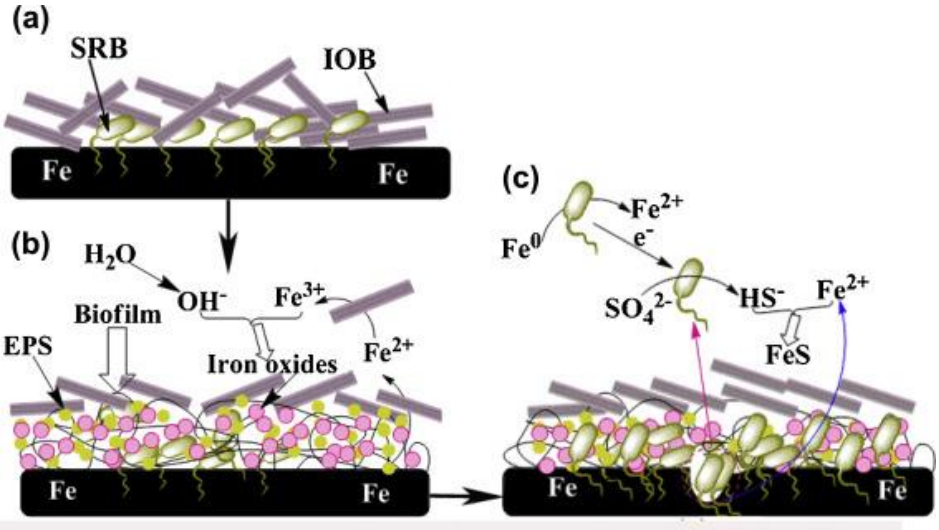


*Figure 3 Scheme of mechanisms of biofilm formation and pitting corrosion in the mixture of SRB and IOB; initial period (a), formation of biofilm (b), and formation and propagation of pitting corrosion (c)[22].*

Generally, oxygen is introduced in the repository during the excavation and operational phases and hence, the environment is oxidizing for first few hundred years of repository. However, oxygen will disappear by microbial consumption or by inorganic reaction and thus, a reducing environment will be established after about 300 years of closure of repository [23]. Under such condition both oxidizing and reducing species along with acid producers are able to invite MIC of metal canister. Some examples different kind of microorganism and their effect in relation to corrosion of metal surface are shown in Table 1. Intact metal canister is the only absolute barrier of disposal system and hence any damage or corrosion in canister may threats the integrity of safety relevant process. The biofilm tends to create nonuniform surface conditions, localized attack might start at some points on the surface leading to localized corrosion, usually in the form of pitting [8]. In contrast, microorganisms can also induce corrosion inhibition by two general mechanisms or their combination: (i) neutralizing the effects of corrosive substances and (ii) forming or stabilizing protective films on a metal surface [16].

*Table 1 Microorganisms and their effect in relation to bio-corrosion of metal surface[21].*

| Type | | Trait | Effect | Reference |
|---|---|---|---|---|
| Sulfate reducers<br>*Desulvovibrio* sp<br>*Desulfomonas* sp | Anaerobic | Use $H_2$ to reduce $SO_4^{2-}$ to $S^{2-}$: precipitation of $H_2S$ and FeS | Cathodic depolarization by hydrogen uptake, anodic depolarization by corrosive iron sulphides | [24-27] |
| Acid producing bacteria and fungi<br>*Clostridium* sp.<br>*Fusarium* sp.<br>*Penicillium* sp.<br>*Hormoconis* sp. | Aerobic and anaerobic | Production of acid eg., nitric acid, sulfuric acid and organic acids | Dissolve iron, chelate copper, zinc and iron | [28, 29] |



The MIND-project has received funding from the European Union's Euratom research and training program (Horizon2020) under grant agreement 661880.

| | | | | |
|---|---|---|---|---|
| Slime forming bacteria<br>*Clostridium* sp.<br>*Bacillus* sp.<br>*Desulfovibrio* sp.<br>*Pseudomonas* sp. | Aerobic and anaerobic | Production of extracellular polymeric substance (biofilm) | Exopolymers capable of binding metal ions | [30-32] |
| Iron oxidizer/Manganese oxidizers<br>*Gallionella* sp.<br>*Leptothrix* sp.<br>*Mariprofundus* sp. | Aerobic | $Fe^{2+}$ to $Fe^{3+}$ and $Mn^{2+}$ to $Mn^{3}$+: Iron oxode and manganese dioxide formation | Depositon of cathodically reactive ferric and manganic oxides | [25, 33, 34] |
| Iron reducers<br>*Pseudomona*s sp.<br>*Shewanella* sp<br>*Geothermobacter* sp | Aerobic | Reduce $Fe^{3+}$ to $Fe^{2+}$, manganese or Iron oxide reduction | Reduction of iron and manganese oxides | [25, 33] |
| Sulphide oxidisers<br>*Thiobacillus* sp. | Aerobic | Oxidises $S^{2-}$ and $SO_3^{2-}$ to $H_2SO_4$ | Acids corrode metal | [35] |

## 1.4 SRPs

### 1.4.1 Sulphate reducing prokaryotes (SRPs)

Under anaerobic environment, MIC is mainly influenced by the activities of sulphate reducing prokaryotes (SRP) which utilize sulfate as a terminal electron acceptor and reduces to sulphide as a result of anaerobic respiration. SRPs are highly specialized microorganisms which can also use sulphite, thiosulphate, sulphur and some can even use nitrate in deprivation of sulfate as a terminal electron acceptor in their energy metabolism. The produced sulphide is a potential corrosive element that may threaten the integrity of metal canister at deep repository condition. Geomicrobiologically, it is dissimilatory sulphate-reducers that are considered important for MIC than assimilatory reducers. Among all genera of sulphate reducing bacteria (SRB) *Desulfovibrio* species is consider as main culprit responsible for corrosion. Similarly, two extremely thermophilic sulphate-reducers, *Archeoglobus fulgidus* and *Archeoglobus profundus* in the domain archaea were discovered as sulphate reducers that can accelerate corrosion. Most of the researches on an anaerobic corrosion have mainly focused on corrosion by SRB.

### 1.4.2 Sulphate reducing bacteria (SRB)

Generally, sulphate-reducing bacteria are heterotrophic which require anaerobic conditions for growth. However, recent studies have shown that few species of SRB are capable of carrying out micro-aerobic respiration and may be autotrophic and lithoautotrophic as well. Low molecular weights organic compound such as lactate, acetate, propionate, amino acid are the main source of carbon. Likewise, hydrogen gas serves as the source of both energy and electron donor for metabolism their metabolism. Phylogenetically and metabolically SRB are most diverse group of bacteria and are also consider unique bacteria because of its role played in biogeochemistry of the environments where they inhabit. SRB are widely distributed in terrestrial, sub terrestrial and marine ecosystem and are capable of producing sulphide under different environmental condition. An overview of some SRB under different temperature and pH condition provided by literature has been presented in Table 2. By now, 60 genera with more than 220 species of SRB have been studied so far [36]. Some of SRB found in extreme physiological condition are *Desulfotomaculum* species, *Desulfovibri*o species and *Desulfomicrobium* species. Moreover, *Desulfotomaculum* is endospore forming species which can exist in dormant phase for long years and revive back to active form of life under a favorable environmental condition. With regard to underground disposal of nuclear waste, active presence of SRB in bentonite buffer and ground water has been reported in many studies [23, 37-40].



The MIND-project has received funding from the European Union's Euratom research and training program (Horizon2020) under grant agreement 661880.

*Table 2 SRP from various site under different temperature and pH provided by literature from Aerts 2009[41]*

| Species | Optimum Temerature | Optimum pH | Sampling site | Electron acceptors | Electron donore | References |
|---|---|---|---|---|---|---|
| *Desulfonatronovibrio hydrogenovorans* | 37 | 9.5-9.7 | Lake Magadi (Kenya) | $SO_4^{2-}$, $SO_3^{2-}$, $S_2O_3^{2-}$ | $H_2$, formate | [42] |
| *Desulfonatronum lacustre* | 37-40 | 9.5 | Lake Khadyn (Tuva, Russia) | $SO_4^{2-}$, $SO_3^{2-}$, $S_2O_3^{2-}$ | $H_2$, formate, ethanol | [43] |
| *lkaliphilus transvaalensis* | 40 | 10 | Mine water (Carletonville, South Africa) | S°, $S_2O_3^{2-}$, fumarate | Organic acid, sugars, starch, alcohols | [44] |
| *Desulfovibrio alkalitolerans* | 43 | 9-9.4 | Heating ducts | $SO_4^{2-}$, $SO_3^{2-}$, $S_2O_3^{2-}$ | $H_2$/ acetate, formate., lactate, pyruvate | [45] |
| *Desulfonatronospir thiodismutans* | 43 | 10 | Soda lake ( Altai, Russia) | $SO_4^{2-}$, $SO_3^{2-}$, $S_2O_3^{2-}$, pyruvate | $H_2$, formate., lactate, ethanol, butanol | [46] |
| *Desulfonatronospira delicata* | 45 | 10 | Lake Wadi al Natrun (Egypt) | $SO_4^{2-}$, $SO_3^{2-}$, $S_2O_3^{2-}$, pyruvate | $H_2$, formate., lactate, ethanol, butanol | [46] |
| *Desulfotomaculum alkaliphilum* | 50-55 | 8.6-8.7 | Cow/pig manure | $SO_4^{2-}$, $SO_3^{2-}$, $S_2O_3^{2-}$ | $H_2$/ acetate, formate., lactate, pyruvate, ethanol | [47] |
| *Thermodesulfovibrio* | 65 | - | - | $SO_4^{2-}$, $SO_3^{2-}$, $S_2O_3^{2-}$ | $H_2$, ethanol | [48] |
| *Thermodesulfobacterium* | 5-70 | - | - | $SO_4^{2-}$, $SO_3^{2-}$ | Acetate, lactate, succinate, fumarate, malate, fatty acids, sugars | |
| *Archaeoglobus* | 82-83 | - | - | $SO_4^{2-}$ | $H_2$, lactate, sugars, peptides, starch | |



The MIND-project has received funding from the European Union's Euratom research and training program (Horizon2020) under grant agreement 661880.

### 1.4.3 Mechansims of MIC by SRB

To study corrosion induced by SRB, understanding the mechanism of corrosion is important. Some of widely known mechanisms of MIC by SRB are as follows:

**1. Cathodic depolarization** (Figure 4): The corrosion of metal by SRB was initially proposed in 1934 by Von Wolzogen Kuehr and Van der Vlugt and a simplified version is presented in the Table 3. This mechanism follows a theory of cathodic depolarization where corrosion by SRB is induced due to depolarization by the oxidation of cathodic hydrogen. A metal becomes polarized when it reacts with water resulting in anodic reaction by losing positive metal ions and hence, in absence of oxygen the free electron reduces the proton of water to produce hydrogen following a cathodic reaction. This hydrogen is expected to be consumed by SRB as good source of energy and electron. The mechanism of cathodic depolarization accelerates the anodic reaction resulting in anodic metal dissolution and subsequently, formation of corrosion product such as FeS and $Fe(OH)_2$ [49].

*Table 3 Cathodic depolarization mechanism by SRB on the metal corrosion*

| | |
|---|---|
| Anodic reaction (1) | $4\,Fe \rightarrow 4Fe^{2+} + 8e^-$ |
| Water dissociation (2) | $8H_2O \rightarrow 8H^+ + 8OH^-$ |
| Cathodic reaction (3) | $8H^+ + 8e^- \rightarrow 8H + 4H_2$ |
| Hydrogen oxidation (4) | $SO_4^{2-} + 4H_2 \rightarrow H_2S + 2H_2O + 2OH^-$ |
| Precipitation (5) | $Fe^{2+} + H_2S \rightarrow FeS + 2H^+$ |
| Precipitation (6) | $3Fe^{2+} + 6OH^- \rightarrow 3Fe(OH)_2$ |
| Total Reaction: | $4Fe + SO_4^{2-} + 4H_2O \rightarrow FeS + 3Fe(OH)_2 + 2OH^-$ |

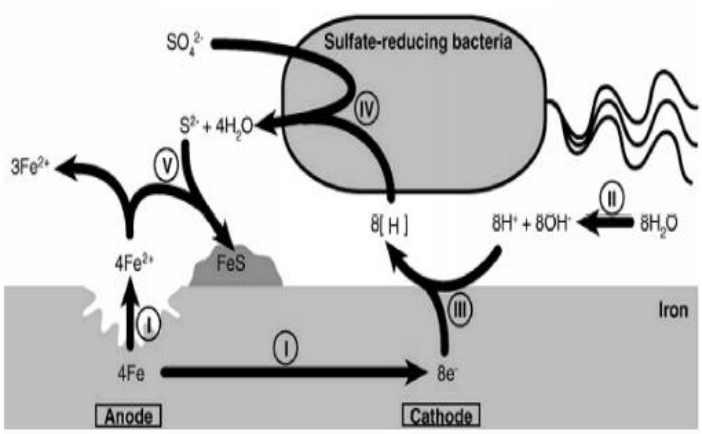


*Figure 4 Scheme of iron surface corrosion induced by SRB based on the process postulated by the cathodic depolarization theory [50] following 5 major steps starting with dissolution of iron, dissociation of water, proton reduction, sulfate reduction and finally, sulphide precipitation.*

**2. Iron sulphides (King's Mechansim**): In 1971 King and Miller suggested that solid FeS formed on the surface of the metal acts as an absorber of molecular hydrogen and then induce in reproduction of iron sulfide. Here, part of the iron below the biofilm becomes anode and the other part covered by iron sulphide behaves as cathode. Thus, the rate of corrosion will remain high. Schematic illustration of this mechanism has been presented in Figure 5 where no film of sulphide are formed after the



The MIND-project has received funding from the European Union's Euratom research and training program (Horizon2020) under grant agreement 661880.

formation of plenty of FeS for commencing a galvanic cell between FeS and Fe while a high corrosion was recorded due to galvanic corrosion [49].

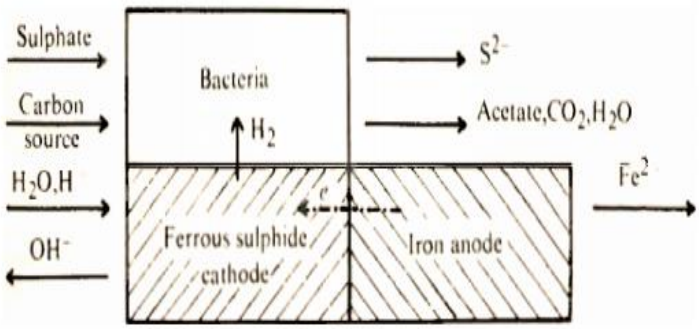


*Figure 5 Corrosion of metal by SRB proposed by King'S Mechanism*

**3. Fe-binding exopolymers**: Microorganisms are capable of producing extracellular polymeric substance (EPS) which usually consists of polysaccharides and nucleic acid. It results in formation of biofilm and the major purpose of biofilm is protection and shelters to microorganisms. The EPS produced by SRB have a unique ability to bind with metal ions and speed up the process of corrosion. SRB with different composition of EPS were observed to have different rate of corrosion[49]. Furthermore, Chan et al., 2002 showed that EPS alone can be a metal corrosion agent. They studied the metal corrosion in two test solution, one with 1% EPS and other without any EPS and the result demonstrated that EPS is a responsible corrosive agent to enhance corrosion [51].

**4. Biocatalytic cathodic sulfate reduction (BCSR) theory:** Oxidation of insoluble iron occurs outside SRB cells while sulphate reduction occurs inside the cells. The electrons released by elemental iron oxidation are transferred from outside the cells across the cell wall to the SRB cytoplasm where sulphate reduction takes place. Organic carbon such as lactate is soluble. Its biocatalyzed oxidation occurs in the SRB cytoplasm. Thus, the released electrons do not need to be transported across the SRB cell wall [4].

According to this theory, electron released by the dissolution of iron at the anode is used to reduce sulphate at the cathode resulting in MIC with the help of biocatalyst. It is believed that because of presence of biocatalysis, following reaction occurs on the surface of the iron resulting in formation of corrosive SRB biofilm.

$$Anodic: 4Fe \rightarrow 4Fe^{2+} + 8e^- \ (Iron\ dissolution)$$
$$Cathodic: SO_4^{2-} + 8H^+ + 8e^- \rightarrow 6HS^- + OH^- + 3H_2O$$

In the supplement of external electrons donor in impressed current cathodic protection condition, a rise in population of sessile SRB may be detected. Additionally, cell wall of SRB carries charges which are attracted to the metal surface. If the environment has insufficient electrons donor, the sessile SRB may attack the iron to fulfil the scarcity of electron for BCSR. Therefore, in order to ensure a steady supply of external electron, a continuous impressed current is desired [52].

## 1.5 MIC of nuclear waste canisters

Candidate container materials such as copper and carbon steel (C-steel) are known to be susceptible to MIC under biofilms [15]. Corrosion occurs under both aerobic and anaerobic conditions and can take the form of general corrosion and localized corrosion, the latter in the form of discrete pitting or general surface roughening. The rate of corrosion will depend on many factors, not least in this case the availability of nutrients. These materials could undergo some corrosion in the presence of surface microbial activity. As for all forms of corrosion to which the container may be susceptible, a


The MIND-project has received funding from the European Union's Euratom research and training program (Horizon2020) under grant agreement 661880.

number of prerequisite conditions are necessary for MIC to occur. In deciding whether MIC is a concern for the overall safety of the disposal system. Microbial influenced corrosion may limit the lifetime of nuclear waste canisters and could influence the corrosion of nuclear waste containers in a number ways. Certain environmental factors such as temperature, pH, radiation, nutrient supply and, in particular, lack of water could severely limit the microbial activity in repositories. Most microorganisms require water activities (aw) above 0.9 to support active metabolism, which corresponds to 60–80% soil saturation. Thus, drying the environment by heating will probably eliminate the microbes initially present in the vicinity of the container. Even though microbial activity in the repository could be expected to be low, due to the above mentioned limiting factors, microbial activity inside the repository cannot be discarded altogether. Some microbial cells, especially those far away from the container, could resist restrictive conditions as dormant bacteria, and move closer to the container when the environmental conditions are less severe. Bacteria naturally occurring in groundwater and rocks could also migrate into the repository through fractures in the concrete and bentonite barriers, thus increasing the risk of microbiologically influenced corrosion (MIC) of the metal canister. It is also important to point out that a significant MIC of the metallic container could occur indirectly from sulfides produced by sulphate reducing bacteria (SRB), at locations remote from the container surface, where microbial activity is not inhibited. The hydration of some bentonite blocks close to the rock, probably due to the penetration of water through cracks in the concrete/rock, produced significant corrosion damage in certain components. This corrosion damage was principally induced by microbial activity. Thus, even though microbial activity in the repository could be expected to be low, MIC cannot be discounted as a potential corrosion mode for the metallic container[53].

## 1.6 Methods for detection of MIC

### 1.6.1 EIS

Electrochemical impedance spectroscopy (EIS) is a non-destructive method for analyzing long-term measurements. It provides a lot of information about the system under investigation (e.g. corrosion rate, the capacity of the electric double layer, morphological characteristics of the surface or dielectric properties) and could be performed *in-situ*.

Output signals, arising from the system (electrochemical cell) responding to an inserted sine wave perturbation signal of small amplitude at different frequencies, are measured. The amplitude $I_m$ and phase shift changes by angle $\varphi$. The overall change in the output signal is characterized by the quantity of the impedance Z having the vector character ($Z = Z' + jZ''$). Impedance is defined by equation:

$$Z = \frac{E(t)}{I(t)} = \frac{E_0 \cdot \sin(\omega t)}{I_0 \cdot \sin(\omega t + \varphi)}$$

Impedance represents the ratio between alternating voltage *E(t)* and current *I(t)* at a given time *t,* where $E_0$ is the amplitude of the voltage, $I_0$ is the amplitude of the current, $\omega$ is the angular frequency, and $\varphi$ is the phase shift between the input voltage and the output current signal. The frequency changes during the measurement to give a characteristic impedance spectrum of the system. Sufficiently small amplitude of the perturbation signal is a necessary condition for the measurement to maintain the linearity of the system behavior.

The obtained data are typically visualized using Nyquist or Bode diagrams (Figure 6). The Nyquist plot shows dependence between real (Z') and imaginary part (Z'') impedance in a complex plane. The imaginary part is plotted versus the real part for each frequency in the measured range, and the values of imaginary and real part are in functionally independent. The Bode diagram shows the phase angle ($\varphi$) and the absolute value of impedance $|Z|$ on the frequency.


The MIND-project has received funding from the European Union's Euratom research and training program (Horizon2020) under grant agreement 661880.

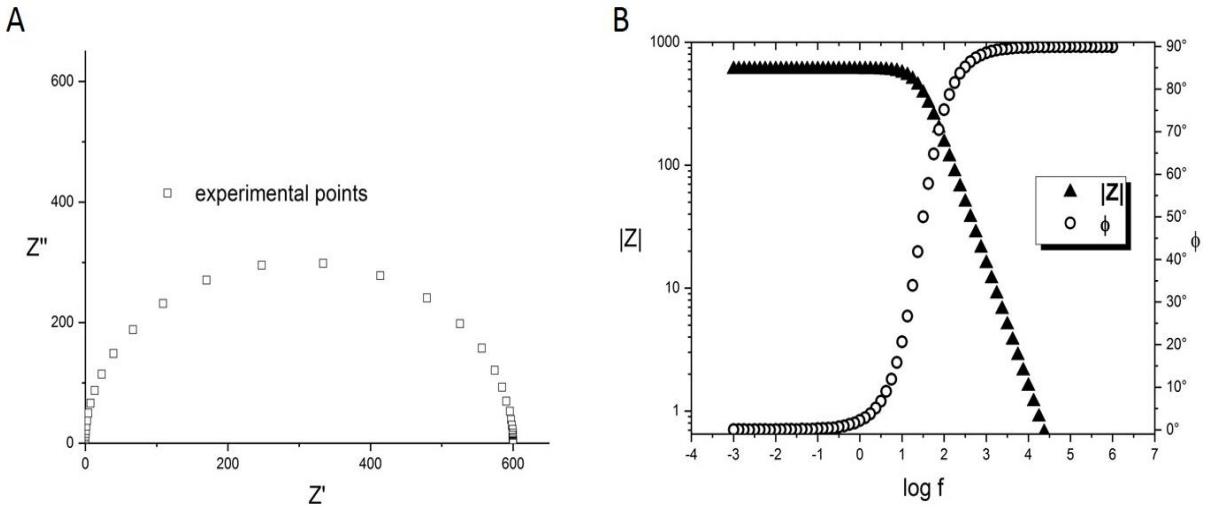


*Figure 6 Example of visualizing of impedance data in the case of parallel circuit of element R and C, R = 600 Ω a C = 0,01 μF: A - Nyquist diagram, B - Bode diagram.*

The impedance spectrum is evaluated by an equivalent circuit, which is used to model interactions on the interface of the working electrode. In other words, experimental impedance values are approximated by impedance of equivalent circuit. Optimal equivalent circuit is formed by a combination of concentric elements (resistance – R, capacity – C and induction – L) and electrochemical elements (constant phase element – CPE, Warburg diffusion impedance – W, etc.). These elements capture the behavior of the measured system and concurrently have a physical meaning. Randles circuit (Figure 7) is a fundamental equivalent circuit in which the total current $I_t$ flowing through the phase interface is divided into a faradian $I_f$ and a charging current $I_c$ of the electric double layer. $R_s$ represents the solution resistance, $C_{dl}$ is the double layer capacitance and $R_p$ is the polarization resistance.

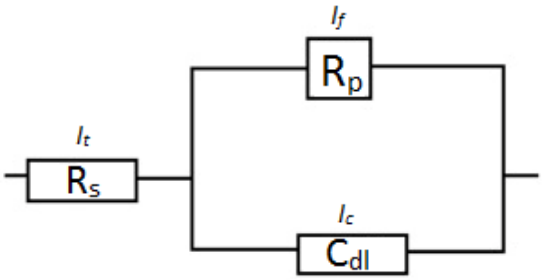


*Figure 7 Randles equivalent circuit*

### 1.6.2 Polarization techniques

Polarization techniques are a part of the DC electrochemical methods that are characterized by the polarization curve (usually dependence between electrode potential and current density). Linear polarization resistance and Tafel extrapolation are typically used as polarization techniques for investigation of a general corrosion. Tafel extrapolation belongs to the destructive methods due to bigger overvoltage that can cause dissolving or precipitating of insoluble corrosion products on the surface of the electrode.

The electrochemical cell uses the working electrode as a corrosion sample (material under evaluation), the counter electrode usually made of platinum or high-density graphite and the reference electrode maintaining a constant potential relative to the working electrode potential. Determination of a polarization curve is usually initiated by measuring the open-circuit corrosion potential ($E_{corr}$) until a steady-state value is achieved (e.g., less than 1.0 mV change over a five-minute period). Next, the potentiostat is set to control at $E_{corr}$ and connected to the polarization cell. If the set-point potential is continuously increased (above $E_{corr}$), an anodic polarization curve is generated; conversely, if the potential is continuously decreased (below $E_{corr}$), a cathodic polarization curve is produced. So the


The MIND-project has received funding from the European Union's Euratom research and training program (Horizon2020) under grant agreement 661880.

polarization curve is composed of partial anodic curve of metal oxidation (metal dissolution) and partial cathodic curve of some environmental components reduction (usually oxygen or hydrogen ions).

The relation between the electrode reaction rate and the potential is described by the Butler-Volmer equation:

$$i_{app} = i_{corr}\left[e^{\left(\frac{2{,}303(E-E_{corr})}{\beta a}\right)} - e^{\left(\frac{2{,}303(E-E_{corr})}{\beta c}\right)}\right] \quad (1)$$

where $i_{app}$ is the applied or measured current density (A/m$^2$), $i_{corr}$ is corrosion current density, $\beta_a$ is the anodic Tafel constant in volts/decade, $\beta_c$ is the cathodic Tafel constant in volts/decade and $(E - E_{corr})$ is the polarization, given by difference between applied and corrosion potential (V). The rearrangement of Equation (1) gives an expression for the polarization resistance, $R_p$:

$$R_p = \frac{\beta_a \cdot \beta_c}{2{,}303 \cdot i_{corr} \cdot (\beta_a + \beta_c)} = \frac{B}{i_{corr}} \quad (2)$$

The slope at the origin of the polarization curve, defined as polarization resistance is inversely proportional to the corrosion rate, where

$$B = \frac{\beta_a \cdot \beta_c}{2{,}303 \cdot (\beta_a + \beta_c)} \quad (3)$$

Classic Tafel analysis is performed by extrapolating the linear portions of a logarithmic current versus potential plot back to their intersection (see Figure 8). The inclinations of the linear parts, so called Tafel lines, express the difficulty of the anodic or cathodic process. The both Tafel lines intersect in the point of coordinates ($E_{corr}$, log $I_{corr}$), that makes possible the estimation of the corrosion current density. At potentials far away from the corrosion potential, the current density reflects the kinetics of only one of the corrosion reactions. Since we assume uniform metal dissolution across the electrode surface, Faraday's laws can be used to convert the corrosion current to the rate of weight loss (g/m$^2$) h or rate of penetration (mm/year).



The MIND-project has received funding from the European Union's Euratom research and training program (Horizon2020) under grant agreement 661880.

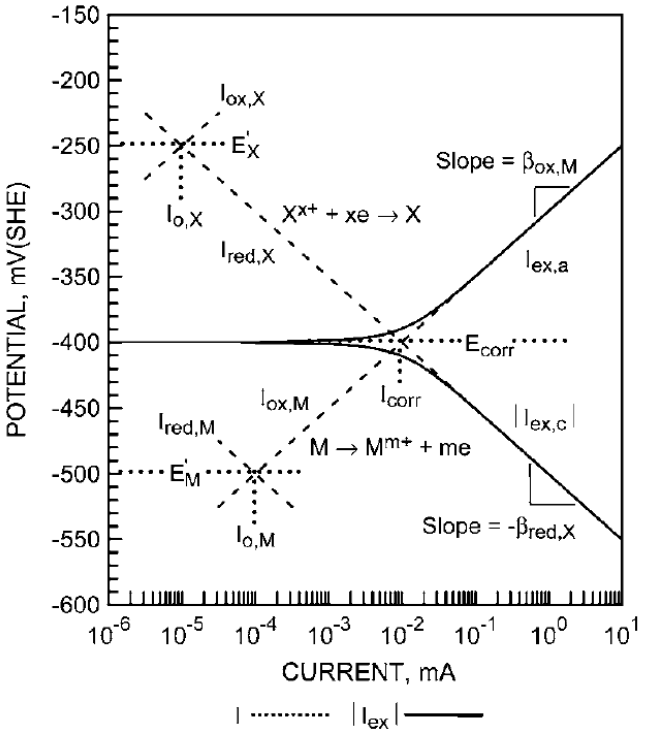


*Figure 8 Schematic experimental polarization curves (solid curves) assuming Tafel behavior for the individual oxidation and cathodic-reactant reduction polarization curves (dashed curves)[54]*

It is important to well-defined linear region (Tafel lines) for the correct interpretation. Two rules should be applied when the Tafel extrapolation is used. For an accurate extrapolation, at least one of branches of the polarization curve should exhibit Tafel behavior (i.e., linear on semilogarithmic scale) over at least one decade of current. In addition, the extrapolation should start at least 50 to 100 mV away from $E_{corr}$. There are several factors that can lead to non-Tafel behavior. For example, the diffusion limitations of a reaction, ohmic losses in a solution, the presence of oxidation reactions that are not metal dissolution and the effect of the buffer presence in a solution.

### 1.6.3 Weight loss analysis

Weight loss analysis is traditional method for measurement of the corrosion rate. The corrosion experiments typically require a time span of several months and involve vigorous cleaning and harsh chemicals to dissolve off the accumulated corrosion products.

A weighed sample (coupon) of the metal (or alloy under consideration) is introduced into the process, and later removed after a reasonable time interval. The coupon is then cleaned of all corrosion products and is reweighed. The weight loss is converted to a corrosion rate (CR), as follows:

$$Corrosion\ Rate(CR) = \frac{Weight\ loss\ (g) \cdot K}{Alloy\ Density\ \left(\frac{g}{cm^3}\right) \cdot ExposedArea\ (cm^2) \cdot Exposure\ Time\ (h)}$$

The constant K can differ to calculate the corrosion rate in various units. If the desired corrosion rate unit is millimeters/year (mmy), the K factor is $8.75 \cdot 10^4$.

The technique requires no complex equipment or procedures, merely an appropriately shaped sample, a carrier for the coupon (coupon holder), and a reliable means of removing corrosion product without disruption of the metal substrate. The method is applicable to all corrosive environments, and gives information on all forms of corrosion. Weight loss measurement is still the most widely used method of determining corrosion loss, despite being the oldest method currently in use.



The MIND-project has received funding from the European Union's Euratom research and training program (Horizon2020) under grant agreement 661880.

The method is commonly used as a calibration standard for other corrosion monitoring methods, such as linear polarization and polarization resistance. In instances where slow response and averaged data are acceptable, weight loss monitoring is the preferred technique [55].

### 1.6.4 SEM

Scanning electron microscopy (SEM) is a technique of major importance and is widely used throughout the scientific and technological communities, permits the observation and characterization of heterogeneous organic and inorganic materials on a nanometer (nm) to micrometer (μm) scale. The popularity of the SEM stems from its capability of obtaining three-dimensional-like images of the surfaces of a very wide range of materials [56]. SEM combines high-resolution imaging with a large depth of field, thanks to the short wavelengths of electrons and their ability to be focused using electrostatic and electromagnetic lenses. To begin with, a fundamental requirement of SEM is the need for high-vacuum conditions throughout the column, typically around $10^{-3}$–$10^{-5}$ Pa ($10^{-5}$–$10^{-7}$ torr), sometimes better, depending on the electron source (some sources, i.e. cold field emission, require ultra-high vacuum conditions on the order of $10^{-8}$ Pa; $10^{-10}$ torr), in order to minimize primary electron scattering and hence maintain a focused beam[56].

There are examples of successful results obtained with high-vacuum SEM using low beam energies and/or a backscattered electron (BSE) detector. Electrons forming the latter signal have relatively high energies and are therefore less sensitive to the electric fields that develop as a result of charge build up, compared to low-energy signal carriers such as secondary electrons [57]. Electrons can be extracted from various sources and driven by an electrical potential along an evacuated column. Electrons generated in this way are called primary electrons, and they can be formed into a finely focused beam and systematically scanned across a surface of interest. Those that are emitted can be collected and used to form an image, diffraction pattern or chemical spectrum [58].

In SEM, the principal electron signals that are used are backscattered electrons (BSEs) and secondary electrons (SEs) [59]. Differences in specimen composition and surface topography affect the generation, transport and escape of these signals. Images formed in an SEM result from variations in electron signal intensity collected at each point (pixel) as the electron beam briefly dwells within the scanned area [58]. Crucially, the size of features that can be resolved is primarily determined by the wavelength λ of the probing radiation: the shorter the wavelength, the smaller the feature that can be seen [56]. So, the shorter wavelength of electrons gives a distinct increase in achievable resolution compared to light. In fact, the resolution for the most advanced TEMs is better than 0.1 nm, enabling individual atoms to be seen. For modern SEM, the maximum resolution is better than 1 nm. This is mainly limited by the physics of electron–specimen interactions [13, 20].

SEM is a well-established basic method to observe the morphology of bacteria adhered on a material surfaces, the morphology of the material surface, and the relationships between [60]. SEM has been used for enumeration of adhered bacteria or tissue large number of samples. It is as a key technique that provides also information about the morphology of biofilm, presence of EPS and the nature of corrosion products (crystalline or amorphous). For the analysis of particles and rough specimens, have been adapted to the analysis of bulk biological and organic samples [61]. The method is based on the use of the ratio between the intensity of the characteristic and background x-rays defined as P/B, where P and B are measured at the same photon energy.

Biofilm morphology and mass are important characteristics that control the kinetics of substrate removal by biofilms. SEM is a powerful technique for revealing the fine structure of living systems and has been applied to biofilms [62]. It has also been of special importance in elucidating biofilm structure for understanding the physiology and ecology of these microbial systems [63]. Biofilm thickness is also especially important for calculation of heat exchange or diffusion rates of antimicrobials or nutrients through a biofilm and for evaluation of the mechanical properties of a biofilm [64].

In its current form, the SEM is both competitive with and complementary to the capabilities offered by other microscopes. It offers much of the same ease of use and image interpretation found


The MIND-project has received funding from the European Union's Euratom research and training program (Horizon2020) under grant agreement 661880.

in the conventional light microscope while providing an improved depth of field, higher magnification, analytical capabilities, and the benefits of image processing. The SEM is also capable of being used for quantitative chemical measurements in solid samples at the micrometer level. EDS and WDS detectors supply the necessary x-ray data. Better spatial resolution approaching the nanometer level can be obtained with the analytical electron microscope, but this capability requires preparing electron-transparent samples [15, 18, 19]. Scanning electron microscopy is a key tool to study the effect of physicochemical properties on adhesion phenomena (pH, roughness, topography, temperature, etc.). SEM plays also a paramount role for assessing the microbial populations, three-dimensional structure, physiology, thickness, etc. SEM proved to be an invaluable method for ultra-structural investigation, allowing imaging of the overall appearance and/or specific features of biofilms formed in different environments, e.g. microbial colonies, individual cells and the presence of inorganic products within the biofilm [65].

### 1.6.5 Raman spectroscopy

Raman spectroscopy is the spectroscopic non-destructive technique used to provide information on molecular vibrations and crystal structures. It can be both for qualitative and quantitative analysis. This method uses a laser light source to irradiate a sample and generates an infinitesimal amount of Raman scattered light. After filtering Rayleigh scattering the Raman spectrum is detected using a CCD camera [66]. The identification features of this method are comparable to Infrared (IR) spectroscopy. Raman and IR spectra are complementary. The characteristic fingerprinting pattern in a Raman spectrum makes it possible to identify substances including polymorphs and evaluate local crystallinity, orientation and stress. Since the discovery of the Raman effect in 1928 by C.V. Raman and K.S. Krishnan, Raman spectroscopy has become an established as well as a practical method of chemical analysis and characterization applicable to many different chemical species [67].

Raman spectroscopy is a technique well suited for the characterization of various oxides and (oxy)hydroxides involved in the corrosion of iron [4, 68]. Therefore, it can be used to identify and localize the phases considered as active in corrosion processes. Also, it offers many advantages which make it very suitable for this purpose. First, the Raman bands usually have narrower bandwidths and are therefore more characteristic and helpful in the analysis of mixtures. Second, sample preparation is minimal, commonly none is required.

Iron oxides and (oxy)hydroxides are sensitive to thermal transformations even at low laser power because they are opaque to visible light and heat up. In fact, temperature rise induces a transformation to the most stable phase, i.e. hematite (α-Fe2O3) [69]. Therefore, for some iron oxides highly sensitive to laser irradiation is usually used a set of density filters to modulate the laser power and avoid any thermal effect on iron (III) compounds [69, 70].

In addition, when Raman spectroscopy is used supported with other techniques, such as the Scanning Electron Microscopy (SEM), a deeper analysis can be performed, based on corrosion products and the morphology of the rust layer, to explain the corrosion behavior of carbon steel [71].

### 1.6.6 Molecular biology analysis (qPCR and DNA sequencing)

In the field of molecular biology, polymerase chain reaction (PCR) is very powerful tool. Specific sequences of DNA template can be amplified or copied using sequence specific oligonucleotides, heat stable DNA polymerase and thermal cycling. PCR is the exponential amplification of DNA based on principle of enzymatic replication which subsequently doubles the number of target molecules with each cycle of amplification. Furthermore, quantitative polymerase chain reactions (qPCR) quantitatively measure the amplification of DNA using fluorescent dyes. qPCR is also known as real-time polymerase chain reaction as this technology measures the amount of DNA after each cycle by means of fluorescent dyes which yield by increasing the fluorescent signal in the direction proportion to the number of PCR copies. Moreover, it helps to monitor the reaction in real time as it occurs and also measures the amount of amplicon precisely at each cycle to achieve accurate quantification of the amount of starting material in the sample. qPCR analysis helps to detect the presence of specific genes


The MIND-project has received funding from the European Union's Euratom research and training program (Horizon2020) under grant agreement 661880.

present in the sample [72]. This technique is more precise and sensitive. Thus, to determine the relative abundance of bacteria, quantitative PCR was employed. Bacterial biomass was quantified using a specific functional gene marker.

Sequencing of genomic DNA is another powerful technique of molecular biology. Next generation sequencing (NGS) is an advanced tool of sequencing method widely used. Library preparation of NGS involves collection of DNA fragments of similar size with known adaptor sequences added to 5' and 3' ends. Library preparation is the most significant step of sequencing technology and is done by the PCR amplification of genomic DNA. Sequencing of bacterial DNA helps to describe composition of bacterial community present in the sample. The NGS platform used for the sequencing in this study is Ion Torrent Personal Genome Machine (PGM, ThermoFisher Scientific).

Ion Torrent PGM sequences the DNA using a semiconductor chip. The chip possesses millions of wells and these wells are responsible for capturing the chemical information resulted from sequencing of DNA and hence, translated into digital information. In this method, hydrogen ion is released when a right nucleotide is incorporated in single strand DNA. Subsequently, the release of hydrogen ion influences the pH of the solution in the well. Therefore, the ion sensitive layers located just beneath the well measure and detect the change in pH and then convert in to voltage. Finally, the change occurred in voltage is recorded highlighting the incorporation of nucleotide and thus the base is coded. In this way, the process of incorporation of nucleotide and change in pH repeated for every 15 second with different nucleotide washing up the chip simultaneously in all well. The raw data obtained from the sequencing should be processed by bioinformatician to prepare it for further interpretation.

## 1.7 Aims of the study

In this report, anaerobic MIC of canister material (12020 carbon steel and 316 L stainless steel) in environments containing natural microbial community dominated by SRB was studied to improve our understanding of the effect of microbiological processes in relation to the repository environment. The experiments were performed under anaerobic conditions (oxygen concentration < 1 ppm volume) in parallel arrangements including sterile controls, and no nutrients were added.

We aimed to describe MIC of the first material, carbon steel, in two different environments during long-term exposure. First, a natural granite underground water (Josef URC, VITA source) containing microbial community dominated by SRB, and second, the synthetic bentonite pore water inoculated with the same VITA water (in the ratio 9:1) were used for the experiments. In the first experiment inoculated with VITA water, the objective was to distinguish the effect of higher temperature (laboratory temperature and 35 °C) on MIC. The corrosion behavior of carbon steel was investigated by electrochemical impedance spectroscopy, weight loss method, potentiodynamic polarization measurements and open circuit potential. The morphology of the carbon steel surface after exposure was investigated using SEM-EDS and characterized by Raman spectroscopy. In order to determine the proliferation of relevant bacterial groups in water as well as biofilm samples, the molecular-biological approach was used (specifically qPCR and 16S rDNA amplicon sequencing).

Experiment with stainless steel was designed to gain better understanding of the influence of natural microbial community dominated by SRB together (Josef URC, source HV1) with the oxygen on the passivation stability of stainless steel.


The MIND-project has received funding from the European Union's Euratom research and training program (Horizon2020) under grant agreement 661880.

# 2 Methods

## 2.1 Experimental design

All samples, measuring cells and instruments were surface-disinfected using ethanol before placing in the glove box with Ar atmosphere. The thermally resistant parts of the experimental equipment (laboratory glassware, trays, etc.) were sterilized at 160 ° C for two hours. The internal working surface of the Argon-purged glove box was disinfected with ethanol and sterilized with UV-C lamp (wavelength 253.7 nm, power 15W, NEXA s.r.o., Slovakia) for 3 hours.

The summary of the experiments is shown in the Table 4. For each experiment, two parallel arrangements were established, one a sterile control and second non-sterile condition. A sterile control was obtained through sterile filtration of the same ground water through a membrane filter with a pore size of 0.22 µm or UV-C sterilizer (in the experiment A).

All the solutions used were deaerated with argon gas (Argon 4.8) in an Argon-purged glove box, where is gaseous oxygen concentration < 1 ppm volume to achieve the reducing condition. The final residual concentration after deaeration of the solution is below the limit of determination of the external oxygen sensor FDO® 925 (WTW, Germany). Only in the experiment A was carried out deaeration during corrosion experiment. The initial concentration of dissolved oxygen was in a non-sterile solution 0,9 mg/l and 5,1 mg/l in a sterile solution.

*Table 4 The detailed summary of the experiments*

| Mark | Type of sample | Environment | Temperature | Duration |
|---|---|---|---|---|
| A | Stainless steel 316 L | HV1 water | $T_{lab.}$ | 111 days |
| B | Carbon steel 12020 | VITA water | $T_{lab.}$ | 240 days |
| C | Carbon steel 12020 | VITA water | 35°C | 293 days |
| D | Carbon steel 12020 | SBPOW inoculated with VITA | $T_{lab.}$ | 2 years |

## 2.2 Media

Natural groundwater was collected from a depth of approximately 100 m from the VITA source and HV1 source at the Josef URC (the Czech Republic; chemical composition provided in Table 5). The water is naturally anaerobic and contains a microbial consortium dominated by SRB.

Synthetic bentonite pore water (SBPOW; chemical composition provided in Table 6) was prepared is based on a proposal for bentonite pore water in equilibrium with bentonite (bentonite "BaM"), referred to chemical analysis the bentonite pore water purging with argon and mixture at laboratory temperature. Preparation of the non-sterile SBPOW was done by inoculation with VITA water in a ratio of 9:1.


The MIND-project has received funding from the European Union's Euratom research and training program (Horizon2020) under grant agreement 661880.

*Table 5 Analysis of the natural ground water from sources HV1 and VITA used in these experiments*

| Analyte | Concentration [mg·l$^{-1}$] | | Limit of quantification |
|---|---|---|---|
| | HV1 | VITA | |
| $Mg^{2+}$ | 12,6 | 12,6 | < 0,1 |
| $Ca^{2+}$ | 60 | 60 | < 0,1 |
| $Na^{+}$ | 54,7 | 54,7 | < 1 |
| $K^{+}$ | 1,79 | 1,79 | < 0,1 |
| $Fe^{2+}$ | 1,01 | 1,01 | < 0,02 |
| $Mn^{2+}$ | 0,11 | 0,11 | < 0,005 |
| $Cr^{3+}$ | < 0,005 | < 0,005 | < 0,005 |
| TOC | 97 | 97 | < 1 |
| $NH_4^{+}$ | < 0,05 | < 0,05 | < 0,05 |
| $Cl^{-}$ | 16,6 | 16,6 | < 2 |
| $NO_2^{-}$ | < 0,05 | < 0,05 | < 0,05 |
| $NO_3^{-}$ | < 2 | < 2 | < 2 |
| $SO_4^{2-}$ | 56,4 | 56,4 | < 10 |
| $PO_4^{3-}$ | 1 | 1 | < 0,05 |
| $F^{-}$ | < 0,05 | < 0,05 | < 0,05 |
| $H_2S$ | 0,08 | 0,08 | < 0,01 |
| Parameter | Value | | |
| Conductivity [µS·cm$^{-1}$] | 667 | 632 | |
| pH | 7,6 | 7,867 | |

*Table 6 Compositon of the Synthetic bentonite pore water used in experiments*

| SBPOW | |
|---|---|
| Component | Content [g.dm$^3$] |
| $MgSO_4 \cdot 7H_2O$ | 2,7279 |
| $NaNO_3$ | 0,8163 |
| NaCl | 0,4191 |
| $KNO_3$ | 0,1328 |
| $Na_2SO_4$ | 0,1462 |
| $KHCO_3$ | 0,1066 |
| $CaCl_2$ | 0,0388 |
| Parameter | Value |
| Conductivity [mS·cm$^{-1}$] | 3800 |
| pH | 8,3 |


The MIND-project has received funding from the European Union's Euratom research and training program (Horizon2020) under grant agreement 661880.

## 2.3 Specimen preparation

Commercial 316 L stainless steel and C15E carbon steel (CSN 12020) were used in this study. The chemical composition of these materials in weight percent is described in Table 7.

*Table 7 Composition of materials used in the experiments*

| | C(%) | Si(%) | Mn(%) | P(%) | S(%) | Cr(%) | Ni(%) | Mo(%) | N(%) |
|---|---|---|---|---|---|---|---|---|---|
| Type 316L | 0,021 | 0,69 | 1,77 | 0,034 | < 0,001 | 16,9 | 10,1 | 20,02 | 0,044 |
| Type C15E | 0,15 | 0,256 | 0,58 | 0,006 | 0,029 | - | - | - | - |

The surface of the specimens was mechanically polished with P500 silicon carbide grinding paper under atmospheric conditions and then in an Argon-purged glove box, following which the specimens were cleaned with de-aerated ethanol. The test specimens for electrochemical experiments, measuring 15 mm in diameter and 3 mm thick in form of the carbon steel and 15 mm in diameter and 1,5 mm thick in form of the stainless steel. The cylindrical carbon steel samples of diameter 10 mm and length 50 mm were used for investigation of weight loss.

## 2.4 Weight loss measurement

The cylindrical carbon steel 12020 samples were used for investigation of mass losses and half of the disc for surface analysis. The experiment was performed in the inoculated bentonite pore water with VITA water in a ratio of 9:1 and sterile bentonite pore water as a negative control (Figure 9). The total volume of each solution was 2 L. The experiment was scheduled for 24 months with the sampling time after 3, 6, 12, 18 and 24 months and last collection will be carried out in January 2019. The corrosion experiment was carried out in an Argon-purged glove box (gaseous oxygen concentration < 1 ppm volume) at laboratory temperature. The corrosion rate was performed by the weight loss measurement according to norms CSN ISO 8407[73], CSN EN ISO 9226[74].

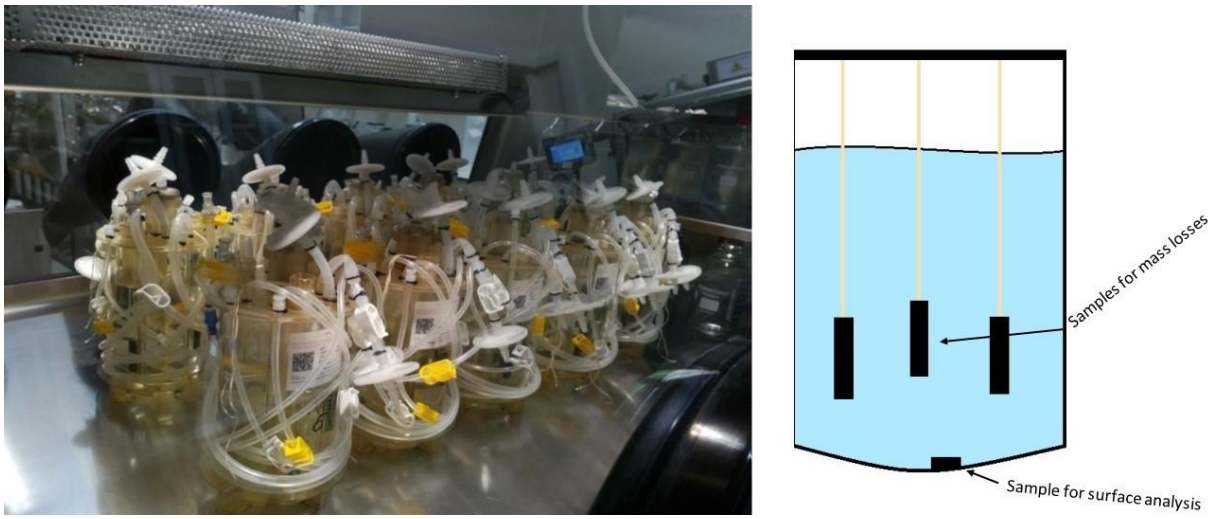


*Figure 9 Design experiment of weight loss exp.*

## 2.5 Electrochemical measurements

Electrochemical measurements were performed with a three-electrode system (Figure 10), was designed using a saturated calomel electrode and two graphite rods as reference and auxiliary



The MIND-project has received funding from the European Union's Euratom research and training program (Horizon2020) under grant agreement 661880.

electrodes by the Gamry Reference 600 potentiostat/galvanostat/ZRA (GAMRY, USA). The working electrode holder had an exposed metal surface area of 1 $cm^2$. EIS measurements were performed with a sinusoidal signal of 10 mV amplitude over a frequency range of 100 kHz – 5 mHz at the corrosion potential (or OCP - open circuit potential). Later the steady-state condition of the corrosion potential allowed to measure of impedance spectrum at low frequencies up to tens of units of µHz. discrete corrosion potential values were obtained before each EIS measurement after steadying of the OCP. The potentiodynamic anodic polarization curves were conducted using a scan rate of 0,1 mV $s^{-1}$ from -100 mV to 600 mV vs OPC and measured after 16 hours of the exposure. The measurement was carried out in an Argon-purged glove box (gaseous oxygen concentration < 1 ppm volume). Analysis of impedance spectra and polarisation curves were performed using ZSimpWin 3.50 software and Gamry Echem Analyst 6.24. The experiment at 35 ° C was controlled by an external sensor (Pt1000 sensor placed in a glass case) using the Heidolph ™ Heat-On Blocks heating system (Heidoph, Germany).

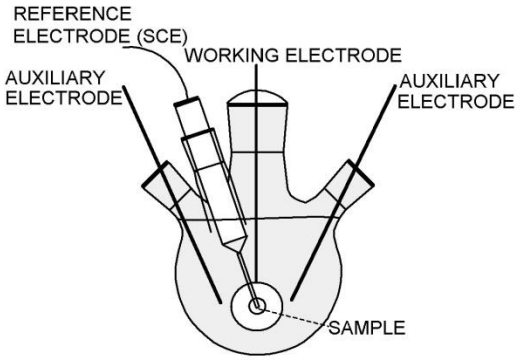


*Figure 10 Design of experimental corrosion cell*

## 2.6 Surface analysis

### 2.6.1 Scanning Electron Microscopy

The steel specimen's surface was examined at the end of the exposure using a LYRA3 scanning electron microscope (Tescan, Czech Republic). Changes in surface morphology were observed with secondary electron detectors (SE and In-beam SE mode) and back-scattered electrons (In-beam BSE mode) at 5 kV accelerating voltage. Energy dispersive X-ray spectroscopy (EDS) was used to determine local chemical composition using unprepared samples. Subsequently, the samples were modified by pouring into polyacrylic resin, then cutting and polishing, and the carbon sputtered with a thickness of 10 nm to provide charging reduction. Cross-section analysis was then performed at 20 kV accelerating voltage.

### 2.6.2 Raman spectroscopy

Raman analysis was performed by micro-Raman spectrometer (DXR2xi, Thermo Scientific, US) with 532 nm laser line coupled with an optical microscope using a 10x magnification objective lens. The power of the laser was 0,5 mW in order to minimize possible phase transition of corrosion products.

## 2.7 Molecular biological techniques

### 2.1.7 DNA extraction and measurement

Bacterial biomass from the water sample was concentrated by using a 0.22 µm GV Durapore® filter membrane through filtration. The membrane filter containing bacterial biomass after filtration



The MIND-project has received funding from the European Union's Euratom research and training program (Horizon2020) under grant agreement 661880.

were stored under -80°C until the DNA extraction. Bacterial DNA from water sample and biofilm were isolated according to the manufacturer instruction using a commercial kit, Power water DNA isolation kit, catalogue number: 14900-50-NF (MO BIO). Quantification of extracted genomic DNA was performed by using a Qubit 2.0 fluorometer (Life Technologies, USA). It uses fluorescent dyes to determine the concentration of nucleic acids.

### 2.7.8 Quantitative polymerase chain reaction (qPCR):

16S rDNA gene was used using primer 16S rRNA to monitor the total changes in bacterial biomass [75]. Likewise, a functional bio-marker genes apsA and dsrA [76] were used for the detection of SRB. These specific primers apsA and dsrA, encode for α sub-unit of adenosine 5' phosphosulphate (APS) reductase and dissimilatory sulphite reductase (DSR) enzymes of SRB, respectively. In the same way, nirK, nirS and nos Z genes[77] were used as a functional marker for identification of denitrifying bacteria. Additionally, genes nirK and nirS encodes nitrite reductase which is the major enzyme of the denitrification process and nosZ encodes catalytic subunit of the nitrous oxide reductase. Similarly, 16S rRNA gene was amplified using specific primers for the identification of family of iron reducing bacteria (IRB), *Geobacteraceae* [78]. Quantitative PCR was performed on a Light cycler® 480 (Roche, Switzerland).

Reaction mixtures were prepared in 10 µl of reaction volume. The mixture contained 2 µl of DNA template, 5 µl KAPA SYBER FASTqPCR kit (Kapa Biosystems. Inc., MA, USA), 0.4 µl of µM forward and reverse primer mixtures (Generi Biotech, Czech Republic, IDT, US) and 2.6 µl ultra-pure water (Bioline, UK). For each DNA sample, reaction was performed in duplicate along with negative control which consists of nuclease free water instead of DNA template. Reaction conditions consisted of an initial 5 min incubation at 95 °C, followed by 45 cycles of denaturation at 95°C for 10 s, annealing at 60 °C for all primer except for *Geobacteraceae* which was 55°C for 15 s and extension 72 °C for 20 s with final extension at 72°C for 3 min. Finally, a melting curve was set for 5 s at 95°C, 1 min at 65°C and final ranging from 60 to 98°C, with a temperature gradient of 40°C per 10 s. Purity of the amplified fragment was determined through observation of a single melting peak. Crossing point values were obtained using the 'second derivative maximum' method included in the LightCycler® 480 Software. The method uses different amplification efficiencies for each primer, determined by measuring the slope of curves constructed from a serial dilution of template DNA from five internal environmental standards. During the evaluation process, a water sample was normalised to dilution and the total amount of DNA extracted. The relative abundance of the bacterial 16S rDNA gene and functional genes was calculated and expressed as a fold change between two states (at a given sampling time and at an initial time) using the delta Cqp method. Based on the approach used, it is necessary to consider each molecular biological marker separately and observe the trends in relative abundance over time.

### 2.7.9 Library preparation

Two consecutive PCR reactions per sample were performed with the use of normal and bar code fusion primers for the library preparation. Primers 530F [79] and 802R [80] were used for amplification of variable V4 region of 16S rDNA gene for sequencing of amplicons. Moreover, the size of the amplicon was kept below 400 bp to cover as much microbial diversity as possible by performing In silico analysis of primers [72].

The PCR conditions for the first PCR were as follows: 95°C for 3 min; 15 cycles at 98 °C for 20 s, 50 °C for 15 s and 72 °C for 45 s; and a final extension at 72 °C for 1 min. The second PCR was performed as follow: 95 °C for 3 min; 35 cycles at 98 °C for 20 s, 50 °C for 15 s and 72 °C for 45 s; with a final extension at 72 °C for 1 min. The quality of the library product was checked by gel-electrophoresis technology. Additionally, the PCR products were purified using the Agencourt Ampure XP system (Beckman Coulter, Brea, USA), and the concentration of the purified PCR products was measured with a Qubit 2.0 fluorimeter (Life Technologies, USA). Then, the barcode-tagged amplicons from different samples were mixed in equimolar concentrations. Sequencing of the amplicons was


The MIND-project has received funding from the European Union's Euratom research and training program (Horizon2020) under grant agreement 661880.

performed on an Ion Torrent PGM using the Ion PGM Hi-Q Sequencing Kit with the Ion 314 Chip following the manufacturer's instructions (Thermo Fisher Scientific).

### 2.1.10. Data processing

Raw reads were split to particular samples by Mothur software [81]. Poor quality reads were trimmed and filtered. Similarly, chimeric sequences were detected using UCHIME [82] and then removed. Silva database version 123 with a bootstrap value set at 80% was used for the classification of the sequences. For clustering of the sequences into operational taxonomic units (OTUs), cut-off value of 97% was employed. Cluster analysis was performed by the use of Vegan package in the R statistical package [83]. Taxa with greater than 1% abundance were visualized as heat map and remaining visualized in graph as unclassified for the microbial analysis of biocorrosion of carbon steel 12020 using VITA water for 240 days at laboratory condition. Similarly, for the investigation of shift in microbial community from the long-term biocorrosion of carbon steel 12020 using synthetic water inoculated with VITA water, DADA2 software package [84] was used for the subsequent processing of the split samples from the raw reads. Taxonomy classification by DADA2 used SILVA database (version 13, www.arb-silva.de).

Accuracy of classification was verified and evaluated against a predefined artificial MOCK community sample created from 4 different taxa up; particularly *Enterococcus*, *Bacillus, Klebsiella* and *Staphylococcus*. Subsequent analyses were performed in R software using Phyloseq library [85].


The MIND-project has received funding from the European Union's Euratom research and training program (Horizon2020) under grant agreement 661880.

# 3 Results a discussion

## 3.1 Corrosion

### 3.1.1 Open circuit potential

The open circuit potential values obtained before the EIS measurements of individual experiments (Table 4), are shown in the Figure 11. In the case of the experiments with carbon steel, we observed the potential shift in the anodic area, indicating the presence of microorganisms on the sample surface. A sharp drops in potential towards the cathodic region suggest local damage of the biofilm coverage (e.g. due the growth of crystals on the surface). On the contrary, it is in stainless steel, the presence of microorganisms decreased the corrosion potential and the corrosion products maintained compact characteristics due to steady potential without a greater tendency to fluctuations.

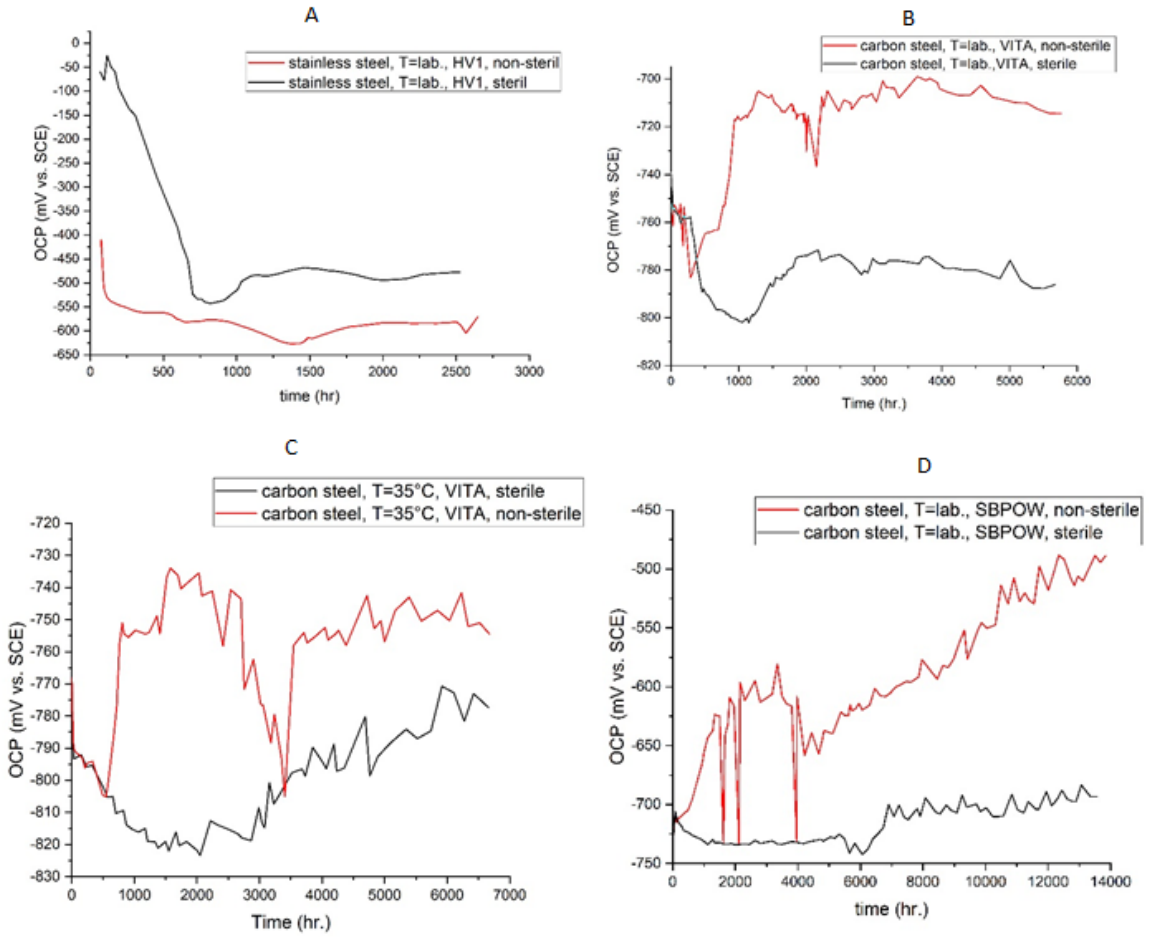


*Figure 11 OPC measurement of the experiments*

### 3.1.2 Polarization curve

The Tafel plots obtained for experiments listed in the Table 4 are shown in Figure 12. The corrosion potential ($E_{corr}$), the corrosion current density ($i_{corr}$) are deduced from the Tafel (log i vs. E) plots representing anodic polarization curve. The results of polarization experiments (Table 8) show that short-term measurements after 16 hours represent small differences to determine the characteristic contrast between the abiotic and biotic systems of the natural microbial community, contra the long-term experiments. These small differences in short-term experiments are due to the use of natural microbial communities instead of the use single bacterial strains.



The MIND-project has received funding from the European Union's Euratom research and training program (Horizon2020) under grant agreement 661880.

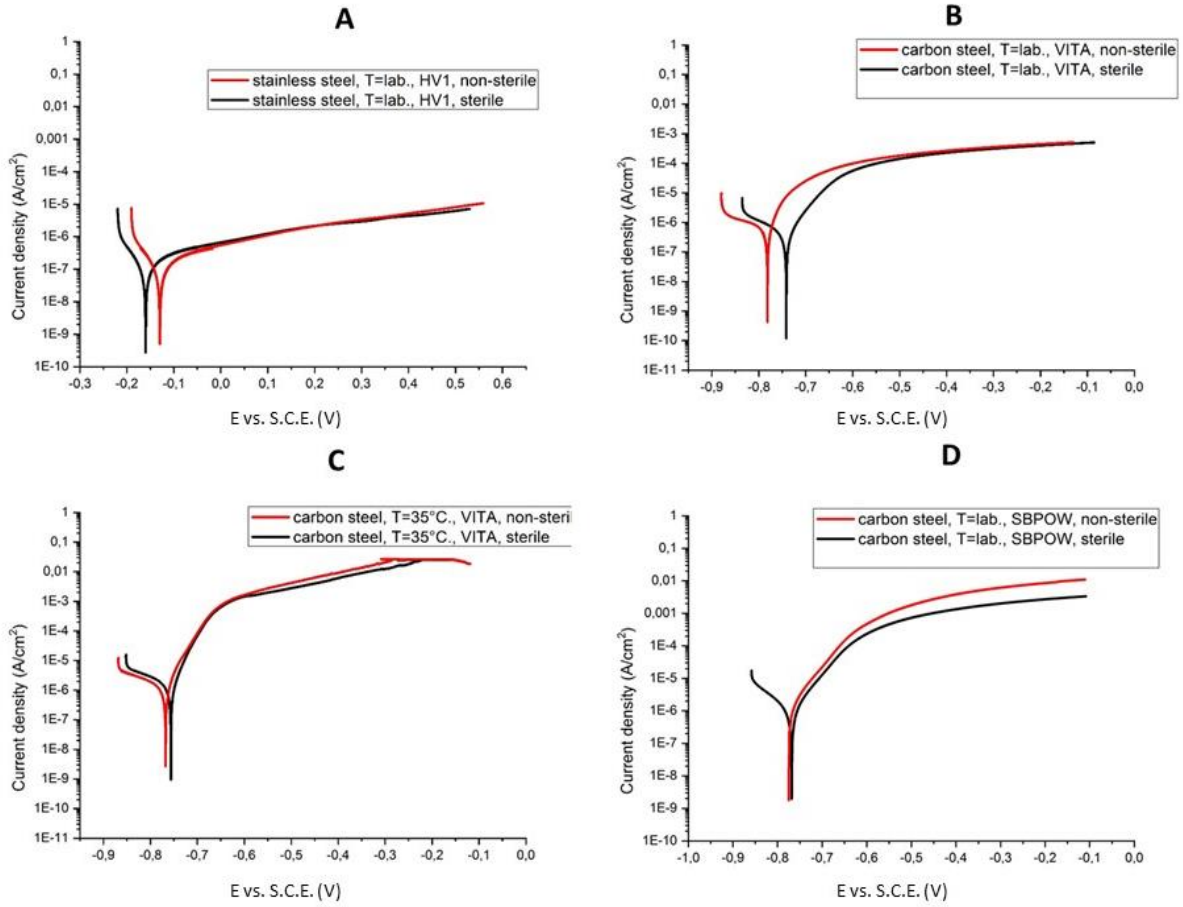


*Figure 12 The Tafel plots for the experiments with stainless steel (A) and carbon steel (B, C, D) exposed to sterile and non-sterile natural granite water (HV1, VITA) and synthetic bentonite pore water (SBPOW).*

Comparing values $I_{corr}$ of the environment of SBPOW and natural granite water shows more aggressive environments of SBPOW solution. All data shows, that the rate of dissolution of the carbon steel and stainless steel was controlled by the diffusion of species through corrosion products film at high anodic overpotentials. Anodic Tafel slope of carbon steel shows metal dissolution reactions from active surfaces after a 16 hour exposure. In case of the carbon steel specimen under sterile condition at laboratory temperature in VITA water exhibited an anodic Tafel slope of 59 mV/decade after a 16 hour exposure. This value is in good agreement with data in the literature representing the anodic dissolution reaction ($Fe = Fe^{2+} + 2e^-$) at 25°C.

*Table 8 The results from polarization experiments show small differences in short-term measurements after 16 hours*

| Mark | Experiment | βa (mV/decade) | βc (mV /decade) | $E_{corr}$ vs. SCE (mV) | $I_{corr}$ (A cm2) | B (mV) |
|---|---|---|---|---|---|---|
| A | Stainless steel, T=lab.,HV1,non-sterlile | 326 | | -130 | 2,18E-07 | 142 |
| | Stainless steel, T=lab.,HV1, sterlile | 381 | | -160 | 2,51E-07 | 165 |
| B | Carbon steel,T=lab., VITA, non-sterile | 42 | - | -780 | 9,53E-07 | 18 |
| | Carbon steel,T=lab., VITA, sterile | 59 | - | -741 | 5,86E-07 | 26 |
| C | Carbon steel, T=35°C, VITA, non-sterile | 40 | | -768 | 1,76E-06 | 17 |
| | Carbon steel, T=35°C, VITA, sterile | 36 | | -756 | 1,72E-06 | 16 |
| D | Carbon steel, T=lab., SBPOW, non-sterile | 61 | - | -775 | 1,33E-06 | 27 |
| | Carbon steel, T=lab.,SBPOW, sterile | 66 | - | -768 | 1,25E-06 | 29 |



The MIND-project has received funding from the European Union's Euratom research and training program (Horizon2020) under grant agreement 661880.

The linear anodic Tafel slopes of stainless steel are more than 300 mV/dec. indicating that the anodic oxidation reactions are under diffusion control for sterile and non-sterile solution.

### 3.1.3 Electrochemical impedance spectroscopy

#### *Stainless steel in natural granite water (source HV1) under laboratory temperature (Experiment A)*

The time evolution of the Bode plot of electrochemical impedance spectra of stainless steel under sterile and non-sterile conditions in natural granite water (source HV1) at laboratory temperature is shown in Figure 13. The deaeration process was ongoing during EIS measurement with different concentration of oxygen at the beginning (concentration of dissolved oxygen was in a non-sterile solution 0,9 mg/l and 5,1 mg/l in a sterile solution).

Initial EIS data of deaeration process in the sterile environment with a higher oxygen concentration were modelled in the circuit description code by the equivalent circuit $R_1(R_2Q_1)(R_3Q_2)$, where $R_1$ is the solution resistance, $R_2$ is the polarization resistance, $Q_1$ is the dispersive double layer capacitance, $R_3$ is resistance of the passive film and $Q_2$ is dispersive capacitance of the passive film. The equivalent circuit $R_1(R_2Q_1)$ was used after the gradual disappearance of the high-frequency time constant during the first 453 hours. During the initial exposure, the values of the modulus of impedance decrease due to the degradation of the passive film, which was able to create at higher concentration of oxygen. The shift of the low-frequency time constant is associated with the corrosion rate and the development of the electric double layer over time. In the non-sterile environment with low oxygen concentration only one time constant was observed during the ongoing experiment. The time evolution of EIS data reveal the absence of passive film produced in the non-sterile environment. EIS spectra remained relatively the same over time.

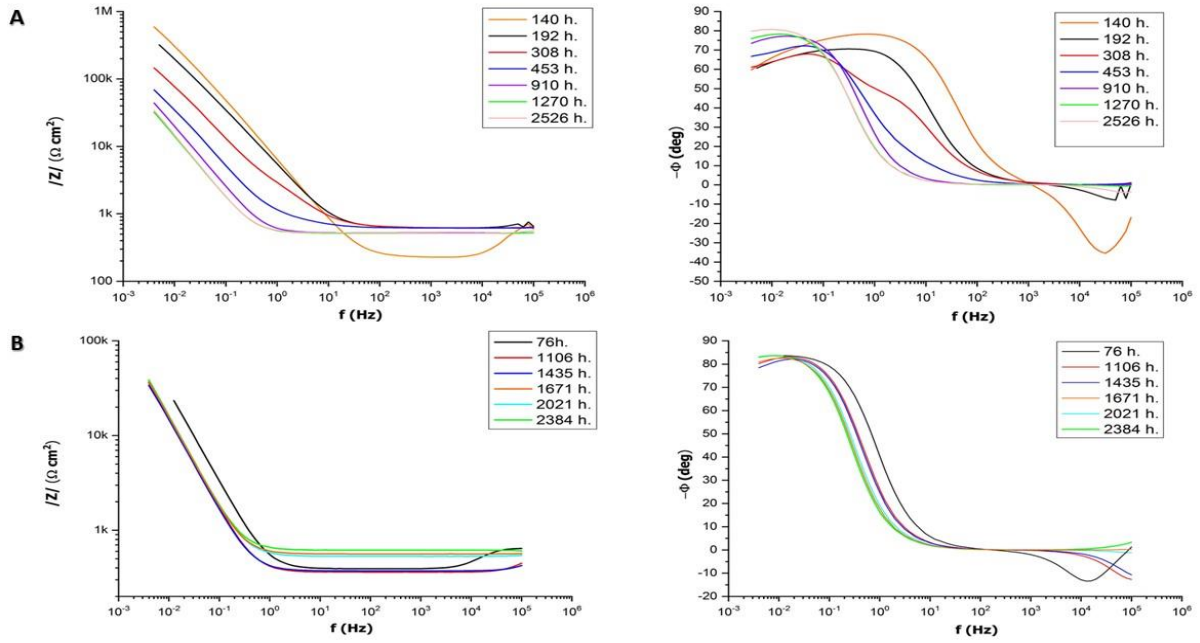


*Figure 13 The time evolution of the Bode plot of EIS of the experiment A under sterile (A) and non-sterile conditions (B) in natural granite water (HV1)*

The natural microbial consortium attached to the stainless steel specimen without forming continuous biofilms explain the absence of a second time constant regarding biofilm formation during whole exposure. This observation is connected with oligodynamic effect and reduced bacterial adhesion due to action of traces of metal ions liberated from the metal surface upon reduction conditions [86].



The MIND-project has received funding from the European Union's Euratom research and training program (Horizon2020) under grant agreement 661880.

Table 9 and Table 10 show the results of EIS measurements performed under sterile and nonsterile conditions at selected exposure times. The accuracy of approximation of experimental data by the equivalent circuits ($\chi^2$) reached similar values in in sterile and non-sterile environments. It ranged in the order of $10^{-4}$ to $10^{-5}$.

*Table 9 The EIS results of exp. A under sterile condition*

| Element → | $R_1$ | $Q_1$ | $n_1$ | $R_2$ | $Q_2$ | $n_2$ | $R_3$ |
|---|---|---|---|---|---|---|---|
| Time (h) ↓ | [Ohm·cm$^2$] | [$\Omega^{-1}s^{-n}cm^{-2}$] | | [Ohm·cm$^2$] | [$\Omega^{-1}s^{-n}cm^{-2}$] | | [Ohm·cm$^2$] |
| 67 | 207 | 8,861E-05 | 0,9219 | 2,2E+06 | 8,86E-05 | 0,9014 | 73520 |
| 96 | 194 | 9,261E-05 | 0,8897 | 1,8E+06 | 4,89E-05 | 0,9135 | 56000 |
| 169 | 616 | 9,497E-05 | 0,8662 | 1,7E+06 | 4,73E-05 | 0,8994 | 58620 |
| 193 | 622 | 5,595E-05 | 0,8356 | 1,2E+06 | 5,60E-05 | 0,8615 | 22320 |
| 453 | 617 | 3,031E-04 | 0,8742 | 3,2E+05 | 3,25E-04 | 0,8126 | 189 |
| 1007 | 525 | 7,306E-04 | 0,9269 | 2,3E+05 | | | |
| 1500 | 480 | 9,471E-04 | 0,9402 | 2,5E+05 | | | |
| 1704 | 477 | 9,428E-04 | 0,9432 | 3,0E+05 | | | |
| 2013 | 498 | 9,403E-04 | 0,9447 | 3,5E+05 | | | |
| 2281 | 513 | 9,326E-04 | 0,9454 | 3,8E+05 | | | |
| 2526 | 522 | 9,260E-04 | 0,9451 | 4,0E+05 | | | |

*Table 10 Results of EIS measurements performed under non-sterile conditions*

| Element → | $R_1$ | $Q_1$ | $n_1$ | $R_2$ |
|---|---|---|---|---|
| Time (h) ↓ | [Ohm·cm$^2$] | [$\Omega^{-1}s^{-n}cm^{-2}$] | | [Ohm·cm$^2$] |
| 76 | 393 | 4,79E-04 | 0,9539 | 1,02E+06 |
| 88 | 395 | 5,19E-04 | 0,9529 | 8,89E+05 |
| 366 | 378 | 7,42E-04 | 0,9423 | 3,59E+05 |
| 564 | 382 | 8,63E-04 | 0,9521 | 3,52E+05 |
| 1106 | 363 | 9,32E-04 | 0,9614 | 3,55E+05 |
| 1435 | 373 | 9,70E-04 | 0,9600 | 2,52E+05 |
| 1671 | 563 | 9,29E-04 | 0,9656 | 4,02E+05 |
| 2021 | 533 | 9,01E-04 | 0,9653 | 7,00E+05 |
| 2384 | 619 | 9,10E-04 | 0,9678 | 7,14E+05 |
| 2566 | 850 | 9,15E-04 | 0,9662 | 5,62E+05 |

Polarization resistance time dependence under sterile and non-sterile conditions shows Figure 14. Polarization resistance under sterile and nonsterile condition was used to calculate the percentage inhibition efficiency. Inhibitory efficiency of microbial consortium containing SRB in natural granite water (source HV1) for stainless steel was 29 % at the end of the experiment.



The MIND-project has received funding from the European Union's Euratom research and training program (Horizon2020) under grant agreement 661880.

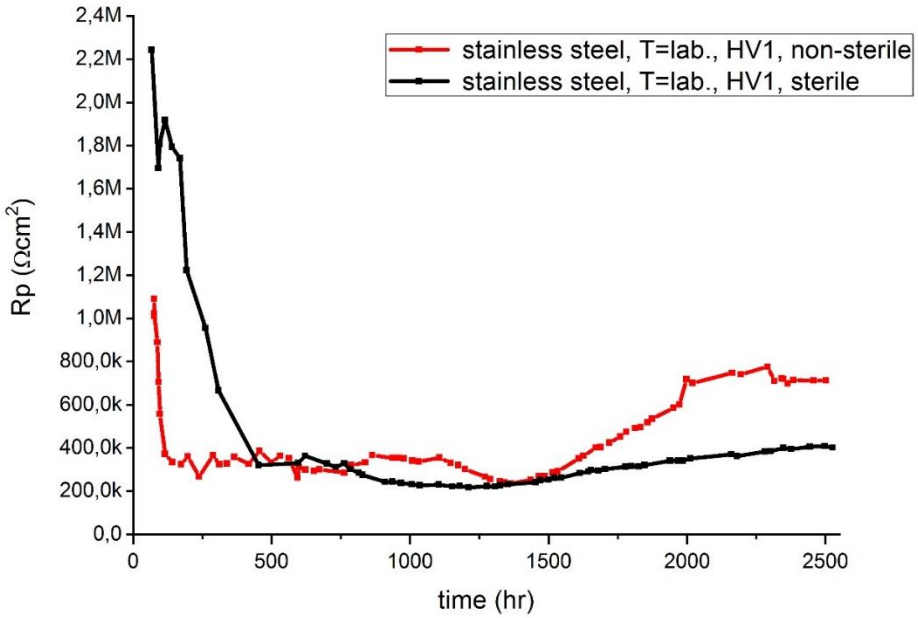


*Figure 14 Time evolution of polarisation resistance of stainless steel at laboratory temperature*

### *Carbon steel in natural granite water (source VITA) under laboratory temperature (Experiment B)*

The time evolution of impedance spectra, measured under sterile and non-sterile conditions, are provided as Bode representations in Figure 15.

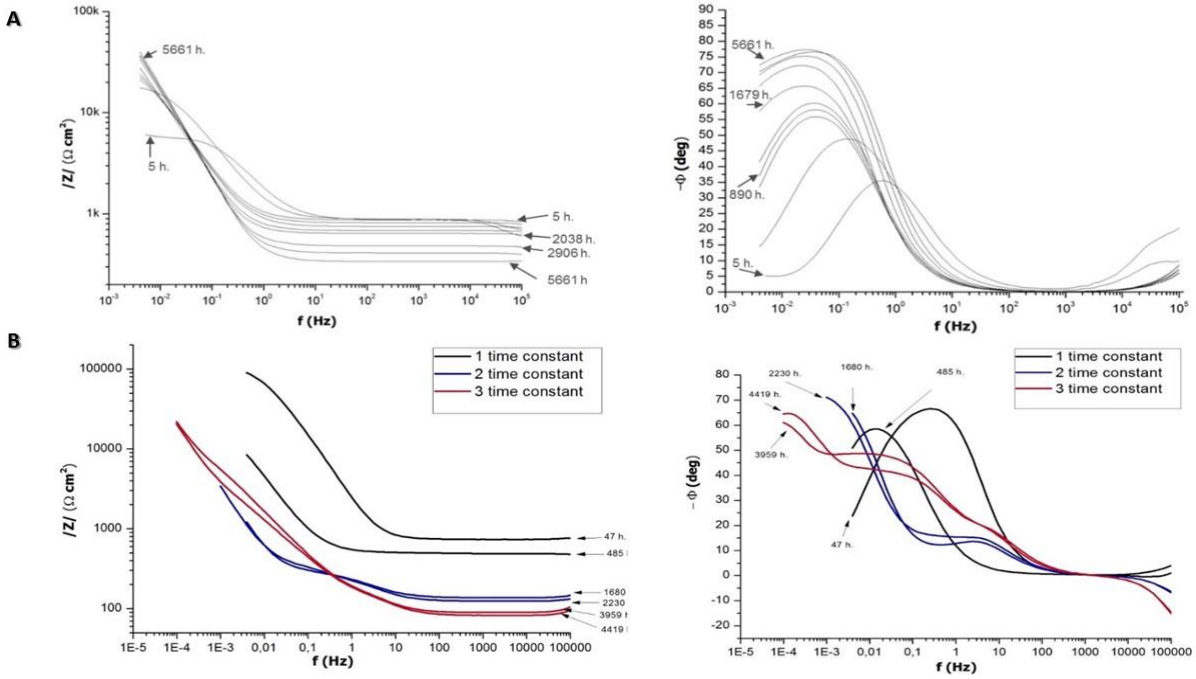


*Figure 15 Bode plot of electrochemical impedance spectra time evolution of carbon steel under sterile (A) and non-sterile conditions (B) .*

High phase shift values at a frequency range of 100-1 kHz appear to be artefacts caused by a parasitic capacitance originating from the electrochemical cell. As such, this part of the spectra was disregarded for further analysis. Spectra measured under sterile conditions are characterized by a single capacitive time constant over the whole measurement period, indicating uniform corrosion of



The MIND-project has received funding from the European Union's Euratom research and training program (Horizon2020) under grant agreement 661880.

the carbon steel. This corrosion stage is modelled in the circuit description code by the equivalent circuit $R_s(R_pQ_{CPE})$, where $R_s$ is the solution resistance, $R_p$ is the polarization resistance and $Q_{CPE}$ is the dispersive double layer capacitance. Table 11 summarizes the results for EIS measurements performed under sterile condition.

The three equivalent circuits (Figure 16) were used gradually for data fitting under non-sterile condition, representing three corrosion stages relating to the biofilm life cycle in three steps, where third step of the seeding dispersal revealed in the form of second layer of biofilm (Figure 2).

*Table 11 Results of EIS measurements performed under sterile conditions*

| Element → / Time (h) ↓ | ***Rs*** [Ohm·cm²] | ***Cdl*** [$\Omega^{-1}s^{-n}cm^{-2}$] | ***n*** | ***Rp*** [Ohm·cm²] |
|---|---|---|---|---|
| 5 | 872 | 1.75E-04 | 0.7862 | 5198 |
| 48 | 876.4 | 2.76E-04 | 0.7739 | 19430 |
| 482 | 867.2 | 5.76E-04 | 0.8081 | 32170 |
| 890 | 814.7 | 5.99E-04 | 0.8195 | 36710 |
| 1295 | 747.5 | 6.10E-04 | 0.8243 | 42770 |
| 1679 | 681.5 | 7.05E-04 | 0.8473 | 82160 |
| 2038 | 640.5 | 7.19E-04 | 0.8949 | 127700 |
| 2906 | 484.3 | 7.13E-04 | 0.9100 | 157300 |
| 3818 | 412.4 | 6.79E-04 | 0.9191 | 208500 |
| 5661 | 301.6 | 7.01E-04 | 0.9082 | 209600 |

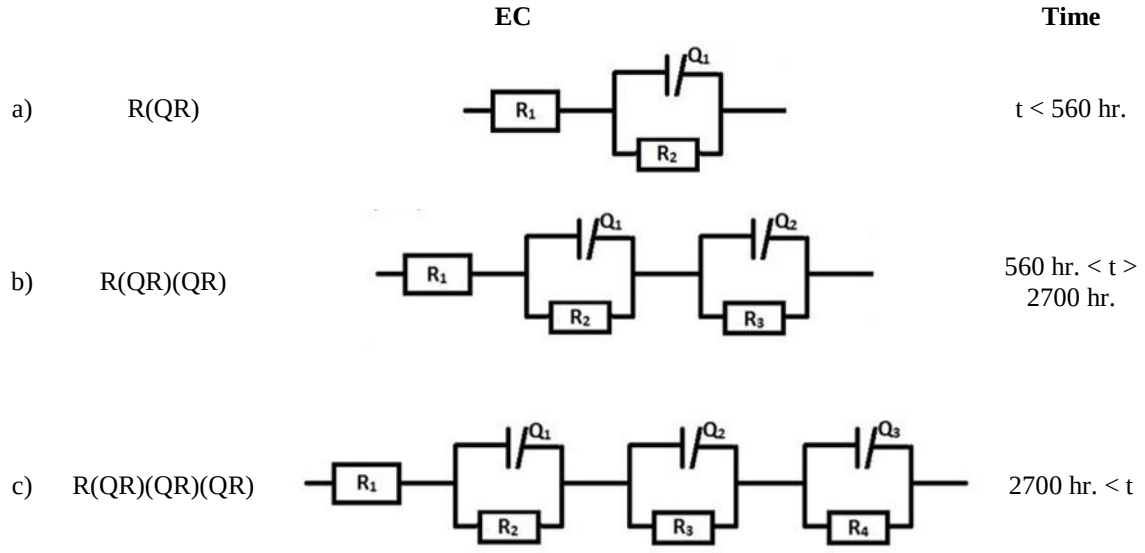


*Figure 16 Equivalence circuits used for electrochemical impedance spectroscopy data fitting and time evolution of corrosion stages.*

The first corrosion stage is characterized by one capacitive time constant, equivalent to the sterile environment, where $R_1$ is the solution resistance, $R_2$ is the polarization resistance and $Q_1$ is the dispersive double layer capacitance.

During early measurements with one time constant, it was difficult to detect presence of microbial activity from the EIS spectra under both sterile and non-sterile conditions without comparison with impedance data. In the non-sterile environment with microbial activity, the main



The MIND-project has received funding from the European Union's Euratom research and training program (Horizon2020) under grant agreement 661880.

differences observed were a more rapid increase in dispersive double layer capacitance and a rapid decrease in solution resistance over time. A second corrosion stage (Figure 16 b) was observed after 23 days, represented by the occurrence of two time constants due to biofilm formation. This corrosion stage was modelled in the circuit description code by the equivalent circuit $R_1(R_2Q_1)(R_3Q_2)$, where $R_3$ represents resistance of the biofilm and $Q_2$ is dispersive capacitance of the biofilm. Values $n_2$ of dispersive capacitance $Q_2$ indicate the presence of the influence of diffusion. The second biofilm time constant appeared in the high frequency area. A third corrosion stage was observed after 112 days and was characterized by a third time constant (Figure 16c), revealing the presence of a second biofilm layer which caused a shift in Faradaic charge transfer to very low frequencies of up to tens of μHz. Impedance measurements at such low frequencies could provide important data for the study of MIC in long-term experiments. This corrosion stage was modelled in the circuit description code by the equivalent circuit $R_1(R_2Q_1)$ $(R_4Q_3)$ $(R_3Q_2)$, where $R_4$ represents the resistance of the second biofilm and $Q_3$ is the second biofilm's dispersive capacitance. Presence of the second biofilm layer was confirmed through SEM analysis. The impedance of the second biofilm layer differed from that of the first by showing lowered dispersion and increased capacitance. Table 12 shown the results for EIS measurements performed under non-sterile conditions.

The accuracy of approximation of experimental data by the equivalent circuit ($\chi^2$) reached similar values in in sterile and non-sterile environments. It ranged in the order of $10^{-4}$ to $10^{-5}$. Table 12 shown the results for EIS measurements performed under non-sterile condition.

*Table 12 Results for EIS measurements performed under non-sterile conditions*

| Element → / Time (h) ↓ | $R_1$ [Ohm·cm$^2$] | $Q_1$ [$\Omega^{-1}s^{-n}cm^{-2}$] | $n_1$ | $R_2$ [Ohm·cm$^2$] | $Q_2$ [$\Omega^{-1}s^{-n}cm^{-2}$] | $n_2$ | $R_3$ [Ohm·cm$^2$] | $Q_3$ [$\Omega^{-1}s^{-n}cm^{-2}$] | $n_3$ | $R_4$ [Ohm·cm$^2$] |
|---|---|---|---|---|---|---|---|---|---|---|
| 6 | 691 | 9.56E-05 | 0.7916 | 43580 | | | | | | |
| 47 | 724.8 | 9.71E-05 | 0.8411 | 105600 | | | | | | |
| 485 | 496.1 | 0.00195 | 0.7933 | 27700 | | | | | | |
| 866 | 308.4 | 0.0111 | 0.9356 | 17300 | 0.0144 | 0.4866 | 297.4 | | | |
| 1295 | 206.8 | 0.01756 | 0.8993 | 25710 | 0.00411 | 0.4387 | 102.2 | | | |
| 1537 | 142.6 | 0.02229 | 0.8983 | 30390 | 0.00175 | 0.4864 | 175.8 | | | |
| 2230 | 100.1 | 0.02785 | 0.8932 | 63370 | 0.0021 | 0.4639 | 298.8 | | | |
| 4239 | 80.32 | 0.05035 | 0.9358 | 85130 | 0.00356 | 0.5608 | 22.65 | 0.00113 | 0.9792 | 3381 |
| 5080 | 82.21 | 0.02807 | 0.8554 | 125800 | 0.00374 | 0.5904 | 20.06 | 0.0013 | 0.9781 | 6891 |

Polarization resistance time dependence under sterile and non-sterile conditions was estimated by fitting by nonlinear least squares (Figure 17).



The MIND-project has received funding from the European Union's Euratom research and training program (Horizon2020) under grant agreement 661880.

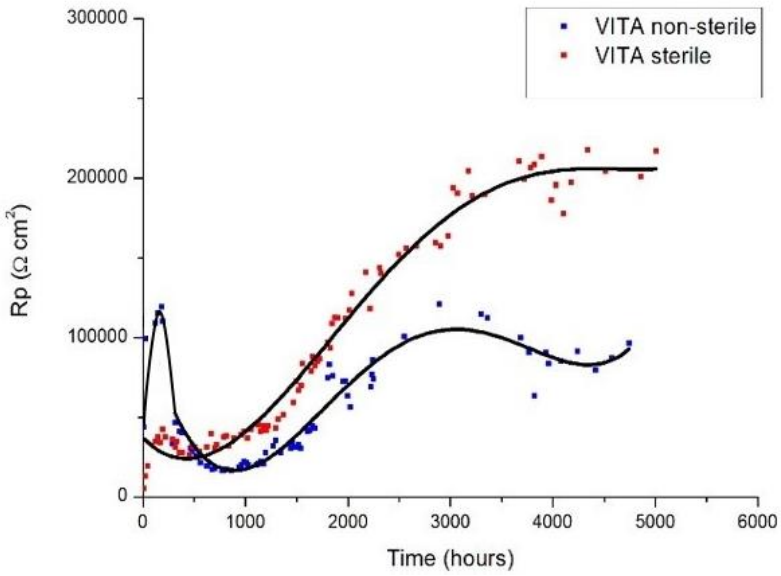


*Figure 17 Time evolution of polarization resistance of carbon steel in sterile and non-sterile environment under laboratory temperature.*

The increased polarization resistance during the early stages of the experiment under non-sterile conditions can be attributed to sedimentation, which has an inhibitory effect on corrosion rate when compared with the sterile environment without colloidal particles. When SRB were present, carbon steel polarization resistance decreased by a factor of two after 240 days, compared with the VITA groundwater under sterile conditions.

### *Carbon steel in natural granite water (source VITA) at T=35°C (Experiment C)*

The impedance spectra measured for carbon steel at 35°C at selected exposure times are shown as a Bode diagram (Figure 18). While in the experiment B at laboratory temperature and under sterile condition, we observed only one time constant during the entire period of exposure, two time constants appeared at 35°C under sterile condition indicating the formation of an oxide layer with dielectric properties. This oxide layer appears in the impedance spectrum after 2989 hours of exposure. Analysis of the impedance spectra was performed by fitting experimental data by the equivalent circuit $R_1(R_2Q_1)$, where $R_1$ is the solution resistance, $R_2$ is the polarization resistance and $Q_1$ is the dispersive double layer capacitance. Consequently for the impedance spectrum with two time constants was used equivalent circuit $R_1(R_2Q_1)(R_3Q_2)$, where $R_3$ represents resistance of the oxide layer and $Q_2$ is dispersive capacitance of the oxide layer.

While at laboratory temperature in experiment B under non-sterile condition, three corrosion stages were observed, experiment C revealed more complicated development. The three equivalent circuits (Figure 16) were used for data fitting under non-sterile condition and four corrosion stages were observed. The first corrosion stage is characterized by one capacitive time constant, equivalent to the sterile environment, where $R_1$ is the solution resistance, $R_2$ is the polarization resistance and $Q_1$ is the dispersive double layer capacitance. A second corrosion stage was observed after 669 hours, represented by the occurrence of two time constants due to biofilm formation. This corrosion stage was modelled in the circuit description code by the equivalent circuit $R_1(R_2Q_1)(R_3Q_2)$, where $R_3$ represents resistance of the biofilm and $Q_2$ is dispersive capacitance of the biofilm. By comparing the experiment under the laboratory temperature, biofilm formation was slower. This suggests, that the higher temperature affected bacterial adhesion. Third corrosion stage was observed after 3544 hours and was characterized by a third time constant. This corrosion stage was modelled in the circuit description code by the equivalent circuit $R_1(R_2Q_1)$ $(R_3Q_2)$ $(R_4Q_3)$, where $R_4$ represents the resistance of the layer of corrosion products and $Q_3$ is dispersive capacitance of the layer of the corrosion products. Fourth corrosion stage was observed after 4717 hours and was characterized by the presence of two



The MIND-project has received funding from the European Union's Euratom research and training program (Horizon2020) under grant agreement 661880.

time constants and shifting time constant of the biofilm to the lower frequency area. This shift time of constant was associated with the detachment of biofilm from surface indicating achievement of decline or death phase.

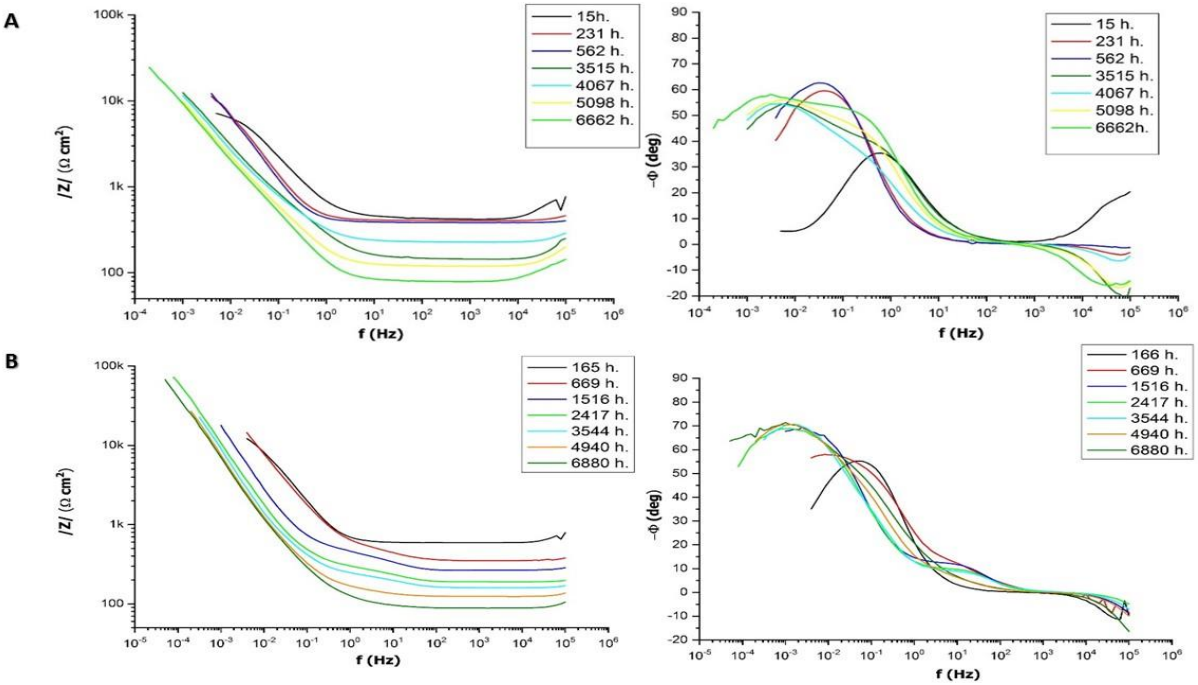


*Figure 18 Bode plot of electrochemical impedance spectra time evolution of carbon steel under sterile (A) and non-sterile conditions (B) at 35°C.*

Table 13 and Table 14 show the results for EIS measurements performed under sterile and nonsterile condition at 35°C.

*Table 13 Results of EIS measurements of carbon steel performed under sterile conditions at 35°C.*

| Element → | $R_1$ | $Q_1$ | $n_1$ | $R_2$ | $Q_2$ | $n_2$ | $R_3$ |
|---|---|---|---|---|---|---|---|
| Time (h) ↓ | [Ohm·cm²] | [$\Omega^{-1}s^{-n}cm^{-2}$] | | [Ohm·cm²] | [$\Omega^{-1}s^{-n}cm^{-2}$] | | [Ohm·cm²] |
| 15 | 426 | 0,000629 | 0,7664 | 8358 | | | |
| 231 | 401 | 0,001222 | 0,8304 | 18850 | | | |
| 562 | 381 | 0,001408 | 0,8417 | 25360 | | | |
| 1211 | 388 | 0,001873 | 0,7831 | 33440 | | | |
| 1548 | 228 | 0,001707 | 0,7345 | 36380 | | | |
| 1834 | 267 | 0,001518 | 0,7053 | 39770 | | | |
| 3515 | 145 | 0,002330 | 0,6972 | 44940 | 0,002777 | 0,8047 | 245 |
| 4067 | 227 | 0,003046 | 0,7290 | 41800 | 0,003579 | 0,7536 | 312 |
| 5098 | 118 | 0,003379 | 0,7168 | 38500 | 0,006810 | 0,8599 | 197 |
| 6662 | 78 | 0,004342 | 0,7472 | 46320 | 0,007248 | 0,8192 | 352 |



The MIND-project has received funding from the European Union's Euratom research and training program (Horizon2020) under grant agreement 661880.

*Table 14 Results of EIS measurements of carbon steel performed under non-sterile conditions at 35°C.*

| Element → / Time (h) ↓ | $R_1$ [Ohm·cm$^2$] | $Q_1$ [$\Omega^{-1}s^{-n}cm^{-2}$] | $n_1$ | $R_2$ [Ohm·cm$^2$] | $Q_2$ [$\Omega^{-1}s^{-n}cm^{-2}$] | $n_2$ | $R_3$ [Ohm·cm$^2$] | $Q_3$ [$\Omega^{-1}s^{-n}cm^{-2}$] | $n_3$ | $R_4$ [Ohm·cm$^2$] |
|---|---|---|---|---|---|---|---|---|---|---|
| 165 | 577 | 0,00086 | 0,7951 | 1,91E+04 | | | | | | |
| 577 | 374 | 0,00103 | 0,7750 | 6,22E+04 | | | | | | |
| 669 | 349 | 0,00091 | 0,7075 | 1,32E+05 | 0,00024 | 0,8535 | 104 | | | |
| 1239 | 272 | 0,00392 | 0,8118 | 1,21E+05 | 0,00076 | 0,6127 | 246 | | | |
| 1743 | 235 | 0,00365 | 0,7872 | 1,46E+05 | 0,00054 | 0,7110 | 171 | | | |
| 2755 | 187 | 0,00703 | 0,8245 | 1,71E+05 | 0,00175 | 0,5173 | 180 | | | |
| 3544 | 158 | 0,00899 | 0,8665 | 9,95E+04 | 0,00967 | 0,8665 | 237 | 0,000681 | 0,7534 | 74 |
| 4047 | 140 | 0,00966 | 0,8683 | 9,04E+04 | 0,00928 | 0,7009 | 308 | 0,001088 | 0,7012 | 43 |
| 4097 | 133 | 0,009759 | 0,8683 | 9,28E+04 | 0,00912 | 0,6919 | 329 | 0,001250 | 0,6843 | 40 |
| 4263 | 135 | 0,01000 | 0,8692 | 8,98E+04 | 0,01008 | 0,7129 | 306 | 0,001868 | 0,6508 | 41 |
| 4717 | 128 | 0,01277 | 0,8942 | 8,61E+04 | 0,00752 | 0,4824 | 1420 | | | |
| 4940 | 122 | 0,01268 | 0,8888 | 9,80E+04 | 0,00807 | 0,4939 | 1263 | | | |
| 5169 | 116 | 0,01255 | 0,8846 | 1,09E+05 | 0,00807 | 0,4946 | 1152 | | | |
| 5848 | 103 | 0,01221 | 0,8749 | 1,23E+05 | 0,00852 | 0,5212 | 892 | | | |
| 6880 | 87 | 0,01194 | 0,8667 | 1,21E+05 | 0,00895 | 0,5443 | 659 | | | |

Polarization resistance time dependence under sterile and non-sterile conditions at 35°C shows Figure 19. Inhibitory efficiency of microbial consortium containing SRB in natural granite water (source VITA) for carbon steel was 62% at the end of the experiment.

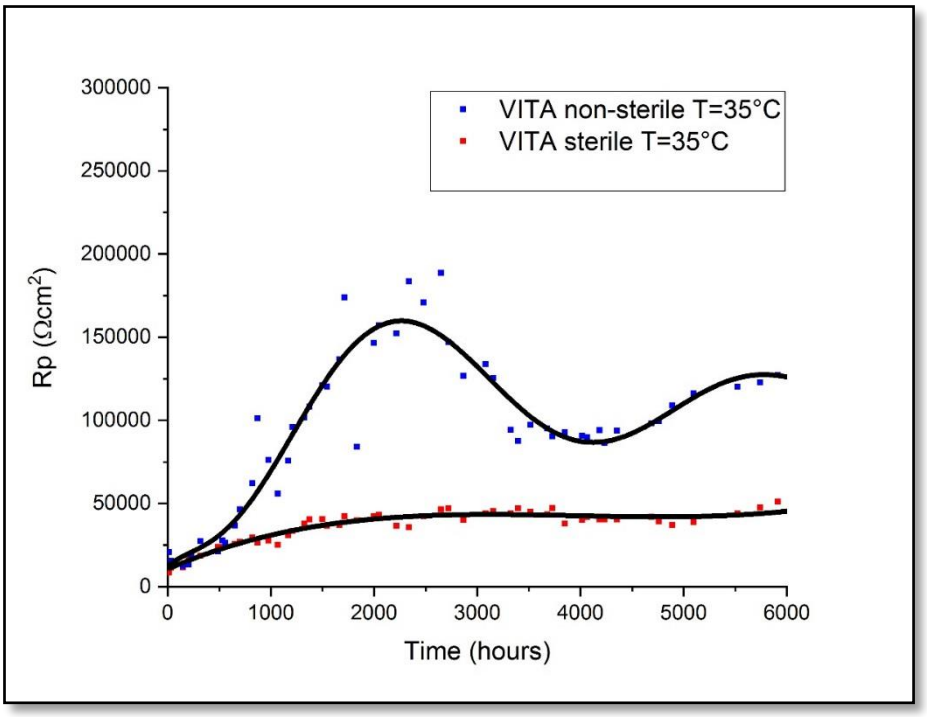


*Figure 19 Time evolution of polarization resistance of carbon steel at 35°C.*



The MIND-project has received funding from the European Union's Euratom research and training program (Horizon2020) under grant agreement 661880.

### 3.1.4 Weight loss method

**Carbon steel in synthetic bentonite pore water (SBPOW) inoculated with VITA water, under laboratory temperature (Experiment D)**

Weight loss data of carbon steel in SBPOW solution under sterile condition and in synthetic bentonite pore water solution inoculated by natural ground water (source VITA) were obtained. The result of the weight loss measurements is summarized in Figure 20. Uniform corrosion of carbon steel was observed in abiotic environment. The apparent corrosion rate in synthetic bentonite pore water solution under sterile condition after 18 months exposure was 0,6 µm/y. This confirms the tendency for the corrosion rate to decrease with increasing exposure time.

In the case of non-sterile environment, severe local attack was observed on each sample after 3, 6 and 12 months, which significantly increases the corrosion rate. The highest corrosion rate was 5,4 µm/y after 6 months.

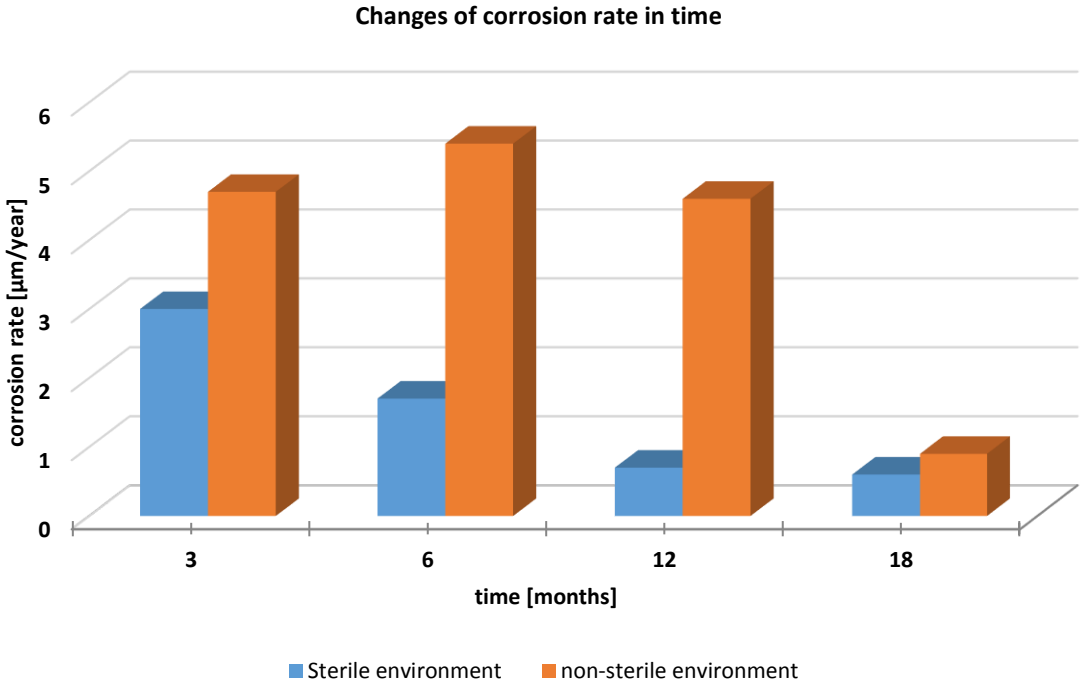


*Figure 20 Average corrosion rates based on weight loss measurements for the carbon steel in sterile synthetic bentonite pore water (SBPOW) and in inoculated SBPOW.*

The samples collected after 18 months of exposure were without local attack in nonsterile conditions and corrosion rate was 0,9 µm/y. This suggests the occurrence of different type of mechanisms and microbial community in the biofilm under nitrate-reducing conditions that can lead not only to local attack but also to uniform corrosion [87].

## 3.2 Surface analysis

### 3.2.1 SEM

SEM showed that, in the presence of bacteria, the carbon steel surface was covered with a relatively thick layer of pompom-shaped biofilm with many cells visible (Figure21). The biofilm



The MIND-project has received funding from the European Union's Euratom research and training program (Horizon2020) under grant agreement 661880.

consisted of microorganisms surrounded and held together by an excreted gelatinous matrix of EPS composed of high molecular weight compounds. The bacteria had a typically cylindrical shape about 2 µm long. Usually, the SE detector mode provided the best surface visualization, when the bacteria looked like dark hyaline objects (Figure 21). The main disadvantage of this mode was the difficulty in finding bacterial cells. Use of the BSE detector improved the imaging contrast between bacterial cells (comprising elements of the lower atomic number) and the steel surface due to the backscatter of electrons, which made areas, where bacteria were located, appear darker (Figure 21). Figure 22 (A, C – non-sterile; B and D – sterile) is revealing the difference between environmental conditions (experiment C), the non-sterile sample displayed the presence of microorganisms by their activity (formed biofilm). The surface analysis suggested a heterogeneous sample surface. The biofilm covering was non-uniform, with some areas showing many flat crystals. The double layer of biofilm (Figure 24) was confirmed by EIS that showed three corrosion stages.

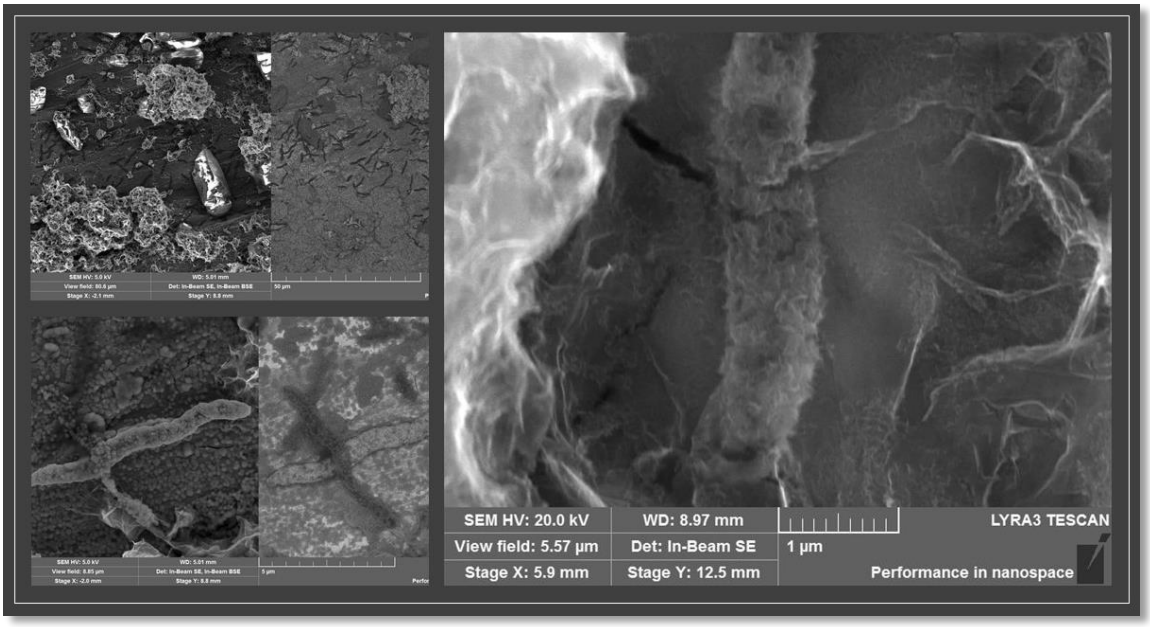


*Figure 21 Experiment C – Biofilm on carbon steel exposed to non-sterile conditions after 293 days incubation; comparison of different detector modes and visualized bacteria*



The MIND-project has received funding from the European Union's Euratom research and training program (Horizon2020) under grant agreement 661880.

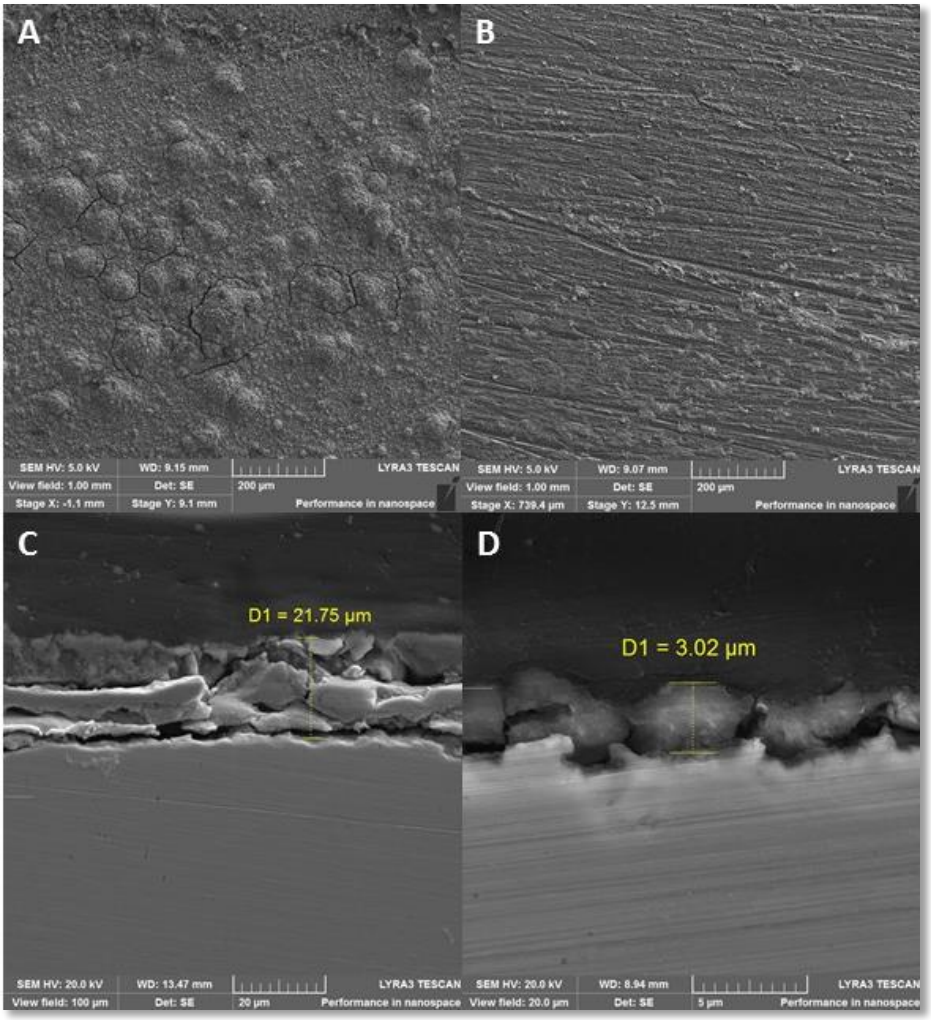


*Figure 22 SEM – Experiment C; T 35°C difference of non-sterile (A, C – 21,75 µm) vs. sterile (B, D – 3,02 µm) conditions*

Local EDS analysis demonstrated that the corrosion products were mainly composed of iron, oxygen, sulphur and carbon. This finding was supported by elemental maps of those areas with bacteria present (Figure 23). The presence of sulphur and iron indicated FeS formation, clearly indicating bacterial activity. Additionally, under non-sterile conditions, black turbidity was observed in the experimental cell and on the surface of the testing coupon. In contrast, no sulphur or signs of microbial activity were detected by SEM/EDS on the sample under sterile conditions.



The MIND-project has received funding from the European Union's Euratom research and training program (Horizon2020) under grant agreement 661880.

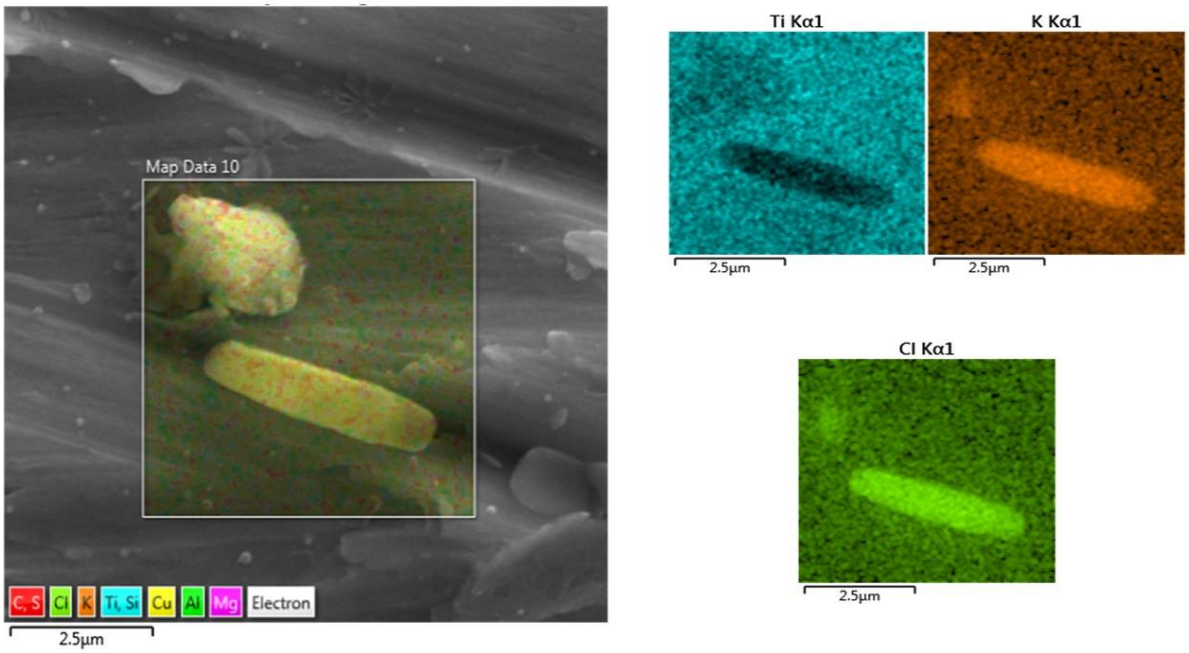


*Figure 23 SEM elemental maps showing composition of area with bacterium (Experiment B).*

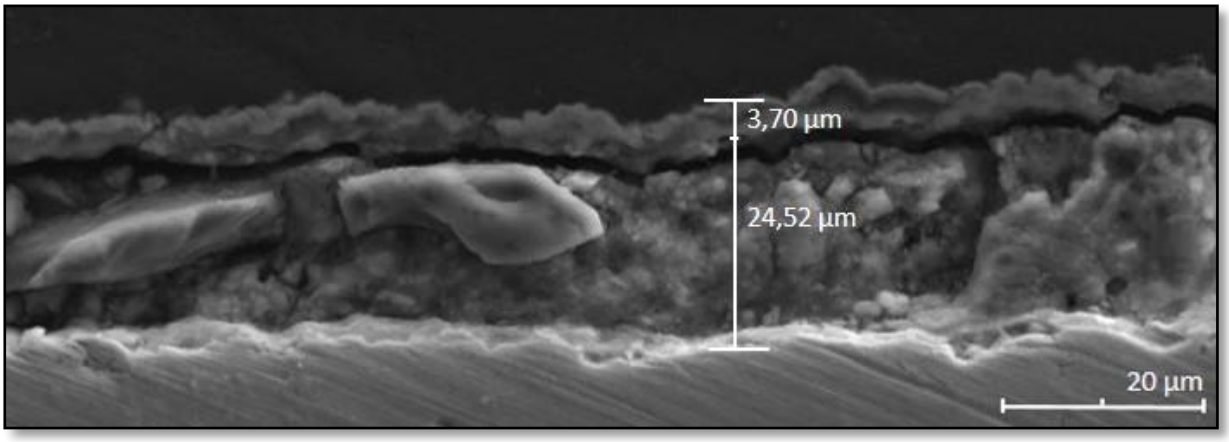


*Figure 24 SEM micrograph showing double layer – cross section of the sample exposed at $T_{lab}$ non-sterile (Experiment B)*



The MIND-project has received funding from the European Union's Euratom research and training program (Horizon2020) under grant agreement 661880.

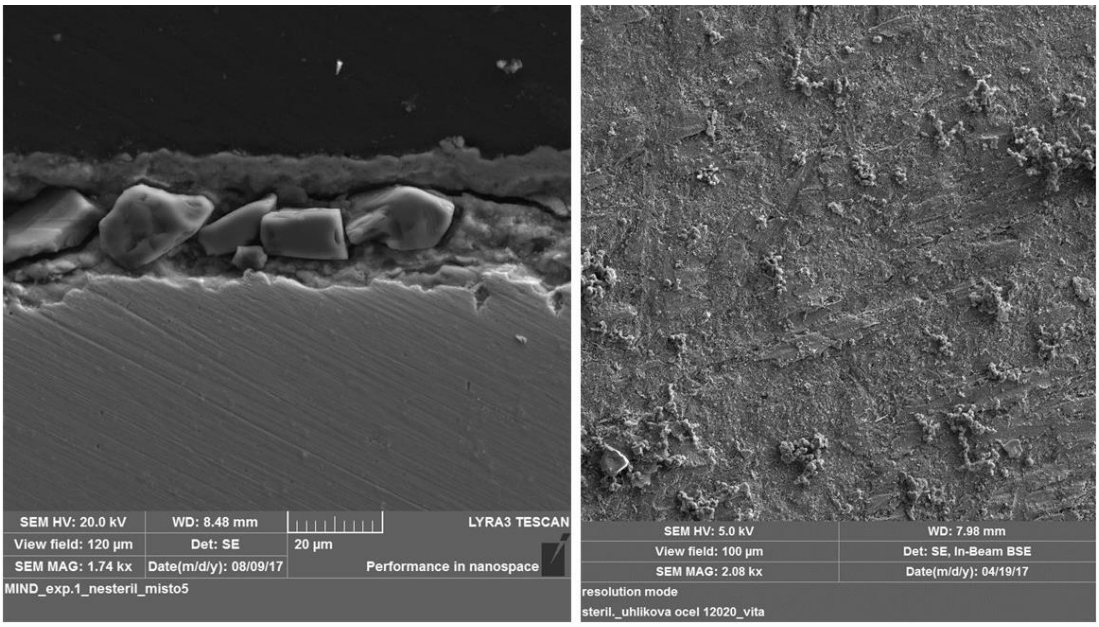


*Figure 25 SEM showing the crystals of the cross-section in non-sterile and surface in the sterile conditions (Experiment B)*

SEM analysis showed that the covering layer was stratified into a thicker (inner layer) and a thinner (outer layer). The composition of these layers differed, the inner layer (spectrum 20) being dominated by iron and oxygen, with a small amount of silicon, while in the outer layer (spectrum 19) comprised iron with oxygen and sulphur dominating (Figure 26 for the EDS spectra).

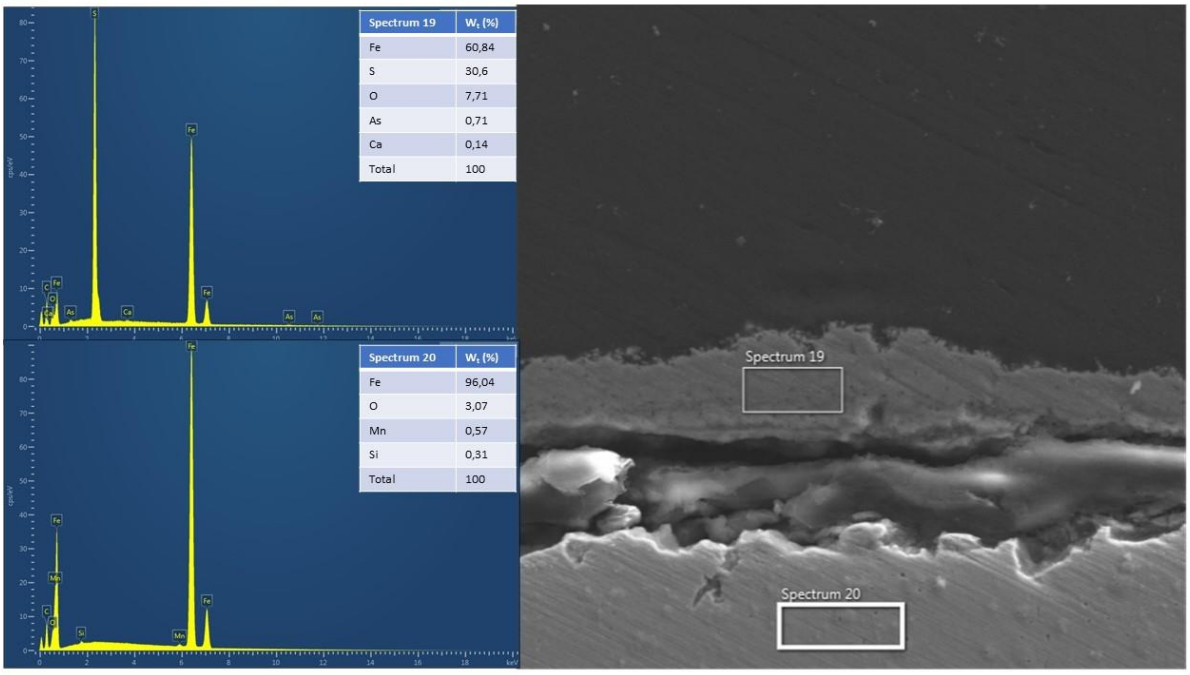


*Figure 26 EDS spectra displaying different composition of layers ( Spectra 19: Fe(60,84), S(30,6), O(7,71), As(0,71), Ca(0,14); Spectra 20: Fe(96,04), O(3,07), Mn(0,57), Si(0,31)) (Experiment B)*



The MIND-project has received funding from the European Union's Euratom research and training program (Horizon2020) under grant agreement 661880.

In the weight loss experiment (Experiment D; still ongoing) the composition of biofilm with bacteria (Figure 27) was dominated by iron and oxygen, with a small amount of carbon and magnesium (Figure 28 is showing the EDS spectra and elemental maps).

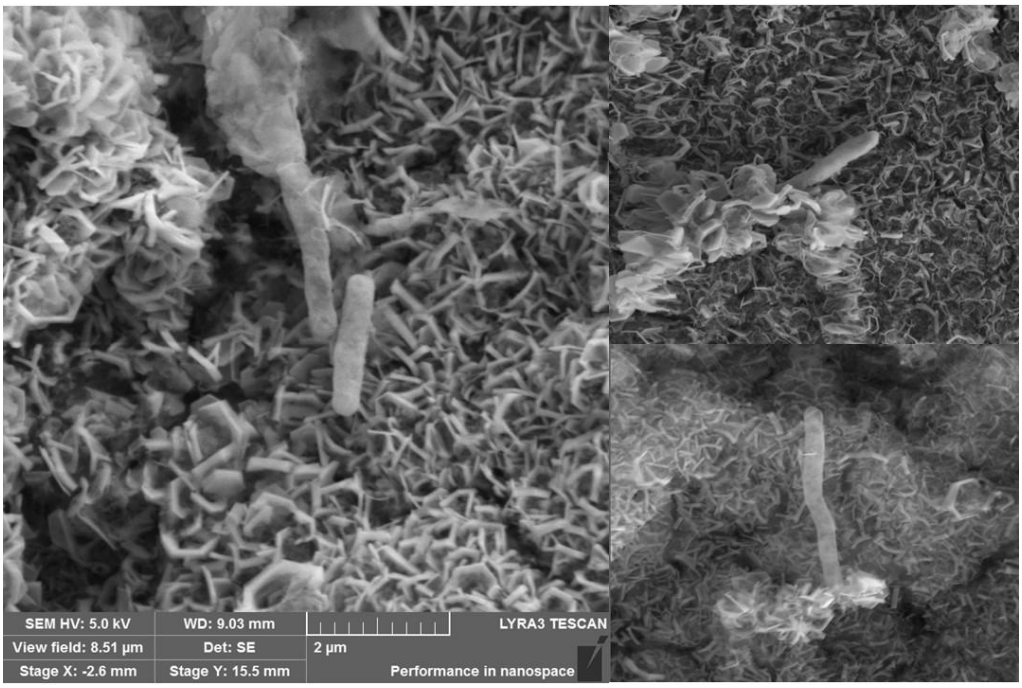


*Figure 27 SEM – Bacteria of the weight loss experiment (Experiment D)*

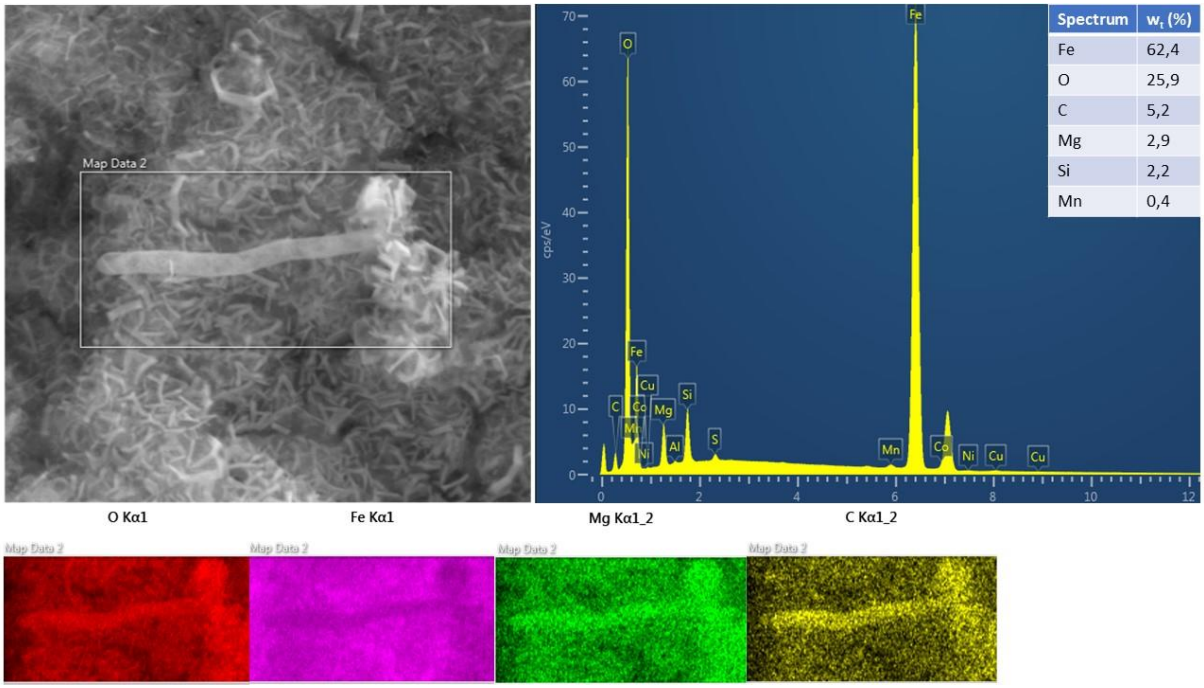


*Figure 28 SEM elemental maps and spectra of compisition (Spectrum: Fe(62,4), O(25,9), C(5,2), Mg(2,9), Si(2,2), Mn(0,4)) (Experiment D)*



The MIND-project has received funding from the European Union's Euratom research and training program (Horizon2020) under grant agreement 661880.

### 3.2.2 Raman spectroscopy

Raman spectroscopy was used to characterize the corrosion products of carbon steel in the different environment, temperature and duration as it is seen in the Table 4. The intensity of the Raman spectra from the experiment A and B were too weak to detect any minerals from the RRUFF library.

#### *Carbon steel in natural granite water (source VITA) at T=35°C (Experiment C)*

The Figure 29 illustrates the spectrum of carbon steel in VITA water under sterile anaerobic conditions after 293 days of incubation with the reference spectra of the Aragonite and the corresponding photography of the sample. There were found five Raman-active bands 153, 180, 207, 705 and the typical intensive bands 1085 $cm^{-1}$ for the group $CO_3^{2-}$. According to RRUFF library this spectrum corresponds to Aragonite (Measured chemistry of Aragonite is $Ca_{1.00}CO_3$).

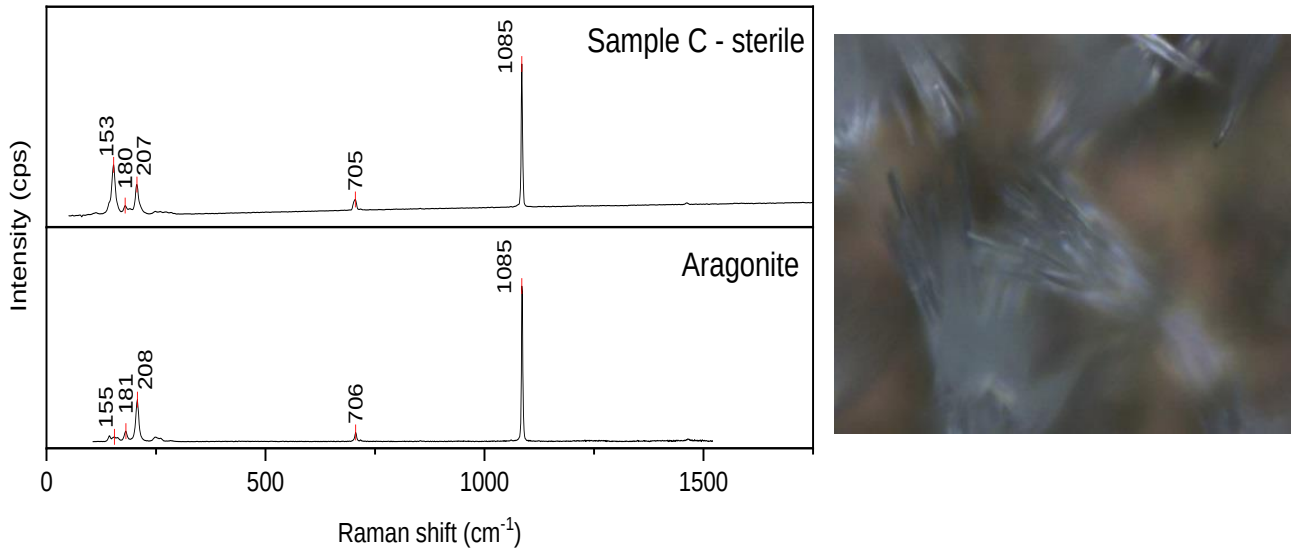


*Figure 29 Raman Spectra of carbon steel in VITA water under sterile anaerobic conditions after 293 days of incubation with the reference spectra of the Aragonite and the corresponding photography of the sample.*

The Figure 30 shows the Raman spectra of the carbon steel exposed in the non-sterile VITA water (rich of SRB). The peaks at 217, 280, 391, 487, 595, 653 and 1286 $cm^{-1}$ were observed and were assigned to Mackinawite. Here was recorded the phenomenon of MIC in anoxic environments involving SRB, microorganisms that produced sulphide species. Thus, in this media where sulphides are not naturally present, the observation of $Fe^{II}$ sulphides (all sulphides have their stronger peak at approximately 250-350 $cm^{-1}$) inside the rust layer is a clear indication that SRB were active and played significant role in the corrosion process [88].



The MIND-project has received funding from the European Union's Euratom research and training program (Horizon2020) under grant agreement 661880.

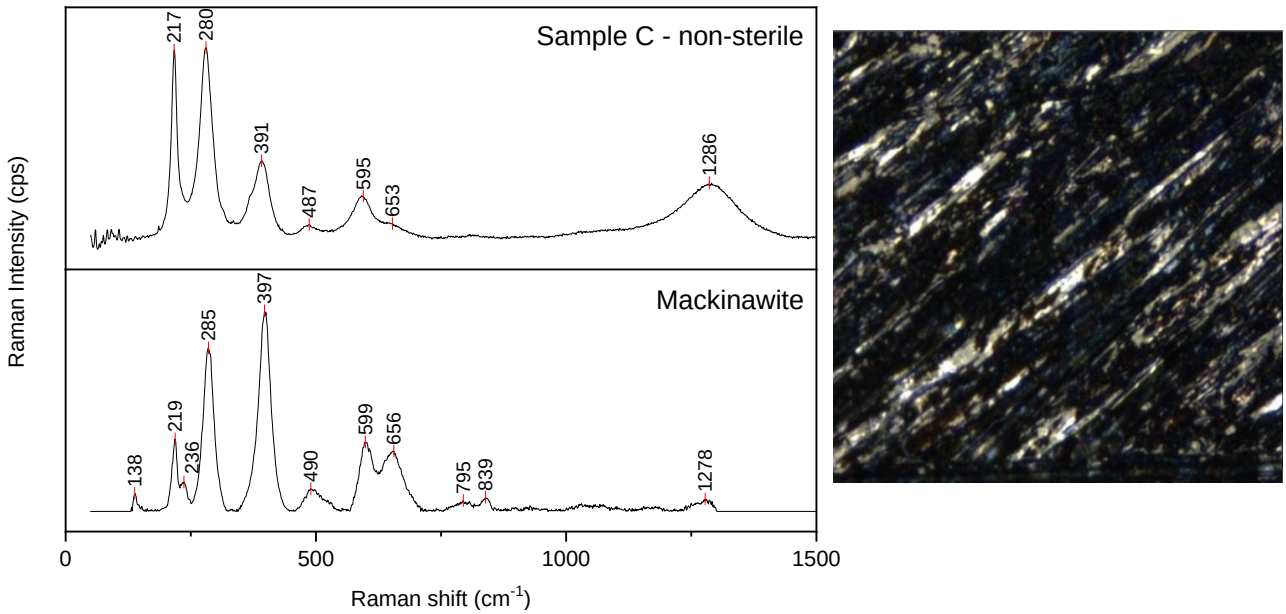


*Figure 30 Raman Spectra of carbon steel under non-sterile anaerobic conditions in VITA water after 293 days of incubation with the reference spectra of the Mackinawite and the corresponding photography of the sample.*

Along with Mackinawite, magnetite was also observed on the surface of carbon steel under non-sterile conditions with the intensive bands 311, 538, 672 $cm^{-1}$ (Figure 31).

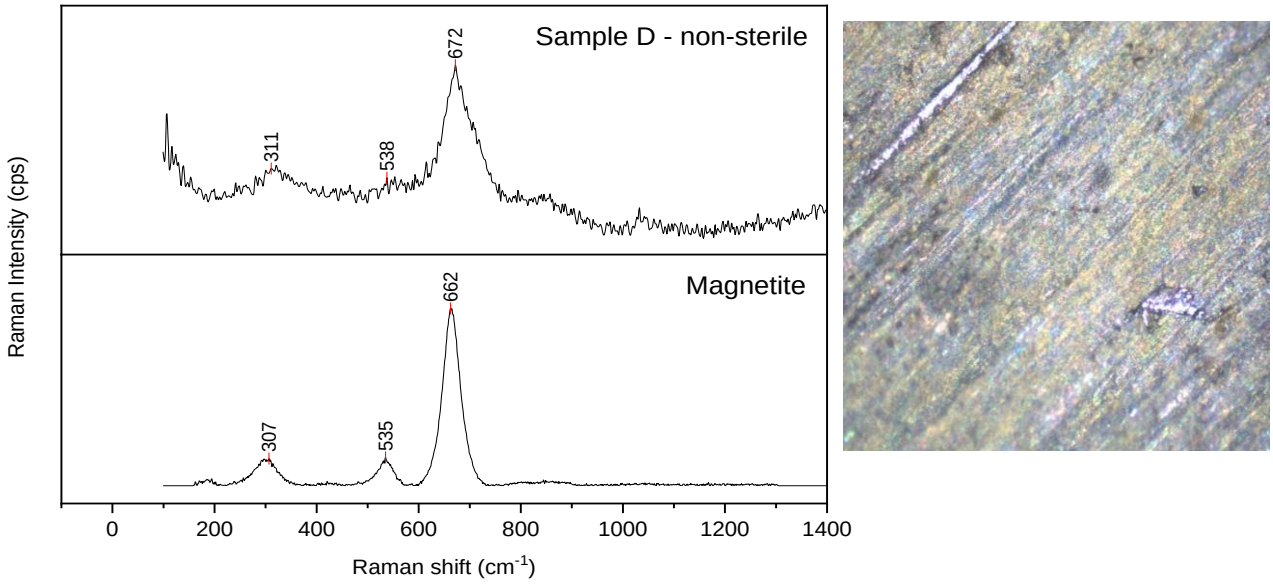


*Figure 31 Raman Spectra of carbon steel under non-sterile anaerobic conditions in VITA water after 293 days of incubation with the reference spectra of the Magnetite and the corresponding photography of the sample.*

### *Carbon steel in synthetic bentonite pore water (SBPOW) inoculated with VITA water, under laboratory temperature (Experiment D)*

The Figure 32 illustrates the Raman spectra of the sample D, which is carbon steel exposed to SBPOW after 12 month of incubation under sterile anaerobic conditions. There were detected three Raman-active bands at 315, 547 and 670 $cm^{-1}$, which corresponds to magnetite. The reference spectrum of magnetite shown in the Raman graph illustrates the magnetite layer. Magnetite ($Fe_3O_4$) is known for its sensitivity to transform into hematite ($Fe_2O_3$) in the presence of oxygen. Although the samples were filled to the cells under anaerobic conditions, their potential oxygen contamination



The MIND-project has received funding from the European Union's Euratom research and training program (Horizon2020) under grant agreement 661880.

cannot be excluded due to the insufficient sealing of the used cells during transportation for Raman measurement. For this reason the hematite spectra was also recorded.

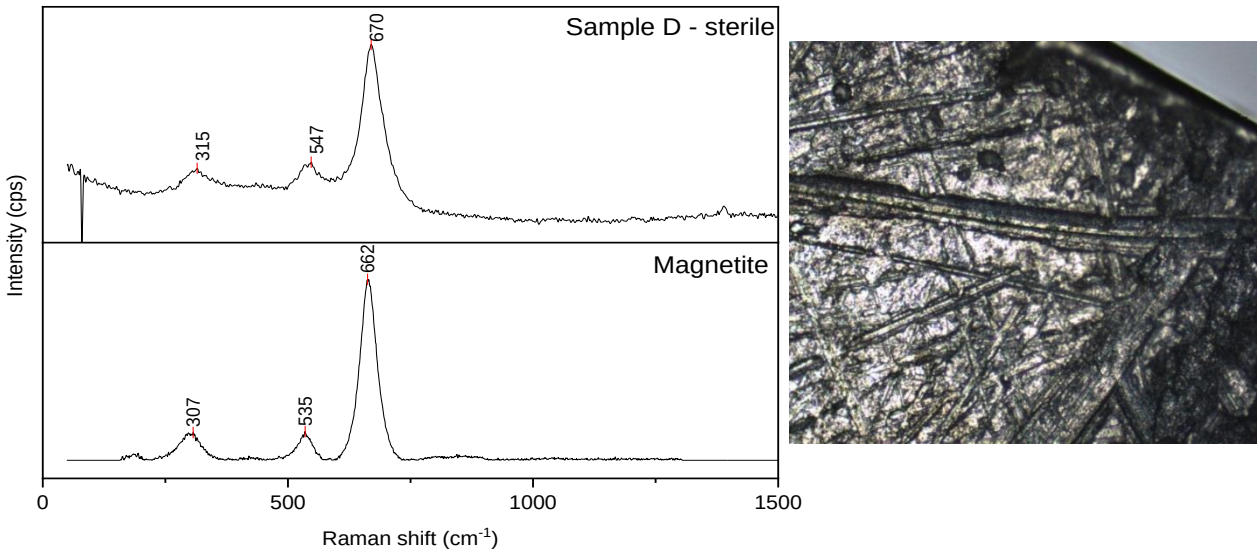


*Figure 32 Raman spectra of carbon steel in SBPOW under sterile anaerobic conditions after 12 month of incubation with the corresponding photography of the sample and reference spectra of the Magnetite.*

After 18 months of incubation in SBPOW inoculated with VITA water, the Raman spectra of carbon steel revealed the presence of four intense bands around 153, 280, 711 and 1086 $cm^{-1}$ (see Figure 33). Narrow intensive band around 1086 is typical for the group $CO_3^{2-}$. According to RRUFF database these bands are assigned to calcite (Measured chemistry of calcite is $(Ca_{0.99}Mg_{0.01})CO_3$).

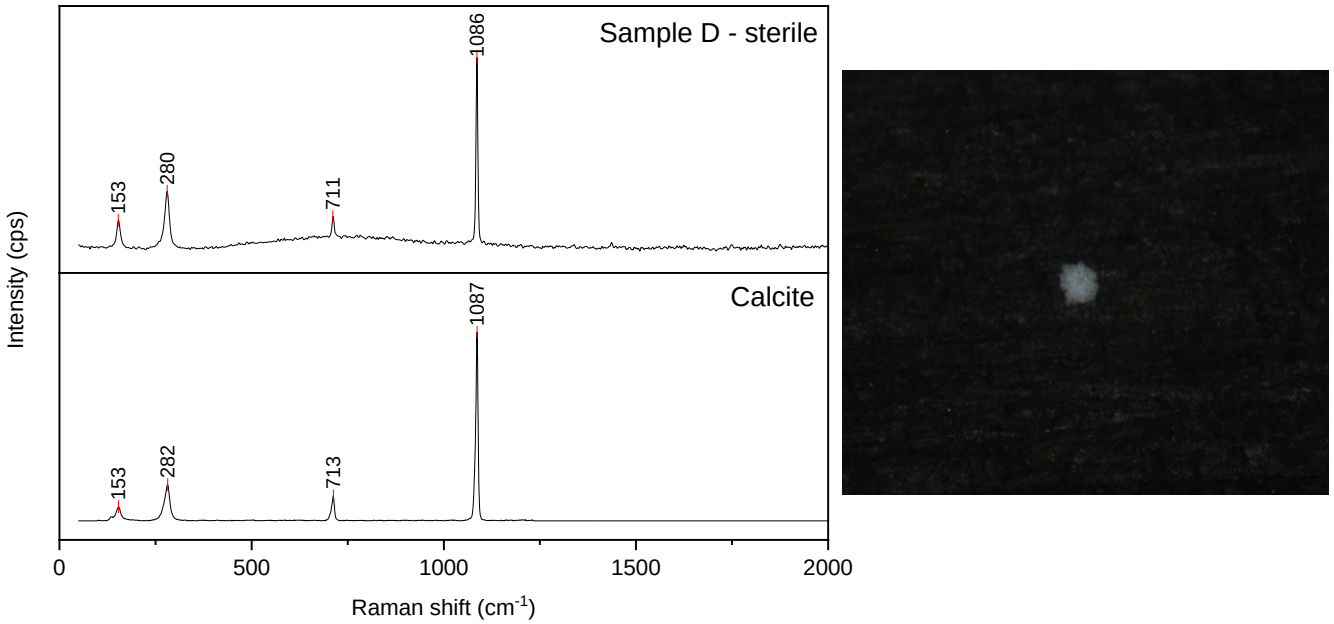


*Figure 33 Raman Spectra of carbon steel in SBPOW under sterile anaerobic conditions after 18 months of incubation with the corresponding photography of the sample and reference spectra of the calcite.*

In the spectrum of the sample D under sterile condition, there were observed following intense bands: 329, 677, 849 and 1037 $cm^{-1}$ that correspond to Larnite – $Ca_2(SiO_4)$ (Figure 34).



The MIND-project has received funding from the European Union's Euratom research and training program (Horizon2020) under grant agreement 661880.

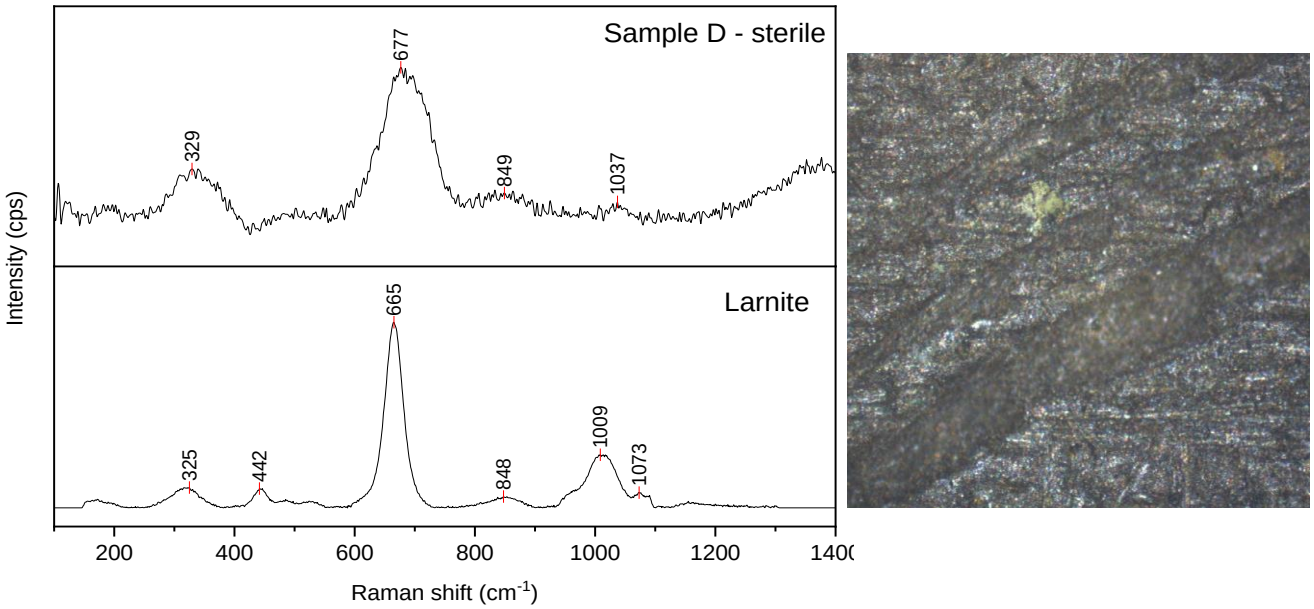


*Figure 34 Raman Spectra of carbon steel in SBPOW under sterile anaerobic conditions after 18 months of incubation with the corresponding photography of the sample and reference spectra of the larnite.*

The Figure 35 shows the Raman spectra of the sample from the Experiment D after 12 months exposed in the SBPOW with the VITA water inoculum under non-sterile conditions. Raman signature peaks at 315, 547 and 670 $cm^{-1}$ were observed and attributed to mackinawite.

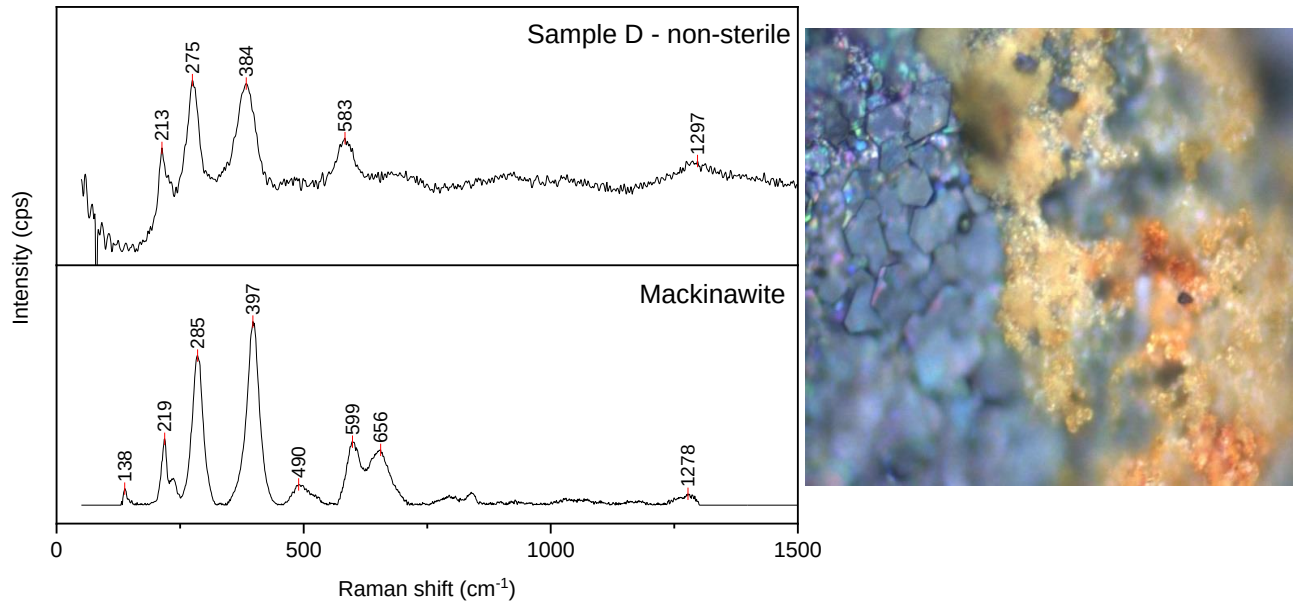


*Figure 35 Raman Spectra of carbon steel in SBPOW in VITA water inoculum under anaerobic conditions after 12 month of incubation with the corresponding photography of the sample (the yellow part) and the reference spectra of the mackinawite.*



The MIND-project has received funding from the European Union's Euratom research and training program (Horizon2020) under grant agreement 661880.

## 3.3 Microbial community analysis

### 3.3.1 qPCR analysis

#### *Stainless steel in natural granite water (source HV1) under laboratory temperature (Experiment A)*

The qPCR analysis from the corrosion of stainless steel 316L (Figure 36) showed a small increase in total bacterial biomass in the end of the experiment. Moreover, SRB (detected by *apsA* gene) was observed to proliferate. *DsrA* gene (SRB) and *nosZ* gene (NRB) followed the similar pattern where only a negligible growth of both genes was detected, while the *Geobacteraceae* and *nirK* gene decreased. *nirS* gene was not detected after 111 days. Even low metabolic activity of SRB could accelerate the process of corrosion of metal canister.

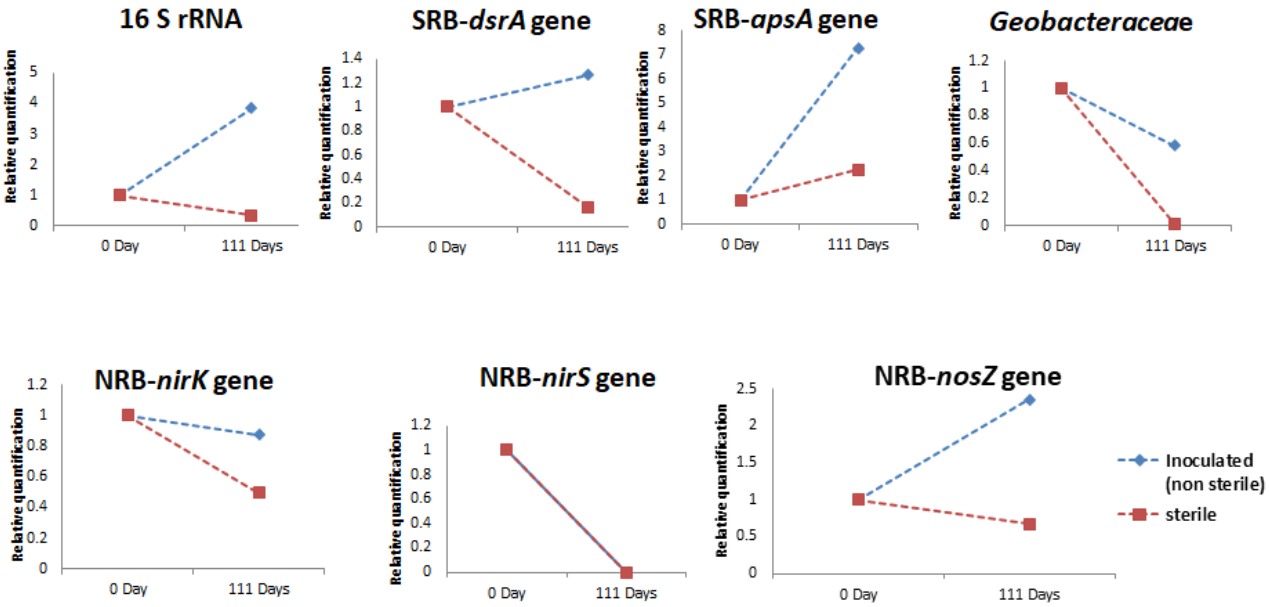


*Figure 36 Relative quantification of bacteria in time with specific gene determined by qPCR analysis using HV1 water as inoculation for 111 days.*

#### *Carbon steel in natural granite water (source VITA) under laboratory temperature (Experiment B)*

The relative abundance of total bacterial biomass was found to be more or less similar after 240 days of incubation (Figure 37). Similar negative response was confirmed for all functional markers except for *nosZ* gene (NRB) that slightly increased during the experiment. NRB are responsible for carrying denitrification in the system. Under the sterile environment any bacterial markers were detected.



The MIND-project has received funding from the European Union's Euratom research and training program (Horizon2020) under grant agreement 661880.

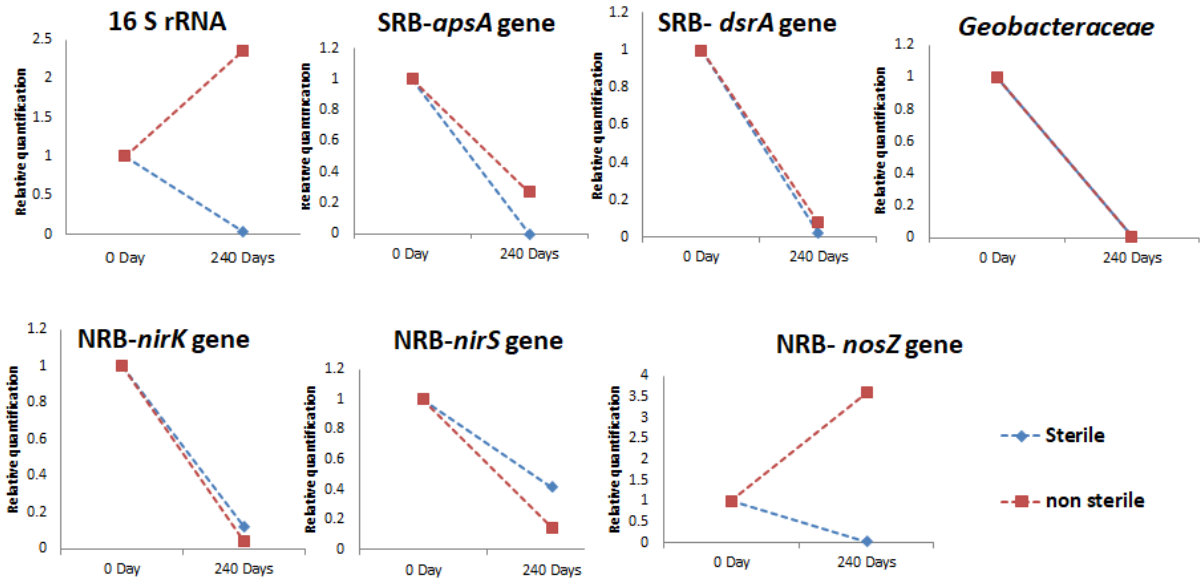


*Figure 37 Relative quantification of bacteria in time with specific gene marker after incubation of 240 days using VITA water determined by qPCR analysis.*

### *Carbon steel in natural granite water (source VITA) at T=35°C (Experiment C)*

qPCR analysis of carbon steel in VITA at 35 °C for 10 months revealed that it follows the similar trend of responses as shown by experiment with carbon steel at laboratory condition for 8 months (240 days). Any remarkable difference in total bacterial biomass including all other functional markers was observed (Figure 38).

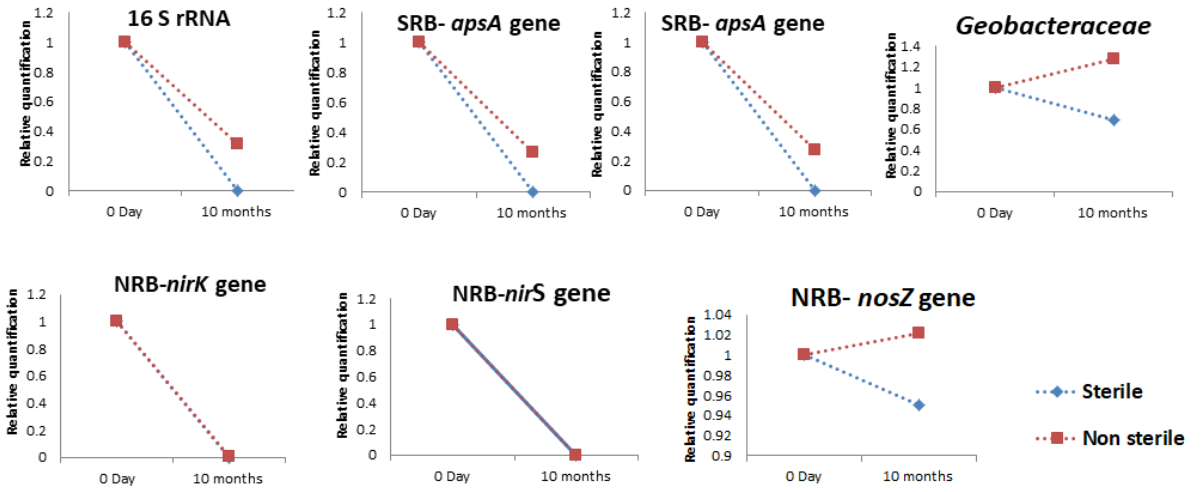


*Figure 38 Relative quantification of bacteria in time with specific gene marker determined by qPCR analysis after incubation at 35 °C for 10 months using VITA water.*

### Carbon steel in synthetic bentonite pore water (SBPOW) under laboratory temperature (Experiment D)

The patterns obtained with SBPOW inoculum in presence and absence of carbon steel were very dissimilar. SRB remained negligible during whole experiment. Any bacteria or genes were detected in the sterile samples. The 16S rRNA, *nirS* and *nosZ* gene results are presented in log form to cover both low and high values.



The MIND-project has received funding from the European Union's Euratom research and training program (Horizon2020) under grant agreement 661880.

During the first three months of anaerobic incubation, the total bacterial biomass including NRB displayed remarkable increase in relative abundance. Total bacterial biomass in the presence of carbon steel remained high until the end of the experiment (18 months), while in the samples without carbon steel biomass increased much more in the first six months reaching very similar level after 18 months. qPCR analysis revealed very high propagation of NRB in agreement with NGS results. Among all the functional markers of NRB, *nosZ* gene responsible for detection of nitrous oxide reductase had shown the highest proliferation. Interestingly it increased more in the samples without carbon steel than with carbon steel after six months. However, the relative levels of nosZ declined by the end of the experiment.

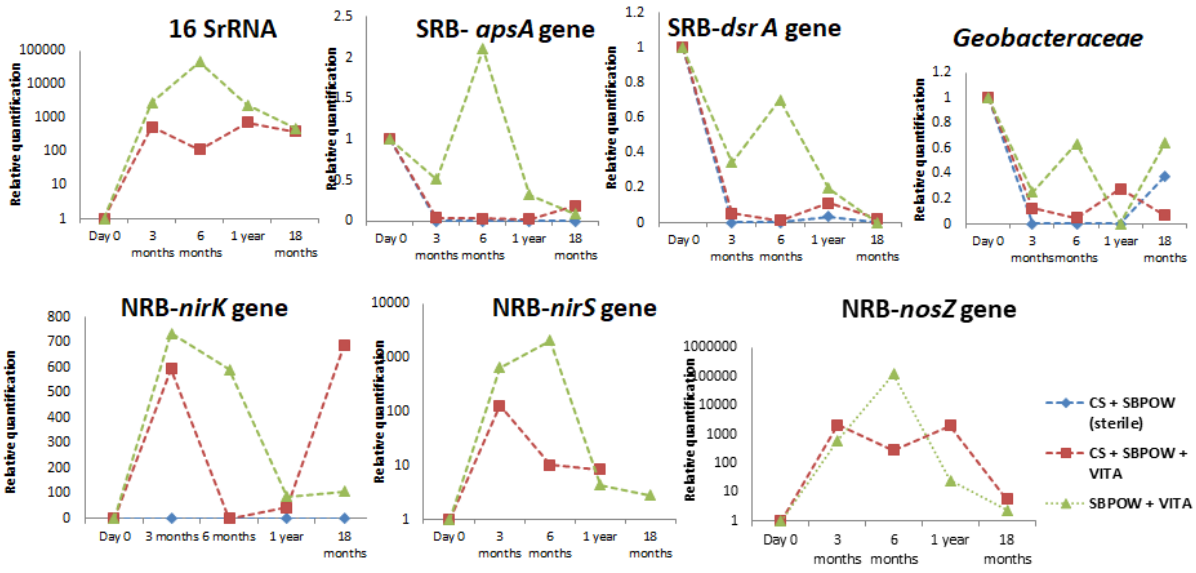


*Figure 39 Relative quantification of bacteria by qPCR analysis with respective gene markers during 18 months of incubation wit carbon steel (CS) in synthetic bentonite pore water (SBPOW) inoculated with VITA water. Note log scale for 16S rRNA, nirS and nosZ.*

Interesting fluctuation was detected for the *nirK* gene. In the presence of steel it dropped down after initial increase and then again remarkably increased by the end of the experiment. In contrast, in the environment where the carbon steel was absent, *nirK* gene showed a decline after strong increase, but it did not increase again as in the sample with carbon steel.

Surprisingly, any such remarkable changes were observed for SRB although they survived in both conditions. The reason behind could be explained by the dominance of NRB favored by SBPOW, because this synthetic water mimics the Czech bentonite leachates which was rich in nitrate. Additionally, the *Geobacteraceae* did not show any positive response to presence or absence of carbon steel revealing the unsuitability of these environmental conditions for its growth.

We can conclude that it was confirmed that denitrifying bacteria were dominant microorganisms present in the experiment. Such a huge proliferation of NRB was caused by the chemical composition of SBPOW which was rich in nitrates and offered to NRB an easy accessible terminal electron acceptor. Furthermore, denitrification indicates a complete reduction of nitrate to nitrogen by the consumption of intermediate product like nitrites, nitric oxide and nitrous oxide. Hence, nitrate was utilized by denitrifying bacteria as a terminal electron acceptor. Some NRB can also be a sulphide oxidizing bacteria which are capable to reduce nitrate to nitrite or nitrogen oxides which can result in the formation of highly corrosive elemental sulphur or polysulfides [89]. Furthermore, generation of gas and increase in pressure can also be accelerated by the active presence of denitrifying bacteria limiting the safety of the radioactive waste repository [90].



The MIND-project has received funding from the European Union's Euratom research and training program (Horizon2020) under grant agreement 661880.

### 3.3.2 Next-generation sequencing

## Carbon steel in natural granite *water* (source VITA) under laboratory temperature (Experiment B)

Results of NGS amplicon sequencing with only taxa over 1% of abundance are shown in Figure 40.

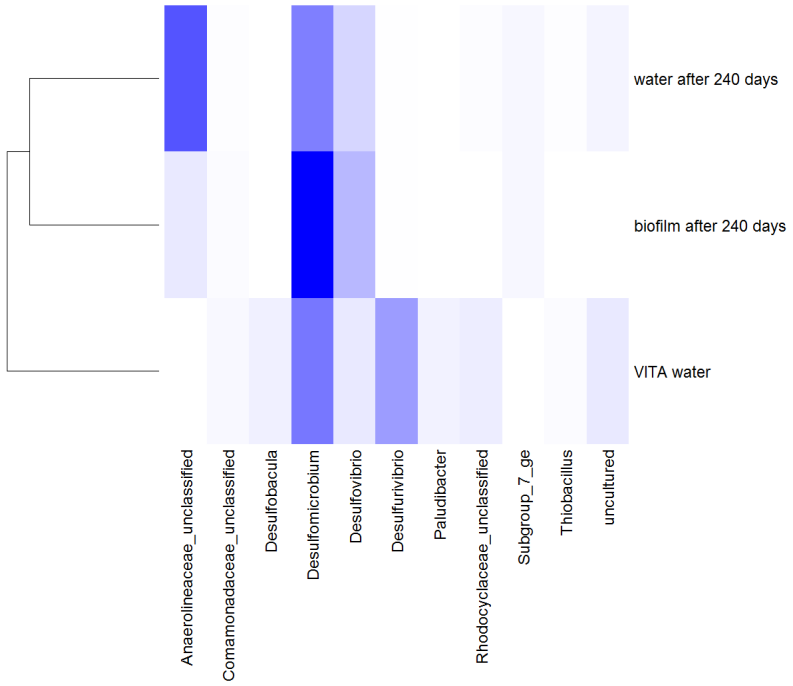


*Figure 40 Heat Map showing the relationship between initial VITA microbial community and microbial community after 240 days in biofilm and water. Results of NGS amplicon sequencing.*

Mesophilic and thermophilic SRB genus like *Desulfobacula, Desulfomicrobium, Desulfovibrio,* and *Desulfurivibrio* were detected in VITA water. They all belong to Deltaproteobacteria. Both water and biofilm were highly dominated by *Desulfomicrobium*. Likewise, *Desulfovibrio*, another sulfide producer, was detected in both the VITA water and, especially, in the biofilm. Organic compound or hydrogen is utilized as source of electron by these heterotrophic species that are suspected to be directly responsible for anoxic corrosion [91]. Moreover, *Desulfomicrobium* can use sulphate, sulphite and thiosulphate as an electron acceptor but not the elemental sulphur [92]. Unlike *Desulfomicrobium*, member of *Desulfovibrio* can use sulphur and also nitrate, nitrite as an electron acceptor to carry denitrification. This genus is well known in the field of bioremediation of toxic metals and chlorinated compounds in water under anaerobic conditions. Surprisingly, *Desulfobacula* and *Desulfurivibrio,* decreased by the end of the experiment comparing to the initial state. On the other side, *Anaerolineaceae*, a Chloroflexi, an obligate anaerobic family, which was low in VITA water, proliferated and was highly abundant in water sample after 240 days. Members of this family are heterotrophic and can utilize hydrogen or sulphide as an electron donor and are biodegraders of n-alkane [93]. Notably, degradation of alkane in nutrient deprived condition similar to repository can provide good source of nutrient to anaerobic bacteria. Another family of *Comamonadaceae* and *Rhodocyclacea*e, facultative anaerobes, were also detected in low amounts. They use nitrate as terminal electron acceptor in absence of oxygen. Generally, a family *Comamonadaceae* was equally present in both water and biofilm while the *Rhodocyclaceae* were moderately less in biofilm than water sample. A chemoorganotrophic, strict anaerobic genus *Paludibacter* was also identified in VITA, but dropped by


The MIND-project has received funding from the European Union's Euratom research and training program (Horizon2020) under grant agreement 661880.

the end of the experiment. Interestingly, *Paludibacter* spp. can produce propionate [94] which can be used as a substrate by SRB for the production of sulphide [95]. In addition, the genus *Thiobacillus*, Betaproteobacteria, is a facultative anaerobe responsible for oxidation of sulphide and reduction of nitrate was detected. While the abundance of *Thiobacillus* in the VITA water was similar to water after 240 days, it was poorly represented in the biofilm. This genus includes acid producing species and hence is considered as key agent of acid mine drainage and for corrosion of concrete materials [96]. As such, species of this genus can play a role in degradation of concrete barrier in waste repositories. Beside this, some members of a class Halophagae (subgroup_7_ge) belonging to the phylum *Acidobacteria* were detected in water sample and biofilm with higher abundance than in initial VITA source.

Investigation of microbial diversity in water and biofilm helps us to understand and consider the impact of these microorganisms in term of corrosion [97]. A study showed that formation of bacterial biofilm is the major key step in initiating MIC. Similarly, the microorganisms living in deep groundwater had higher ability to form biofilm on the surface of carbon steel. It was also revealed that localized accelerating corrosion develops rapidly in presence of biofilm [91].

## Carbon steel in natural granite water (source VITA) at T=35°C (Experiment C)

Results of NGS amplicon sequencing with only taxa over 1% of abundance are shown in Figure 41.

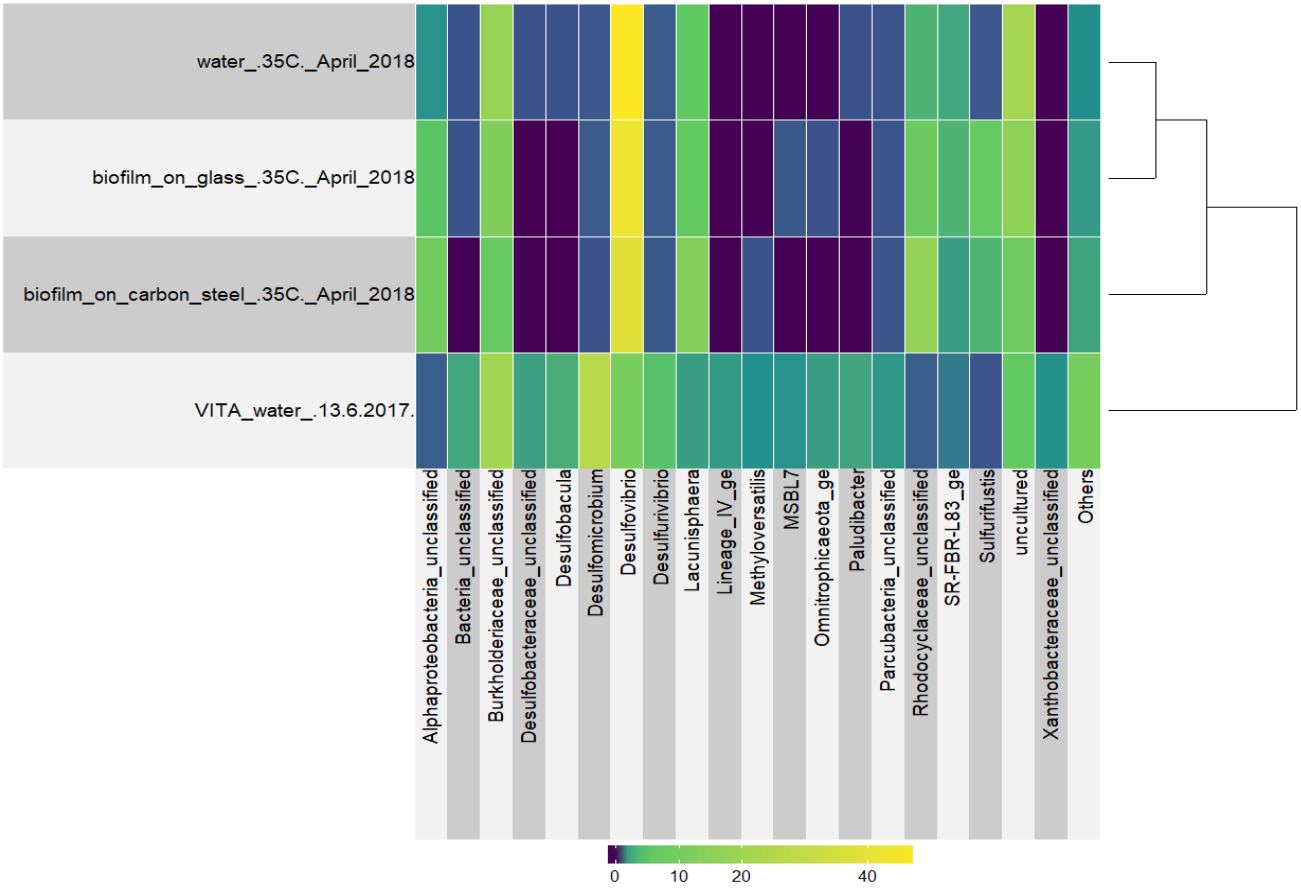


*Figure 41 Heat Map showing the relationship between initial microbial community in VITA water and microbial community in water, biofilm on glass and biofilm on carbon steel. Results of NGS amplicon sequencing (only taxa with abundance over 1% are visualised)*



The MIND-project has received funding from the European Union's Euratom research and training program (Horizon2020) under grant agreement 661880.

The VITA water was rich in microbial diversity comparing to water and biofilm after 10 months. SRB and many unclassified taxa were detected. SRB belonging to phylum Deltaproteobacteria such as *Desulfobacula, Desulfomicrobium, Desulfovibrio,* and *Desulfurivibrio* were identified in initial VITA water source. However, by the end of experiment, *Desulfovibrio* was the only the dominant and most abundant genus in water as well as in biofilm on glass and on carbon steel. The members of this genus are believed to be a major culprit for carrying out MIC [89]. Surprisingly, the other SRB members decreased over the period of experiment.

Unclassified Alphaproteobacteria increased over 10 months little bit more in biofilm than in water. The members of this phylum might be facultative anaerobes here. Likewise, unclassified family of *Burkholderiaceae,* which are facultative anaerobes, slightly decreased toward the end of the experiment forming higher abundance in water and biofilm on glass than in biofilm on carbon steel. They reduces nitrate in absence of oxygen. Moreover, an increase of *Lacunisphaera* belonging to phylum *Verrucomicrobia* was noticed by the end of incubation. The optimal temperature for the growth of this bacterial taxa is between 10 to 38°C and the experimental temperature of 35°C could favor its growth. Typical member of this group is aerobic and can be found in freshwater and soil however, some species may exist as facultative anaerobes as well [105]. Similarly, another unclassified family of Rhodocyclaceae was recorded in higher abundance while the proliferation was slightly higher in biofilm on carbon steel than biofilm on glass and water. Rhodocyclaceae are facultative anaerobes and are able to reduce nitrate under anaerobic condition. Furthermore, a genus *Sulfurifustis* belonging to phylum Gamaproteobacteria that oxidizes thiosulphate, tetrathionate and elemental sulphur was found to grow in both the biofilms but not in water. The normal temperature for the growth of this genus is 28-46°C [98]. In contrast, other taxa such as Lineage_IV_ge, Methyloversatilis, MSBL7, Omnitrophicaeota_ge, *Paludibacter*, Unclassified Parcubacteria and Xanthobacteraceae which are generally nitrate reducers decreased dramatically by the end of the experiment.

### Carbon steel in synthetic bentonite pore water (SBPOW) inoculated with VITA water, under laboratory temperature (Experiment D)

The VITA water was primarily dominated by SRB such as *Desulfurivibrio* and *Desulfomicrobium* and by facultative anaerobe *Sulfuritalea* that is sulphide oxidizer and nitrate reducer. The NGS amplicon sequencing results of genus with relative abundance over 1% is presented in Figure 412. In general, the microbial diversity declined during the first 3 months. Two biofilm marked as A and B was from each sampling day and it was a duplicate sample. In the experimental condition without carbon steel, the microbial community was more diverse after 6 months than after 18 months. Surprisingly, NRB highly proliferated throughout the experiment and outcompeted SRB. As mentioned earlier, the SBPOW mimics the bentonite leachate, which was rich in nitrate, and hence; it favors and promotes the growth of NRB in the absence of oxygen and suppresses SRB.


The MIND-project has received funding from the European Union's Euratom research and training program (Horizon2020) under grant agreement 661880.

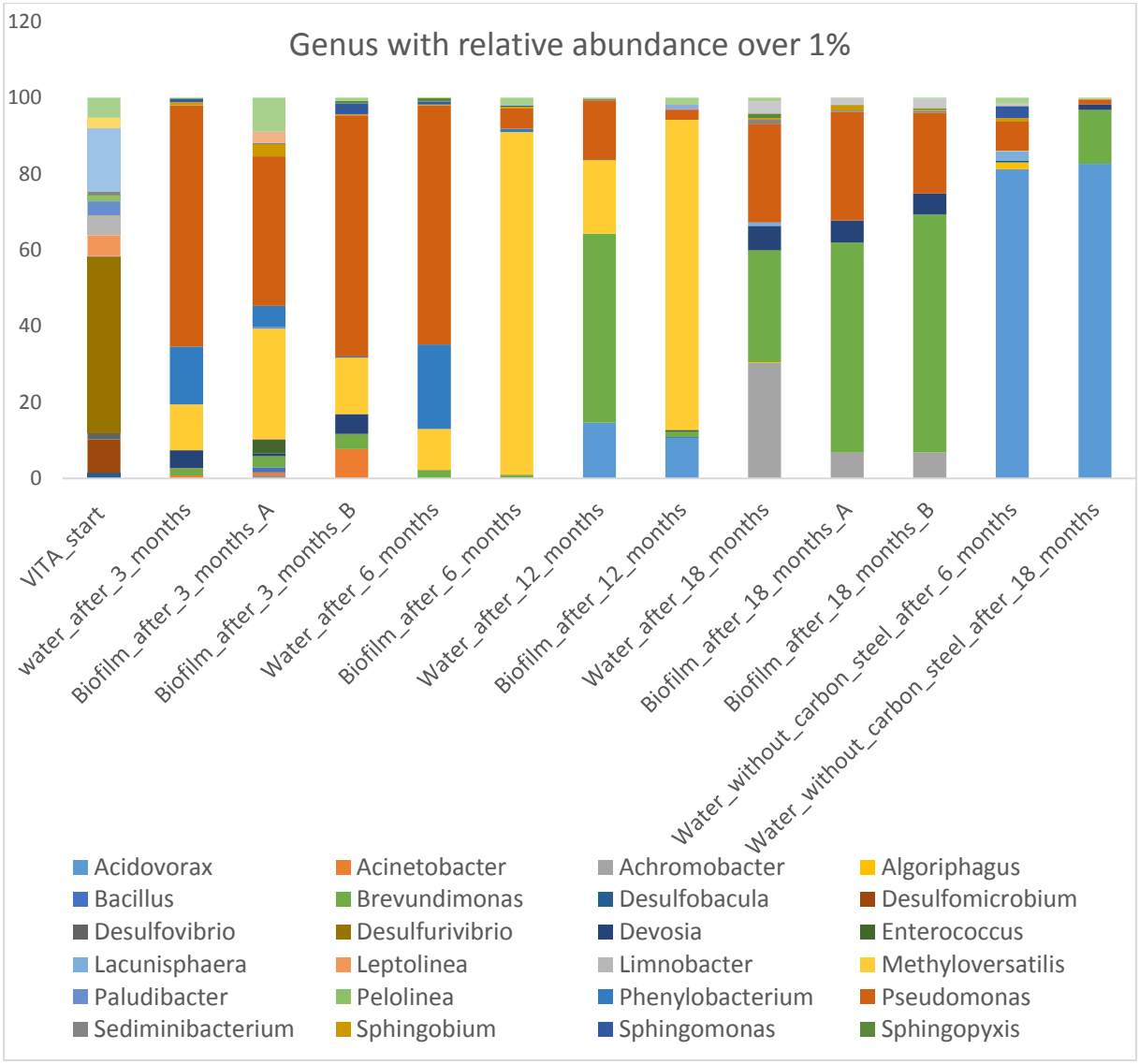


*Figure 412 Results of NGS amplicon sequencing showing genus with relative abundance over 1% .*

*Pseudomonas* belonging to Gammaproteobacteria and facultative anaerobes highly proliferated and was the most dominant genus for the first 6 months contributing to more than 60% of total abundance in water and biofilm B after 3 months. However, it decreased by the end of 1 year and increased again gaining 20-25% of abundance by the end of 18 months. This genus was also present in samples without carbon steel after 6 months though it declined by 18 months under the same conditions. The member of this genus are heterotrophic and are typical nitrate reducers and can grow at temperature of 42 °C [99]. Similarly, a heterotrophic, denitrifying bacteria *Phenylobacterium* was present for the first 6 months but it was not able to proliferate after that and the reason could be the competition with other NRB like *Methyloversatilis*. The species of the genus *Phenylobacterium* belong to Alphaproteobacteria, facultative anaerobes that use nitrate as terminal electron acceptor under anoxic environment and use organic compounds as electron donor [100]. The biofilm after 6 and 12 months was dominated by the genus *Methyloversatilis* resulting in more than 80% of abundance. They belong to Betaproteobacteria and are heterotrophic facultative anaerobes and use nitrate in absence of oxygen [101]. Nonetheless, their abundance fall dramatically after 18 months. Interestingly, *Acinetobacter*, a Gammaproteobacteria which might have fallen below detection limit in VITA water was observed after the first 3 months in a very low abundance and disappeared completely after 6 months. Generally, *Acinetobacter* is heterotrophic aerobe [102] and could not sustain in anaerobic environment. Similarly, *Devosia,* Alphaproteobacteria, proliferated only in the first 3 months



The MIND-project has received funding from the European Union's Euratom research and training program (Horizon2020) under grant agreement 661880.

and after 18 months contributed to about 5% of biomass. This genus is normally aerobic, but was also isolated from deep-sea sediments with temperature 25-30 °C [103]. Any growth of this genus was detected during the period of 6-12 months even though, its presence was noticed more or less in same ratio in water and both the biofilms after 18 months. Additionally, a very small abundance of *Devosia* was also recorded in the sample without carbon steel after 18 months. Furthermore, *Acidovorax,* Betaproteobacteria was detected clearly after 12 months though only a very small abundance was found in biofilm A after 3 months. Members of this genus are facultative anaerobes and hydrogen or organic compound can serve them as electron donor, they can reduce nitrate under anaerobic conditions [104]. Surprisingly, *Acidovorax* was the only dominant genus (80%) confirmed in the samples without carbon steel after 6 and 18 months. Moreover, the genus *Brevundimonas, A*lphaproteobacteria, was noticed in very low abundance until 6 months of period but after 12 months the growth of this genus increased dramatically. They are nitrate reducers and facultative anaerobes that commonly utilize organic compound as electron donor. The optimum temperature for this genus is 30 °C and pH 7.5 to 8 [105]. The member of *Brevundimonas* were well adopted to the environment after 18 months being the most abundant one among others achieving 29% in water and over 50% in both biofilms. Likewise, the genus *Achromobacter*, Betaproteobacteria was observed only after 18 months while any sign of this genus was detected in earlier sampling point including VITA water similarly to *Acinetobacter*. Since the NGS result showed the genus abundance with more than 1 % only, the genus *Achromobacter* might have fallen below 1%. They are also facultative anaerobes and are heterotrophs which use either nitrate or nitrite as electron acceptor and hydrogen or organic compound as electron donor [106]. Additionally, the two heterotrophic taxa *Thalassobaculum* and *Lacunisphaera* appeared with a low abundance after 6 months in samples without carbon steel. The *Thalassobaculum* belongs to Alphaproteobacteria and are facultative anaerobes with a capability to reduce nitrate [107] whereas *Lacunisphaera* which belongs to Verrucomicrobia is generally aerobic [108]. Additionally, *Algoriphagus,* heterotrophic bacteria was noticed in a very low abundance in water after 18 months with carbon steel and after 6 months without carbon steel. The members of this genus are usually halotolerant [109]. Interestingly, some of the taxa that have been labelled as aerobes were detected in some sampling points while the experiment was carried under anaerobic condition. In general, the taxa like *Acinetobacter, Devosia, Lacunisphaera* and *Algoriphagus* are marked as aerobes however, there might have different species of these genuses present in water which were able to reduce nitrate as terminal electron acceptor in absence of oxygen and thus were facultative anaerobes.

NRB are capable of inducing metal corrosion. According to bioenergetics, iron oxidation coupled with nitrate reduction provides energy for the respiration for NRB which can lead to MIC [110]. Marine *Pseudomonas aeruginosa,* a NRB was observed to accelerate the pitting corrosion of 2304 duplex steel by 6.2 times higher than abiotic control in 14 days [111]. Furthermore, it has been demonstrated that *Bacillus licheniformis,* a NRB influenced corrosion of carbon steel C1018 when grown as biofilm causing a 14.5 µm pit depth and 0.89 mg/cm$^2$ normalized weight loss in one week lab tests. Unlike SRB corrosion, NRB corrosion has been reported only occasionally in the literature [110].


The MIND-project has received funding from the European Union's Euratom research and training program (Horizon2020) under grant agreement 661880.

# 4 Conclusions

This study was to focused on anaerobic microbial corrosion of canister material in environments containing natural microbial community dominated by sulphate-reducing bacteria. Particularly, MIC of stainless steel and carbon steel was studied in laboratory conditions.

The unstable passivity and MIC inhibition of stainless steel was observed in the granite groundwater under anaerobic conditions at laboratory temperature.

In the case of a carbon steel exposed to natural granite water at laboratory temperature, we observed biofilm life cycle in three steps, where third step of the seeding dispersal revealed in the form of second layer of biofilm. The formation of a biofilm on the carbon steel surface accelerated the corrosion rate. Polarization resistance of carbon steel decreased by a factor of two after 240 days. Molecular biological analysis of the water and biofilm showed dominance of *Desulfomicrobium* along with *Desulfovibrio species.* These species are considered to be active in corrosion under anaerobic condition.

On the contrary, the formation of biofilm on the carbon steel surface in natural granite water at 35°C inhibited corrosion rate by barrier effect. Molecular biological analysis of the water and biofilm showed only dominance of *Desulfovibrio* whereas the other SRB initially present (*Desulfobacula, Desulfomicrobium, Desulfovibrio*) declined over time.

Severe local attack was observed only in the case of weight loss experiments with carbon steel using synthetic bentonite pore water inoculated with VITA water for samples taken after 3, 6 and 12 months. The samples collected after 18 months of exposure were without local attack under non-sterile conditions. Members of NRB highly proliferated in carbon steel presence using synthetic bentonite pore water inoculated with VITA**.** *Pseudomonas, Methyloversatilis and Brevundimonas* belonged to the most abundant NRB. The synthetic water mimics the Czech bentonite leachate, which was rich in nitrate hence; it favored the growth of bacteria that could reduce nitrate. Iron oxidation coupled with nitrate reduction provides energy for the NRB respiration which may lead to MIC.

SEM images showed the biofilm formation. The microbial presence was proved through the corrosive products by EDS analysis and a varying of corrosion layer thickness between sterile versus non-sterile conditions. Moreover, in the experiment with carbon steel using only VITA water at laboratory temperature, two corrosion layers were observed. SEM analysis clearly supported the rightness of the EIS results.

Raman analysis of the carbon steel in natural granite water at 35°C and in synthetic bentonite pore water showed that the surface was essentially covered with magnetite in the end of the experiment. However, local depressions were filled with calcite or aragonite. Moreover, in the case of non-sterile conditions the mackinawite was recorded on the carbon steel as a proof of presence SRB and possible MIC. Except for the carbon steel after 18 months of exposition in SBPOW, there was not found any presence of sulphide species on the surface.



The MIND-project has received funding from the European Union's Euratom research and training program (Horizon2020) under grant agreement 661880.

# 5 Acknowledgement

The MIND-project has received funding from the European Union's Euratom research and training program (Horizon2020) under grant agreement 661880 The MIND-project.

# 6 References


1. Zhou, Z., *Modeling of Microbial Induced Corrosion on Metallic Pipelines Resulting from Biomethane and the Integrity Impact of Biomethane on Non-Metallic Pipelines*. 2012.
2. Féron, D., *Nuclear corrosion science and engineering*. 2012: Elsevier.
3. Beech, I.B. and J. Sunner, *Biocorrosion: towards understanding interactions between biofilms and metals.* Current Opinion in Biotechnology, 2004. **15**(3): p. 181-186.
4. Degen, I. and G. Newman, *Raman spectra of inorganic ions.* Spectrochimica Acta Part A: Molecular Spectroscopy, 1993. **49**(5-6): p. 859-887.
5. Li, Y., et al., *Anaerobic microbiologically influenced corrosion mechanisms interpreted using bioenergetics and bioelectrochemistry: A review*. 2018.
6. Vert, M., et al., *Terminology for biorelated polymers and applications (IUPAC Recommendations 2012)*, in *Pure and Applied Chemistry*. 2012. p. 377.
7. Little, B.J. and J.S. Lee, *Microbiologically Influenced Corrosion*. 2007: Wiley.
8. Stoodley, P. and P. Dirckx, *Biofilm formation in 3 steps*. 2003.
9. Jin, J. and Y. Guan, *The mutual co-regulation of extracellular polymeric substances and iron ions in biocorrosion of cast iron pipes.* Bioresource technology, 2014. **169**: p. 387-394.
10. Paula, M.S.d., et al., *Carbon steel corrosion induced by sulphate-reducing bacteria in artificial seawater: electrochemical and morphological characterizations.* Matéria (Rio de Janeiro), 2016. **21**(4): p. 987-995.
11. Clark, M.E., et al., *Transcriptomic and proteomic analyses of Desulfovibrio vulgaris biofilms: Carbon and energy flow contribute to the distinct biofilm growth state.* Bmc Genomics, 2012. **13**: p. 17.
12. Hall-Stoodley, L. and P. Stoodley, *Evolving concepts in biofilm infections*. 2009.
13. Verwey, E.J.W. and J.T.G. Overbeek, *Theory of the stability of lyophobic colloids*. 1955.
14. Lewandowski, Z. and H. Beyenal, *Fundamentals of biofilm research*. 2013: CRC press.
15. Little, B., et al., *Impact of biofouling on the electrochemical behavior of 304 stainless steel in natural seawater.* Biofouling, 1991.
16. Fletcher, M. and G.D. Floodgate, *An electron-microscopic demonstration of an acidic polysaccharide involved in the adhesion of a marine bacterium to solid surfaces.* Journal of General Microbiology, 1973.
17. Xu, D. and T. Gu, *Bioenergetics explains when and why more severe MIC pitting by SRB can occur.* Corrosion/2011 Paper, 2011(11426).
18. Dall'Agnol, L.T., C.M. Cordas, and J.J. Moura, *Influence of respiratory substrate in carbon steel corrosion by a Sulphate Reducing Prokaryote model organism.* Bioelectrochemistry, 2014. **97**: p. 43-51.
19. Beech, I.B. and J. Sunner, *Biocorrosion: Towards understanding interactions between biofilms and metals*. 2004.
20. Madigan, M.T., et al., *Brock Biology of Microorganisms*. 2014.
21. Kip, N. and J.A. Van Veen, *The dual role of microbes in corrosion.* The ISME journal, 2015. **9**(3): p. 542.
22. Liu, H., et al., *Corrosion behavior of carbon steel in the presence of sulfate reducing bacteria and iron oxidizing bacteria cultured in oilfield produced water.* Corrosion Science, 2015. **100**: p. 484-495.
23. Pedersen, K., *Metabolic activity of subterranean microbial communities in deep granitic groundwater supplemented with methane and H 2.* The ISME journal, 2013. **7**(4): p. 839.
24. Enning, D., et al., *Marine sulfate-reducing bacteria cause serious corrosion of iron under electroconductive biogenic mineral crust.* Environmental microbiology, 2012. **14**(7): p. 1772-1787.
25. Rao, T., et al., *Carbon steel corrosion by iron oxidising and sulphate reducing bacteria in a freshwater cooling system.* Corrosion Science, 2000. **42**(8): p. 1417-1431.




The MIND-project has received funding from the European Union's Euratom research and training program (Horizon2020) under grant agreement 661880.

26. Venzlaff, H., et al., *Accelerated cathodic reaction in microbial corrosion of iron due to direct electron uptake by sulfate-reducing bacteria.* Corrosion Science, 2013. **66**: p. 88-96.
27. Wikieł, A.J., et al., *Impact of Desulfovibrio alaskensis biofilms on corrosion behaviour of carbon steel in marine environment.* Bioelectrochemistry, 2014. **97**: p. 52-60.
28. Usher, K., A. Kaksonen, and I. MacLeod, *Marine rust tubercles harbour iron corroding archaea and sulphate reducing bacteria.* Corrosion Science, 2014. **83**: p. 189-197.
29. Little, B., R. Staehle, and R. Davis, *Fungal influenced corrosion of post-tensioned cables.* International biodeterioration & biodegradation, 2001. **47**(2): p. 71-77.
30. San, N.O., H. Nazır, and G. Dönmez, *Microbial corrosion of Ni–Cu alloys by Aeromonas eucrenophila bacterium.* Corrosion Science, 2011. **53**(6): p. 2216-2221.
31. Stadler, R., et al., *First evaluation of the applicability of microbial extracellular polymeric substances for corrosion protection of metal substrates.* Electrochimica Acta, 2008. **54**(1): p. 91-99.
32. Stadler, R., et al., *Influence of bacterial exopolymers on cell adhesion of Desulfovibrio vulgaris on high alloyed steel: corrosion inhibition by extracellular polymeric substances (EPS).* Materials and Corrosion, 2010. **61**(12): p. 1008-1016.
33. Lee, J.S., et al., *Iron cycling at corroding carbon steel surfaces.* Biofouling, 2013. **29**(10): p. 1243-1252.
34. Linhardt, P., *Twenty years of experience with corrosion failures caused by manganese oxidizing microorganisms.* Materials and Corrosion, 2010. **61**(12): p. 1034-1039.
35. LI, S.-M., et al., *Corrosion behavior of steel A3 influenced by Thiobacillus ferrooxidans.* Acta Physico-Chimica Sinica, 2008. **24**(9): p. 1553-1557.
36. Barton, L.L. and G.D. Fauque, *Biochemistry, physiology and biotechnology of sulfate-reducing bacteria.* Advances in applied microbiology, 2009. **68**: p. 41-98.
37. Bengtsson, A. and K. Pedersen, *Microbial sulphate-reducing activity over load pressure and density in water saturated Boom Clay.* Applied Clay Science, 2016. **132**: p. 542-551.
38. Masurat, P., S. Eriksson, and K. Pedersen, *Evidence of indigenous sulphate-reducing bacteria in commercial Wyoming bentonite MX-80.* Applied Clay Science, 2010. **47**(1-2): p. 51-57.
39. Pedersen, K., et al., *Mobility and reactivity of sulphide in bentonite clays–implications for engineered bentonite barriers in geological repositories for radioactive wastes.* Applied Clay Science, 2017. **146**: p. 495-502.
40. Stroes-Gascoyne, S., et al., *The effects of the physical properties of highly compacted smectitic clay (bentonite) on the culturability of indigenous microorganisms.* Applied Clay Science, 2010. **47**(1-2): p. 155-162.
41. Aerts, S., *Effect of geochemical conditions on bacterial activity.* SCK CEN, Belgium, 2009.
42. Zhilina, T., et al., *Desulfonatronovibrio hydrogenovorans gen. nov., sp. nov., an alkaliphilic, sulfate-reducing bacterium.* International Journal of Systematic and Evolutionary Microbiology, 1997. **47**(1): p. 144-149.
43. Pikuta, E., *Desulfonatronum lacustre gen. nov., sp. nov.: a new alkaliphilic sulfate-reducing bacterium utilizing ethanol.* Микробиология, 1998. **67**(1): p. 123-131.
44. Takai, K., et al., *Alkaliphilus transvaalensis gen. nov., sp. nov., an extremely alkaliphilic bacterium isolated from a deep South African gold mine.* International Journal of Systematic and Evolutionary Microbiology, 2001. **51**(4): p. 1245-1256.
45. Abildgaard, L., et al., *Desulfovibrio alkalitolerans sp. nov., a novel alkalitolerant, sulphate-reducing bacterium isolated from district heating water.* International journal of systematic and evolutionary microbiology, 2006. **56**(5): p. 1019-1024.
46. Sorokin, D.Y., et al., *Sulfidogenesis under extremely haloalkaline conditions by Desulfonatronospira thiodismutans gen. nov., sp. nov., and Desulfonatronospira delicata sp. nov.–a novel lineage of Deltaproteobacteria from hypersaline soda lakes.* Microbiology, 2008. **154**(5): p. 1444-1453.



The MIND-project has received funding from the European Union's Euratom research and training program (Horizon2020) under grant agreement 661880.

47. Pikuta, E., et al., *Desulfotomaculum alkaliphilum sp. nov., a new alkaliphilic, moderately thermophilic, sulfate-reducing bacterium.* International journal of systematic and evolutionary microbiology, 2000. **50**(1): p. 25-33.
48. Rabus, R., T.A. Hansen, and F. Widdel, *Dissimilatory sulfate-and sulfur-reducing prokaryotes*, in *The prokaryotes*. 2006, Springer. p. 659-768.
49. Kakooei, S., M.C. Ismail, and B. Ariwahjoedi, *Mechanisms of microbiologically influenced corrosion: a review.* World Appl. Sci. J, 2012. **17**(4): p. 524.
50. Mori, K., H. Tsurumaru, and S. Harayama, *Iron corrosion activity of anaerobic hydrogen-consuming microorganisms isolated from oil facilities.* Journal of bioscience and bioengineering, 2010. **110**(4): p. 426-430.
51. Chan, K.Y., L.C. Xu, and H.H.P. Fang, *Anaerobic electrochemical corrosion rug of mild steel in the presence of extracellular polymeric substances produced by a culture enriched in sulfate-reducing bacteria.* Environmental Science & Technology, 2002. **36**(8): p. 1720-1727.
52. Gu, T. and D. Xu, *Demystifying MIC mechanisms.* CORROSION 2010, 2010.
53. Druyts, F. and B. Kursten, *SACNUC. Sulphur-Assisted Corrosion in Nuclear Waste Disposal Systems*. 2008, SCK• CEN, Mol, Belgium.
54. Stansbury, E.E. and R.A. Buchanan, *Fundamentals of electrochemical corrosion*. 2000: ASM international.
55. Jones, D.A., *Principles and Prevention of Corrosion, 2nd.* Ed. Upper Saddle River, NY: Prentice Hall, 1996: p. 168-198.
56. Goldstein, J., et al., *Scanning Electron Microscopy and X-Ray Microanalysis: A Text for Biologists, Materials Scientists, and Geologists*. 2012.
57. Goodhew, P.J., J. Humphreys, and R. Beanland, *Electron Microscopy and Analysis.* Taylor and Francis, 2001.
58. Reimer, L., *Scanning Electron Microscopy: Physics of Image Formation and Microanalysis*. 1998.
59. Seiler, H., *Secondary electron emission in the scanning electron microscope.* Journal of Applied Physics, 1983.
60. Peters, G., R. Locci, and G. Pulverer, *Adherence and growth of coagulase-negative staphylecocci on surfaces of intravenous catheters.* Journal of Infectious Diseases, 1982.
61. Echlin, P., *Ice crystal damage and radiation effects in relation to microscopy and analysis at low temperatures.* J Microsc, 1991.
62. Eighmy, T.T., D. Maratea, and P.L. Bishop, *Electron microscopic examination of wastewater biofilm formation and structural components.* Applied and Environmental Microbiology, 1983.
63. Blenkinsopp, S.A. and J.W. Costerton, *Understanding bacterial biofilms.* Trends in Biotechnology, 1991.
64. Körstgens, V., et al., *Influence of calcium ions on the mechanical properties of a model biofilm of mucoid Pseudomonas aeruginosa.* Water science and technology : a journal of the International Association on Water Pollution Research, 2001.
65. El, S., et al., *Scanning Electron Microscopy (SEM) and Environmental SEM: Suitable Tools for Study of Adhesion Stage and Biofilm Formation*. 2012.
66. Bumbrah, G.S. and R.M. Sharma, *Raman spectroscopy–Basic principle, instrumentation and selected applications for the characterization of drugs of abuse.* Egyptian Journal of Forensic Sciences, 2016. **6**(3): p. 209-215.
67. Tsuboi, M., *Infrared and Raman spectroscopy*. Vol. 1. 1974: Academic Press: New York.
68. Monnier, J., et al., *A methodology for Raman structural quantification imaging and its application to iron indoor atmospheric corrosion products.* Journal of raman spectroscopy, 2011. **42**(4): p. 773-781.
69. Dubois, F., et al., *Raman mapping of corrosion products formed onto spring steels during salt spray experiments. A correlation between the scale composition and the corrosion resistance.* Corrosion Science, 2008. **50**(12): p. 3401-3409.



The MIND-project has received funding from the European Union's Euratom research and training program (Horizon2020) under grant agreement 661880.

70. Neff, D., et al., *Raman imaging of ancient rust scales on archaeological iron artefacts for long-term atmospheric corrosion mechanisms study.* Journal of Raman Spectroscopy: An International Journal for Original Work in all Aspects of Raman Spectroscopy, Including Higher Order Processes, and also Brillouin and Rayleigh Scattering, 2006. **37**(10): p. 1228-1237.
71. Surnam, B.Y.R., et al., *Investigating atmospheric corrosion behavior of carbon steel in coastal regions of Mauritius using Raman Spectroscopy.* Matéria (Rio de Janeiro), 2016. **21**(1): p. 157-168.
72. Němeček, J., et al., *Stratification of chlorinated ethenes natural attenuation in an alluvial aquifer assessed by hydrochemical and biomolecular tools.* Chemosphere, 2017. **184**: p. 1157-1167.
73. ISO, I., *8407: 2009 (E). Corrosion of Metals and Alloys—Removal of Corrosion Products from Corrosion Test Specimens.* International Standards Organization: Geneva, Switzerland, 2009.
74. ISO, E., *9226. Corrosion of Metals and Alloys: Corrosivity of Atmospheres: Determination of Corrosion Rate of Standard Specimens for the Evaluation of Corrosivity.* International Organization for Standardization, Geneva, Switzerland, 1992.
75. Clifford, R.J., et al., *Detection of bacterial 16S rRNA and identification of four clinically important bacteria by real-time PCR.* PloS one, 2012. **7**(11): p. e48558.
76. Ben-Dov, E., A. Brenner, and A. Kushmaro, *Quantification of sulfate-reducing bacteria in industrial wastewater, by real-time polymerase chain reaction (PCR) using dsrA and apsA genes.* Microbial ecology, 2007. **54**(3): p. 439-451.
77. Geets, J., et al., *Real-time PCR assay for the simultaneous quantification of nitrifying and denitrifying bacteria in activated sludge.* Applied microbiology and biotechnology, 2007. **75**(1): p. 211-221.
78. Wei, N. and K.T. Finneran, *Influence of ferric iron on complete dechlorination of trichloroethylene (TCE) to ethene: Fe (III) reduction does not always inhibit complete dechlorination.* Environmental science & technology, 2011. **45**(17): p. 7422-7430.
79. Dowd, S.E., et al., *Evaluation of the bacterial diversity in the feces of cattle using 16S rDNA bacterial tag-encoded FLX amplicon pyrosequencing (bTEFAP).* BMC microbiology, 2008. **8**(1): p. 125.
80. Claesson, M.J., et al., *Comparison of two next-generation sequencing technologies for resolving highly complex microbiota composition using tandem variable 16S rRNA gene regions.* Nucleic acids research, 2010. **38**(22): p. e200-e200.
81. Schloss, P.D., et al., *Introducing mothur: open-source, platform-independent, community-supported software for describing and comparing microbial communities.* Applied and environmental microbiology, 2009. **75**(23): p. 7537-7541.
82. Edgar, R.C., et al., *UCHIME improves sensitivity and speed of chimera detection.* Bioinformatics, 2011. **27**(16): p. 2194-2200.
83. Oksanen, F., et al., *Vegan: community ecology package. 2011.[R packa version 2.0-2] http://CRAN.* R-project. org/package= vegan.
84. Callahan, B.J., et al., *DADA2: high-resolution sample inference from Illumina amplicon data.* Nature methods, 2016. **13**(7): p. 581.
85. McMurdie, P.J. and S. Holmes, *phyloseq: an R package for reproducible interactive analysis and graphics of microbiome census data.* PloS one, 2013. **8**(4): p. e61217.
86. Sreekumari, K.R., Y. Sato, and Y. Kikuchi, *Antibacterial Metals—A Viable Solution for Bacterial Attachment and Microbiologically Influenced Corrosion—.* Materials transactions, 2005. **46**(7): p. 1636-1645.
87. Miller, R.B., et al., *Uniform and pitting corrosion of carbon steel by Shewanella oneidensis MR-1 under nitrate-reducing conditions.* Applied and environmental microbiology, 2018: p. AEM. 00790-18.
88. Colomban, P., *Potential and drawbacks of Raman (micro) spectrometry for the understanding of iron and steel corrosion*, in *New Trends and Developments in Automotive System Engineering*. 2011, InTech.



The MIND-project has received funding from the European Union's Euratom research and training program (Horizon2020) under grant agreement 661880.

89. Joo, J.O., et al., *Effective bioremediation of Cadmium (II), nickel (II), and chromium (VI) in a marine environment by using Desulfovibrio desulfuricans.* Biotechnology and Bioprocess Engineering, 2015. **20**(5): p. 937-941.
90. Bertron, A., et al., *Physico-chemical interactions at the concrete-bitumen interface of nuclear waste repositories*, in *International Workshop Nucperf 2012: Long-Term Performance of Cementitious Barriers and Reinforced Concrete in Nuclear Power Plant and Radioactive Waste Storage and Disposal*, V. Lhostis and R. Gens, Editors. 2013.
91. Rajala, P., et al., *Microbially induced corrosion of carbon steel in deep groundwater environment.* Frontiers in Microbiology, 2015. **6**.
92. Thevenieau, F., et al., *Desulfomicrobium thermophilum sp nov., a novel thermophilic sulphate-reducing bacterium isolated from a terrestrial hot spring in Colombia.* Extremophiles, 2007. **11**(2): p. 295-303.
93. Sherry, A., et al., *Anaerobic biodegradation of crude oil under sulphate-reducing conditions leads to only modest enrichment of recognized sulphate-reducing taxa.* International Biodeterioration & Biodegradation, 2013. **81**: p. 105-113.
94. Ueki, A., et al., *Paludibacter propionicigenes gen. nov., sp. nov., a novel strictly anaerobic, Gram-negative, propionate-producing bacterium isolated from plant residue in irrigated rice-field soil in Japan.* International journal of systematic and evolutionary microbiology, 2006. **56**(1): p. 39-44.
95. Glombitza, C., et al., *Formate, acetate, and propionate as substrates for sulfate reduction in sub-arctic sediments of Southwest Greenland.* Frontiers in microbiology, 2015. **6**: p. 846.
96. Peccia, J., et al., *Development and application of small-subunit rRNA probes for assessment of selected Thiobacillus species and members of the genus Acidiphilium.* Applied and environmental microbiology, 2000. **66**(7): p. 3065-3072.
97. Libert, M., et al., *Impact of microbial activity on the radioactive waste disposal: long term prediction of biocorrosion processes.* Bioelectrochemistry, 2014. **97**: p. 162-168.
98. Kojima, H., A. Shinohara, and M. Fukui, *Sulfurifustis variabilis gen. nov., sp. nov., a sulfur oxidizer isolated from a lake, and proposal of Acidiferrobacteraceae fam. nov. and Acidiferrobacterales ord. nov.* International journal of systematic and evolutionary microbiology, 2015. **65**(10): p. 3709-3713.
99. Garrity, G.M., et al., *Bergey's Manual of Systematic Bacteriology. Volume 2: The Proteobacteria.* Part B: The Gammaproteobacteria, 2005.
100. Aslam, S., R.J. Hamill, and D.M. Musher, *Treatment of Clostridium difficile-associated disease: old therapies and new strategies.* The Lancet infectious diseases, 2005. **5**(9): p. 549-557.
101. Lu, H., M. Kalyuzhnaya, and K. Chandran, *Comparative proteomic analysis reveals insights into anoxic growth of M ethyloversatilis universalis FAM 5 on methanol and ethanol.* Environmental microbiology, 2012. **14**(11): p. 2935-2945.
102. Choi, A.M., S.W. Ryter, and B. Levine, *Autophagy in human health and disease.* New England Journal of Medicine, 2013. **368**(7): p. 651-662.
103. Jia, Y.-Y., et al., *Devosia pacifica sp. nov., isolated from deep-sea sediment.* International journal of systematic and evolutionary microbiology, 2014. **64**(8): p. 2637-2641.
104. Whitman, W.B., *Bergey's manual of systematics of Archaea and Bacteria*. 2015: Wiley Online Library.
105. Yoon, J.-H., et al., *Brevundimonas terrae sp. nov., isolated from an alkaline soil in Korea.* International journal of systematic and evolutionary microbiology, 2006. **56**(12): p. 2915-2919.
106. Vandamme, P., et al., *Achromobacter animicus sp. nov., Achromobacter mucicolens sp. nov., Achromobacter pulmonis sp. nov. and Achromobacter spiritinus sp. nov., from human clinical samples.* Systematic and applied microbiology, 2013. **36**(1): p. 1-10.
107. Zhang, G.I., C.Y. Hwang, and B.C. Cho, *Thalassobaculum litoreum gen. nov., sp. nov., a member of the family Rhodospirillaceae isolated from coastal seawater.* International journal of systematic and evolutionary microbiology, 2008. **58**(2): p. 479-485.



The MIND-project has received funding from the European Union's Euratom research and training program (Horizon2020) under grant agreement 661880.

108. Rast, P., et al., *Three novel species with peptidoglycan cell walls form the new genus Lacunisphaera gen. nov. in the family Opitutaceae of the verrucomicrobial subdivision 4.* Frontiers in microbiology, 2017. **8**: p. 202.
109. Nedashkovskaya, O.I., et al., *Description of Algoriphagus aquimarinus sp. nov., Algoriphagus chordae sp. nov. and Algoriphagus winogradskyi sp. nov., from sea water and algae, transfer of Hongiella halophila Yi and Chun 2004 to the genus Algoriphagus as Algoriphagus halophilus comb. nov. and emended descriptions of the genera Algoriphagus Bowman et al. 2003 and Hongiella Yi and Chun 2004.* International journal of systematic and evolutionary microbiology, 2004. **54**(5): p. 1757-1764.
110. Xu, D., et al., *Laboratory investigation of microbiologically influenced corrosion of C1018 carbon steel by nitrate reducing bacterium Bacillus licheniformis.* Corrosion Science, 2013. **77**: p. 385-390.
111. Zhou, E., et al., *Accelerated corrosion of 2304 duplex stainless steel by marine Pseudomonas aeruginosa biofilm.* International Biodeterioration & Biodegradation, 2018. **127**: p. 1-9.


The MIND-project has received funding from the European Union's Euratom research and training program (Horizon2020) under grant agreement 661880.